République Algérienne Démocratique Et Populaire

Ministère De L'enseignement Supérieur Et De La Recherche Scientifique
Université Mohamed Khider De Biskra

Faculté des Sciences Exactes et Sciences de la Nature et de la Vie
Département de Sciences de la matière

Ref : ……..

Thèse présentée en vue de l'obtention du diplôme de :

Doctorat en physique
Option : **Physique des couches minces**

Thème:

Synthèse et caractérisations d'oxyde semiconducteurs de type p en couches minces par chimie douce pour des applications photovoltaiques

Présentée par:
Saadi Boutheina

Soutenue le: 14 / 02 / 2024

Devant le jury :

Abdelouahab Ouahab	Professeur	Université de Biskra	Président
Saâd RAHMANE	Professeur	University de Biskra	Encadreur
Slimane CHALA	MCA	University de Boumerdès	Examinateur
Elhachmi GUETTAF TEMAM	MCA	University de Biskra	Examinateur

Democratic and Popular Republic of Algeria
Ministry of Higher Education and Scientific Research
University Mohamed Khider of Biskra

Faculty of Exact Sciences and Science of Nature and Life
Department of Material Sciences

Ref : ……..

Thesis Presented to obtain the degree of

Doctorate in Physics

Option: **Physics of thin films**

Entitled:

Synthesis and characterizations of p-type oxide semiconductors thin films by mild chemistry for photovoltaic applications

Presented by:
Saadi Boutheina

Publicly defended on: 14 / 02 / 2024

In front of the Jury committee composed of:

Abdelouahab Ouahab	Professor	University of Biskra	President
Saâd RAHMANE	Professor	University of Biskra	Supervisor
Slimane CHALA	MCA	University of Boumerdes	Examiner
Elhachmi GUETTAF TEMAM	MCA	University of Biskra	Examiner

Dedication

I dedicate this thesis

To my dear parents who supported me in this thesis

To my husband and his parents

To my beautiful daughter, ***Ala Errahmane*** *and my son,* ***shouaib***

To all my sisters and brothers

To my second mother, may God have mercy on her.

To all my friends

Thank you a lot for your support, encouragement, and love, and may God bless them.

ACKNOWLEDGEMENT

First and foremost, thanks and praise are addressed to Allah, who has allowed me to accomplish this work.

I would like to express my deepest gratitude to my supervisor, Professor **Saad Rahmane**. I am very grateful to my supervisor for being paramount to the realization of this thesis and also for his constant encouragement and patience, which helped me continue during tough moments and helped develop my research skills. I will be eternally grateful to you.

I am honored that Pr. **Abdelouahab Ouahab**, Professor at Mohamed Khider University of Biskra, has agreed to chair the jury of my thesis.

I am also thankful to Mr **Sliman Chala**, MCA at Boumerdes University has agreed to chair the jury of my thesis.

I would also like to thank Pr **Elhachmi Guettaf Temam**, MCA in University Mohamed Khider of Biskra, who agreed to accept to belong to the jury and to examine my work.

My deepest sincere gratitude to Pr. Tibermacine Toufik, who helped me do the electrical tests of my work. I am also very grateful to the engineers at LPCMA laboratory, head of MEB Mr. Gasmi Brahim and head of DRX Mrs. Touhami.

thanks Mrs. **Nadjette Belhamra**, **Aicha Kater**, **Bencharef Zahia** and **chaouche Nadjette** for encouraging me.

My thanks also go to all of my colleagues from our laboratory (Laboratoire de Physique des Couches Minces et Applications « LPCMA »)

Last but not least, I owe a great deal to my entire family for their unwavering support and confidence in my capacity to accomplish so much.

TABLE OF CONTENTS

Chapter II: Influence of precursors on Cr_2O_3 thin films properties

Part one: Experimental details

Part Two: Influence of precursors on Cr_2O_3 thin films properties

Chapter III: Influence of substrate temperature on Cr_2O_3 thin films properties

LIST OF FIGURES

LIST OF TABLES

INTRODUCTION

In order to realize high-performance electronic devices such as light-emitting diodes (LEDs), transparent pn-junctions, transparent electronics, and thin-film transistors (TFTs), highly effective p-type TCOs are required. Relatively few p-type TCOs have been identified, and when compared to their n-type counterparts, they exhibit relatively inferior characteristics, such Poor conduction. The poor hole mobility of p-type TCOs is mostly caused by the shape of their valence band (VB) due to the strong localization of holes at oxygen 2p levels, resulting in the formation of a deep acceptor level. However, incorporating appropriate cations with energy levels close to or higher than the O 2p level can disrupt this localization. This leads to the dispersion of the valence band by hybridizing the cation outer shell orbital with the anion 2p orbital, reducing the hole's effective mass, which in turn augments the hole's mobility. This improves the p-type electrical conductivity in the material. Along with that, the optimization of deposition parameters plays a vital role in improving the optical and electrical properties.

Our job in this research work was to synthesize efficient p-type TCO thin-film by pneumatic spray system (SP) technique. Chromium oxide Cr_2O_3 was selected as our candidate material. Cr_2O_3 is a highly versatile material and its films have been used in a variety of applications, such as organic solar cells hole-transporting layer [1], Photodetector and Solar Cell [2], electronics [3], gas sensors [4] and corrosion [5]. There are many different thin film deposition methods that have been used to create Cr_2O_3 thin films, including dc magnetron sputtering [6], CVD [7], pulsed laser deposition (PLD) [8], sol gel method [9] and spray pyrolysis [10]. Among of these methods, spray pyrolysis has a lot of benefits, such as simplicity and low cost, moderate temperature operation, control of thickness, and solution flow rate control.

Hence, this work is aimed to demonstrating the appropriate conditions for synthesizing thin films for various applications by varying the concentration of precursor, substrate temperature, and effect of Indium and copper doped Cr_2O_3 thin films to improve the optical and electrical properties of chromium oxide thin films. This research is done at the University of Biskra's Physics of Thin Films and Applications laboratory (LPCMA).

We have characterized our films by different analysis techniques. X-ray Diffraction analysis (XRD) was used to measure structural properties such as the crystalline quality and nature of the layers, the size of the crystallites, the lattice parameters, and the evaluation of the stresses. Scanning electron microscopy (SEM) made it possible to analyze the surfaces and their

morphology and chemical composition by X-ray energy dispersive spectroscopy (EDX). UV-visible spectrophotometer made it possible to discuss the optical characteristics such as: the spectrum of the transmittance, the optical gap energy, the Urbach energy. Finally, the four-point technique was used to measure electrical characteristics such as electrical resistivity.

This thesis is organized into five chapters:

The first chapter gives a definition of P-type transparent conducting oxides (TCOs) and a bibliographic overview of chromium oxide by introducing its structural, optical, and electrical properties and its multiple applications. Summarized some of the various methods used for depositing Cr_2O_3 films in the literature, such as physical vapor deposition (PVD), chemical vapor deposition (CVD), sol gel, and spray pyrolysis. It also contains characterization methods that have been used for optical, electrical, morphological, and crystallographic measurements.

The second chapter presents in the first part a description of the experimental homemade pneumatic spray system (SP) technique employed in this work. The preparation and characterization of chromium oxide (Cr_2O_3) films deposited by pneumatic spray technique on glass substrates with different precursor concentrations using chromium chloride and chromium nitrate ranging from 0.02 to 0.08 M is presented in the second part.

In the third chapter, we studied the effect of substrate temperature on the structural, morphological, optical, and electrical properties of chromium oxide films by carrying out a series from 350 to 550 °C.

Chapter four deals with the influence of indium-doped chromium oxide films prepared by pneumatic spray on glass substrates with different concentrations of indium (0, 2, 4, 6, and 8 wt.%).

Chapter five presents the effects of doping by copper with various concentrations (0, 2, 4, 6, and 8 wt.%) on the structural, morphological, optical, and electrical properties of Cr_2O_3 thin films.

Finally, we provide a general conclusion including the essential results of the characterization of chromium oxide thin films with future outlooks about the results obtained in this thesis.

References

[1] P. Qin *et al.*, "Organic solar cells with p-type amorphous chromium oxide thin film as hole-transporting layer," *Thin Solid Films*, vol. 519, no. 13, pp. 4334–4341, 2011, doi: 10.1016/j.tsf.2011.02.013.

[2] P. Cr, N. T. Photodetector, and C. Applications, "Porous-Spherical Cr_2O_3 -$Cr(OH)_3$ - Polypyrrole/Polypyrrole Nanocomposite Thin-Film Photodetector and Solar Cell Applications," 2023.

[3] P. Makushko *et al.*, "Flexomagnetism and vertically graded Néel temperature of antiferromagnetic Cr_2O_3 thin films," *Nat. Commun.*, vol. 13, no. 1, pp. 1–13, 2022, doi: 10.1038/s41467-022-34233-5.

[4] E. Ahmed and M. Saeed, "Synthesis and characterization of Cr_2O_3 : Al thin films by plasma of R . F . magnetron sputtering for gas sensing application," vol. 10, pp. 4450–4455, 2023.

[5] A. M. Oje, A. A. Ogwu, S. U. Rahman, A. I. Oje, and N. Tsendzughul, "Effect of temperature variation on the corrosion behaviour and semiconducting properties of the passive film formed on chromium oxide coatings exposed to saline solution," *Corros. Sci.*, vol. 154, no. April, pp. 28–35, 2019, doi: 10.1016/j.corsci.2019.04.004.

[6] K. Khojier, H. Savaloni, and N. Z. Dehnavi, "Structural , mechanical and tribological characterization of chromium oxide thin films prepared by post-annealing of Cr thin films," no. November, 2013, doi: 10.1016/j.apsusc.2013.07.123.

[7] T. Ivanova, M. Surtchev, and K. Gesheva, "Characterization of CVD Chromium Oxide Thin Films," vol. 513, no. 2, pp. 507–513, 2001.

[8] S. Punugupati, J. Narayan, and F. Hunte, "Room temperature ferromagnetism in epitaxial Cr_2O_3 thin films grown on r-sapphire," vol. 193907, pp. 1–6, 2015.

[9] A. Zekaik, H. Benhebal, and B. Benrabah, "Synthesis and characterization of Cu doped chromium oxide (Cr_2O_3) thin films," *High Temp. Mater. Process.*, vol. 38, no. 2019, pp. 806–812, 2019, doi: 10.1515/htmp-2019-0037.

[10] V. B. Kamble and A. M. Umarji, "Chromium Oxide thin films by Ultrasonic Nebulized Spray Pyrolysis of Aqueous Combustion Mixture for Gas Sensing Application".

Chapter I: *CHROMIUM OXIDE, PREPARATION, AND CHARACTERIZATION TECHNIQUES*

Introduction

The subsequent chapter gives a definition of P-type transparent conducting oxides (TCOs) and a bibliographic overview of chromium oxide. We will focus on chromium oxide (Cr_2O_3) by introducing its structural, optical, and electrical properties. And present applications of Cr_2O_3.

Various methods have been used in the literature for depositing Cr_2O_3 films, such as physical vapor deposition (PVD), chemical vapor deposition (CVD), sol gel, and spray pyrolysis. In order to determine the optical, electrical, morphological, , and crystallographical characteristics of chromium oxide films, characterization methods, which include X-ray diffraction (XRD), scanning electron microscopy (SEM), spectrophotometry UV -visible, and four-point are used.

I.1. P-type transparent conducting oxides (TCOs)

Transparent conductive oxides, also known as TCOs, exhibit an unusual combination of two characteristics. They have high conductivities and are transparent in the visible spectrum. Research on p-type transparent conductive oxides has considerably increased interest in these materials in order to manufacture transparent electronics based on the production of p-n hetero-junctions. They are needed for a wide range of applications, including solar cells, flat panel displays, touch screening, light-emitting diodes, and transparent electronics[1,2]. But compared to n-type TCOs, p-type TCOs still suffer greatly from lower conductivities and transparencies. In 1993, Sato et al.[3] published the first study on the deposition of p-type TCOs via the synthesis of NiO. The P-type conductivity of the delafossite $CuAlO_2$ was first investigated in 1997 by Kawazoe et al.[4] .The synthesis of highly conductive p-type TCOs is challenging due to their valence band (VB) structure and is shown schematically in **Figure I.1**. Because oxygen has a high electronegativity in p-type semiconductor oxides, oxygen 2p levels produce a strongly confined valence band edge that has a strong ionic character. The high ionicity of these compounds is attributed to the energetic position of the oxygen level, which is situated at energy lower than the valence orbital of the metallic cations. This will result in a large effective mass of the holes, i.e., a flat valence band structure[5–7]. Another factor is the low formation energy of intrinsic donor defects such as cation interstitials or anion vacancies, which act as hole killers [1]. This will result in reduced holes' mobility and, finally, low electrical conductivity. Here, Chromium (III) oxide (Cr_2O_3) is regarded as a potential p-type TCO. Cr_2O_3 has a hexagonal structure with the chromium cations filling up 2/3 of the octahedral sites. Tetrahedrally coordinated oxide ions inside the lattice are helpful

for p-type conductivity because they help minimize the localization of the O 2p electrons to the oxide ions [5, 8, 9]. The conductivity and the optical properties of Cr_2O_3 can be improved dramatically by doping.

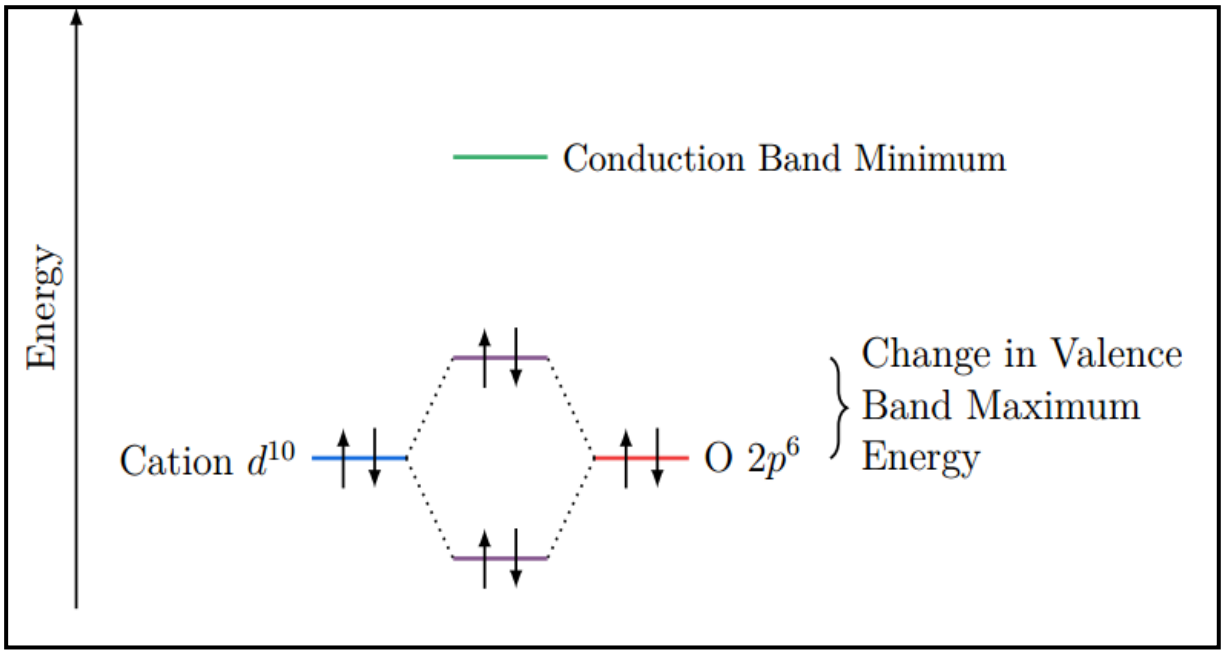

Figure I.1: Chemical bond between a metal cation and an oxygen anion. The top of the valence band has mixed character consisting of the oxygen $2p^6$ and the metal d^{10}. The cation has a closed d^{10} shell, to prevent *d-d* transitions, and thus coloration (visible light absorption) of the material[5].

I.2. Main chromium oxides

Some of the most important chromium oxides' qualities will be recognized in this chapter. Chromium has a variety of oxidation states and oxides, such as CrO, CrO_2, CrO_3, and Cr_2O_3 [10]. As shown in the table I.1. The review will be focused on chromium oxide (Cr_2O_3), the material of interest for this work, because it is a very stable phase of chromium oxide.

Table I.1: *Oxidation state of chromium oxide[10].*

Oxidation state	+3	+4	+6	Intermediate
Cr	Cr_2O_3	CrO_2	CrO_3	Cr_3O_8, Cr_2O_5, Cr_5O_{12}, etc.

I.2.1. Chromium (IV) dioxide (CrO_2)

Chromium dioxide is a highly interesting compound that is metastable at atmospheric pressure, decomposing into Cr_2O_3 when heated and exposed to ambient air [11,12]. It has metallic conductivity and its ferromagnetic properties; (CrO_2) is an important material for applications in magnetic and magnetoelectronic devices. Is the only stoichiometric binary oxide with a Curie temperature of ~ 390 °K that is a ferromagnetic (FM) half metal (spin-polarization, Pn, of ~ 100%) [13]. It exhibits half-metallic behavior with relatively low electrical resistance. Compared to the other half-metal possibilities, it is likewise ferromagnetic at room temperature. These properties of CrO_2 make this material a perfect substance for developing spintronic devices [14]. The first band-structure calculation that identified CrO_2 as a half-metallic ferromagnet was performed by Irkhin and Katsnelson [15].

The structural characterization of chromium oxide was first presented by Michel and Benard in 1943, it has a tetragonal unit cell with a rutile-type structure having the space group P4'/rnnm. Cr^{4+} is bonded to six equivalent O^{2-} atoms to form a mixture of corner and edge-sharing CrO_6 octahedral [11]. The corner-sharing octahedral tilt angles are 50°. The chromium atoms are octahedrally coordinated by oxygen atoms with a small distortion to orthorhombic symmetry. Rutile-type structure of chromium oxide is shown in **figure I.2**. The refined tetragonal cell parameters are a=4.421Å, c=2.916 Å with c/a = 0.6596, and volume = 56.99 $Å^3$.

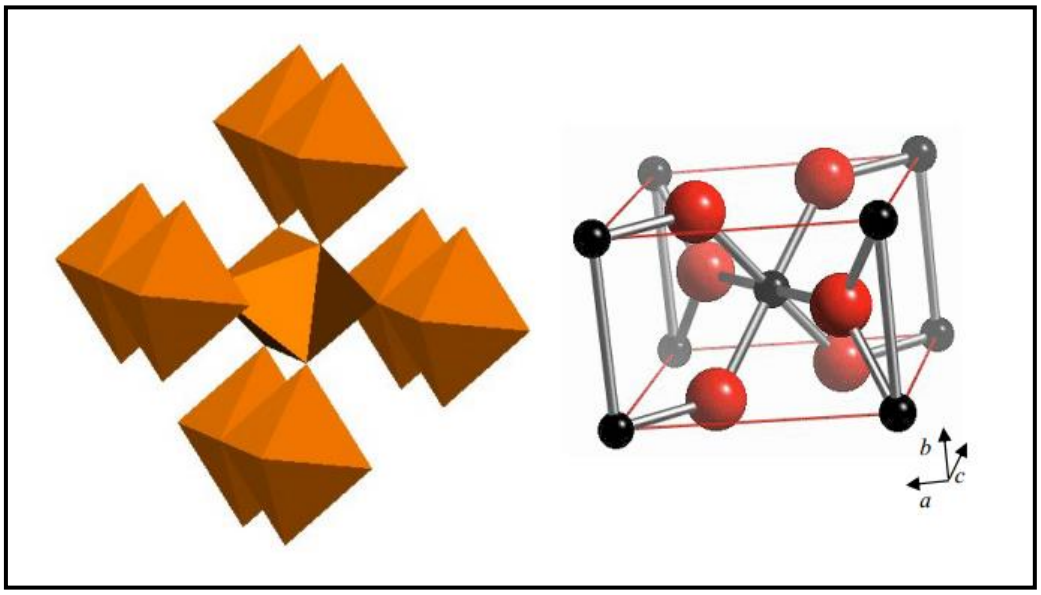

Figure I.2: scheme of the CrO_2 rutile crystal structure detailing the "CrO_6" octahedral arrangement (left panel) and unit cell (right panel) with dark balls representing chromium atoms[11].

CrO_2 is a metastable phase and easily decomposes to Cr_2O_3 even at room temperature. It must often be produced at high oxygen pressures. Therefore, precise tuning and knowledge of the synthesis conditions are required. Under normal growing circumstances, it has been difficult to fabricate high-quality thin films of CrO_2. Therefore, they have utilized a CVD, PVD and molecular beam epitaxy (MBE) techniques to grow high-quality thin films of CrO_2.

I.2.2. Chromium (VI) oxide, CrO_3

CrO_3 is one of the many oxidation states of chromium oxide. It is a powerful oxidizing agent and a strong acid as well when dissolved in water, with a melting point of 197 °C. It decomposes into lower oxidation state chromium oxides like Cr_8O_{21}, Cr_2O_5, CrO_2, and Cr_2O_3 once it reaches the boiling point (250 °C) [10,11]. It has been reported that CrO_3 complexes exhibit antibacterial activity against Pseudomonas Eruginosa Bacteria. CrO_3 is used in various pharmaceutical and chemical industries [16]. Chromium (CrO_3) is important as heterogeneous catalyst, coating material, wear resistance, advanced colorant, pigment and solar energy collector [17].

Bystrom and Wilhelmi (1950), who gathered two-dimensional photographic data, made the first determination of the crystal structure of chromium trioxide.CrO_3 crystal structure is made up of chains of CrO_4 tetrahedral that are linked at the corners by oxygen. The refined Orthorhombic cell parameters are a=4.789 Å, b=8.557 Å, c=5-743 Å with volume = 235.4 $Å^3$ and Space group: C2cm [18].

I.2.3. Chromium (III) oxide, Cr_2O_3

Louis Nicolas Vauquelin discovered chromium in 1797. He isolated chromium (III) oxide (Cr_2O_3) by treating the mineral crocoite ($PbCrO_4$) with hydrochloric acid. He chose the name chromium, from the Greek term chroma meaning color, since all compounds containing chromium are colored. The first applications of chromium compounds were as pigments for dyeing (e.g. wallpaper or wool). Common examples are chrome red ($PbCrO_4$·PbO), green chromium oxide (Cr_2O_3) and chrome yellow ($PbCrO_4$) [19]. Chromium oxide (chromia, Cr_2O_3) is a p-type metal oxide semiconductor (MOS) and the most stable of several oxides of chromium in the under standard conditions (i.e. a temperature below 1600°C and oxygen pressures below 1 atm) [20, 21].

The chromium oxide (Cr_2O_3) contains elemental composition: 68.43% of chromium and 31.57% of oxygen, the theoretical density of Cr_2O_3 is 5.23 g/cm^3 and the molecular weight of 151.99 g/mol. The electronic distribution of the elements is [Ar] $3d^5$ $4s^1$ for the chromium atom [22, 23].

Chromium oxide has many uses due to its physical and chemical properties. With a néel temperature (TN) of 307°K, Cr_2O_3 is antiferromagnetic. Nevertheless, chromia nanoparticles can modify this behavior to weak ferromagnetism and even superparamagnetism [11, 24]. Due to its high melting and boiling points (2330 °C and 3000 °C, respectively), it can be used as a refractory material and because of its extreme hardness of 29.5 GPa, it can be added to materials to make them more resistant to chemicals and heat [23, 25].

I.2.3.1. Structure of chromium oxide Cr_2O_3

According to Kouvo and Vuorelainen, eskolaite (Cr_2O_3) is a naturally occurring mineral that forms iodomorphic crystals, is isostructurally related to corundum and hematite, and occurs naturally in the mineral eskolaite [26]. Chromium (III) oxide has a rhombohedral or hexagonal structure, being the corundum-type crystal structure with space group R3-C [11]. Chromium (III) oxide (Cr_2O_3) consists of a slightly distorted hexagonally packed lattice of oxygen anions, with the chromium cations filling up 2/3 of the octahedral sites. The oxide ions within the lattice are tetrahedrally coordinated [5]. **Figure I.3** represents the conventional hexagonal unit cell, which contains six formula units. The oxygen anions form a pseudo-hexagonal, close-packed structure, with Cr^{3+} cations occupying two-thirds of the octahedral interstices. The structure contains oxygen layers alternated with chromium bilayers along the c-axis of the hexagonal lattice. Each bilayer consists of two perfectly planar triangular lattices whose combined projections build an ideal honeycomb structure with one atom from each sublayer as the two-basis element. A close look at the local environment of Cr^{3+} cations shows that CrO_6 is not a perfect octahedron. The Cr^{3+} cation is displaced (upward in Figure I.3b) along the C_3 axis relative to the octahedral center, making two equilateral triangles formed by three oxygen ions each. Due to a slight rotation of the upper and lower oxygen ion triangles (dotted lines in Figure I.3c), the exact symmetry of the Cr^{3+} cations in Cr_2O_3 is C_3 [27]. The lattice parameters of Cr_2O_3 are a = 4.958 Å and c = 13.594 Å and table I.2 summarizes some of the structural properties of Cr_2O_3.

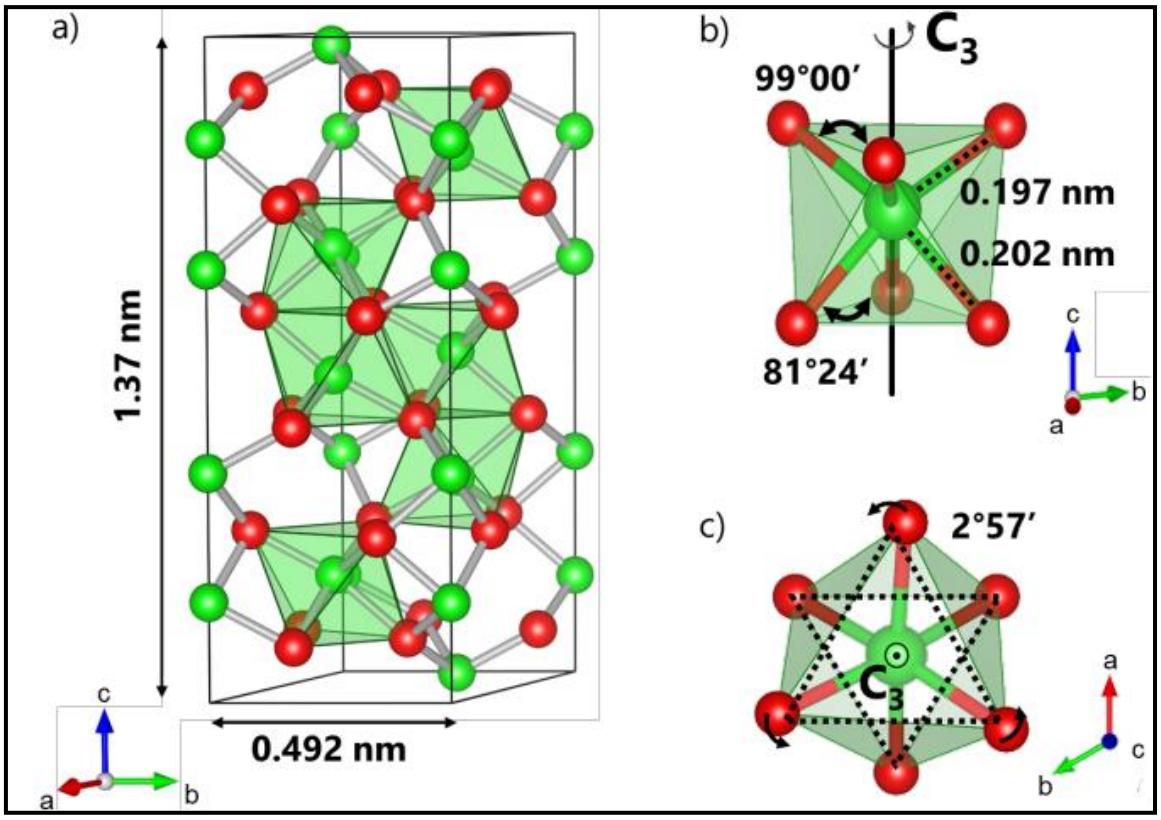

Figure I.3 : (a) Close-packed hexagonal unit cell of Cr_2O_3, where trivalent Cr cations (green) bonded to six oxygen anions (red) form trigonal distorted octahedra. (b) The Cr^{3+} ions lie along the threefold axis with Cr-O bond lengths of 0.197 nm and 0.202 nm, and O–Cr–O angles of 81°24’ and 99°00’. (c) A rotation angle of 2°57’ is observed between the upper and lower oxygen triangles (depicted in black dotted lines) [27].

Table I.2: *structural properties of Cr_2O_3 eskolaite phase.*

Structural	Data	Ref.
Colour	Green	
Space group	R3-C	
Lattice type	Rhombohedral	
z	6	[11]
a_0 (nm)	0.495876	
c_0 (nm)	1.359420	
Molecular mass, M (g mol^{-1})	151.99	
Density, ρ (g cm^{-3})	5.231	

I.2.3.2. Optical and Electrical properties of Cr_2O_3:

Cr_2O_3 is optically transparent due to its large band gap. The energy separating the valence band from the conduction band is known as the band gap (Eg). The solid's chemical make-up and crystalline structure have a significant impact on this gap's value. The Cr_2O_3

band gap is reported to be 3.4 eV. T. Ivanova et al. [28] deposited the chromium films using CVD, and they obtained an optical band gap energy of 2.95 eV for the chromium oxide thin film annealed at 400 °C and 3.2 eV for the film treated at a temperature of 500 °C. Y. PARSA [29] summarized the band gap values for chromium oxide (Cr_2O_3) reported in the literature. The band gap energy was estimated using models or measured using various techniques, as shown in **Figure I.4**. He found that the values of the chromium gap were between 2.6 and 3.8 eV, both for the measured values and for the values estimated by modeling (DFT).

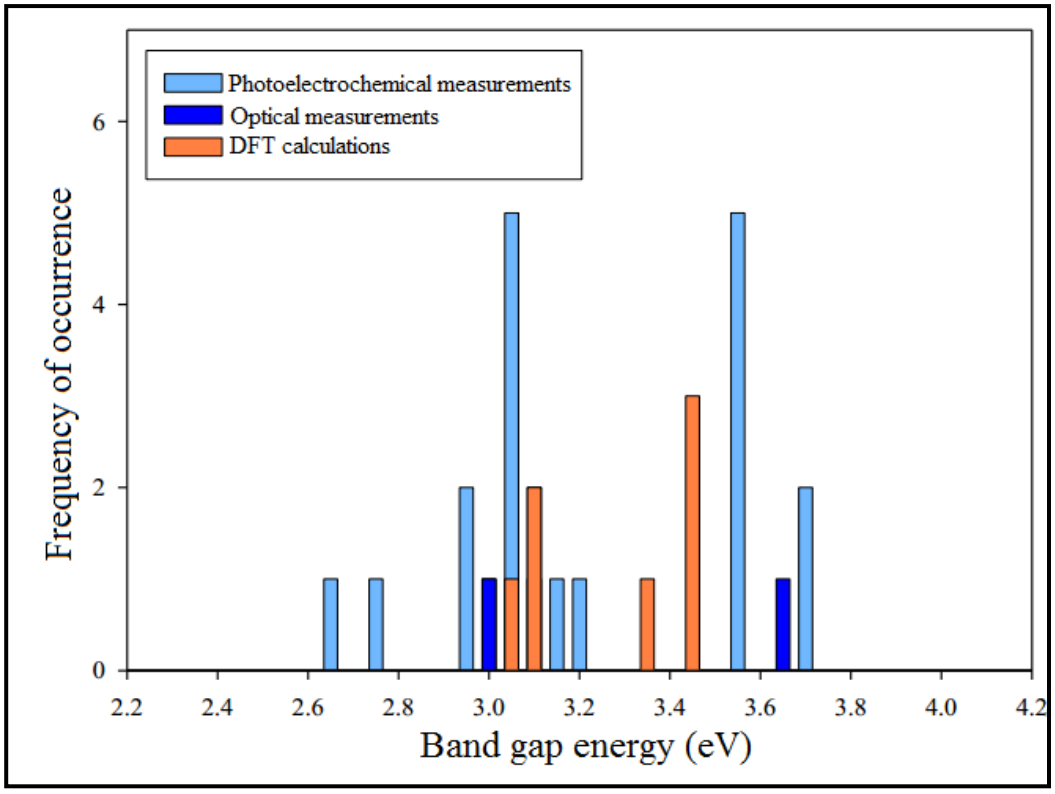

Figure I.4: Summary of chromiun band gap energy values available in the literature [29].

Due to the octahedral field, the Cr 3d states are split into two sub-bands: the triple degenerate t_{2g} and the double degenerate E_g. To fully comprehend the optical and electrical properties of this material, it is imperative to comprehend the energy positions of these two bands and their respective contributions to the valence band maximum and conduction band minimum.

McClure (1963) [30] examined the optical absorption spectra of Cr_2O_3. These spectra are connected to electronic changes in Cr^{3+}-ions' $3d^3$ states [31]. The electronic configuration

of Cr^{3+} ions is [Ar] $3d^3$. In absorption measurements, only two broad absorptions are typically observed, located at 455 and 600 nm, as shown in **Figure I.5** , which are brought about by the d-d transition of Cr^{3+} ions in octahedral sites and are assigned to $^4A_{2g} \rightarrow {}^4T_{1g}$ at the higher energy region and $^4A_{2g} \rightarrow {}^4T_{2g}$ at the lower energy region, respectively [19, 32, 33].

The octahedral coordination of the Cr ions (with $3d^3$ configuration) splits these d levels into the t_{2g} and E_g levels, with the t_{2g} being occupied and the Eg unoccupied. This gives rise to transitions that are dipole forbidden but quadruple allowed at the typical energies of 2.1 and 2.7 eV, respectively. Even though these weak transitions give the material a slight green color, it remains highly transparent throughout the visible spectrum in thin film form [5].

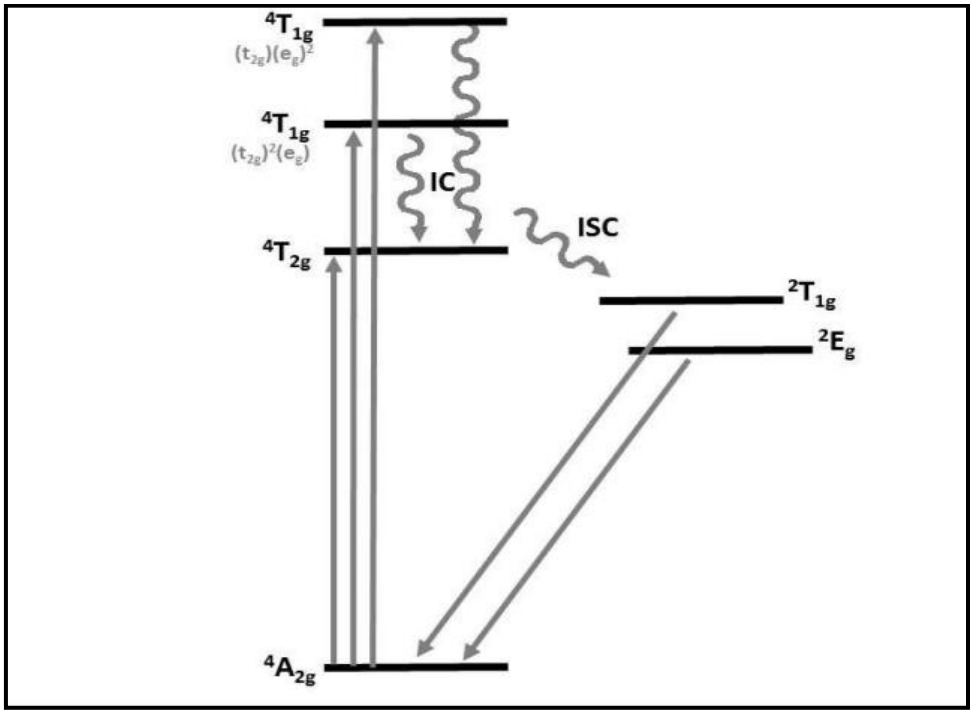

Figure I.5: Energy level diagram for chromium(III) complexes, where IC stands for internal conversion and ISC for intersystem crossing.

From an electrical point of view, chromium oxide is an insulator in its stoichiometric form, often reported to show native yet very poor p-type conductivity [5, 29].

Chromium oxide (Cr_2O_3) has attracted a lot of attention as a p-type TCO. However, its poor conductivity led to the use of dopants like Li, Ca, Zn, and Mg to enhance its electrical characteristics. Li and Ca doping only results in insulating properties [1]. On the other hand,

doping with magnesium has been dramatically improved the conductivity of Cr_2O_3 to values approaching 0.1 S cm^{-1} [34].

Chromium oxide's electrical conductivity and thermoelectric power were measured by Young et al. [35] between 1000 and 1800 °K. According to the measurements, Cr_2O_3 is an n-type semiconductor at low oxygen partial pressures and changes to a p-type semiconductor at high oxygen partial pressures. At temperatures exceeding 1200 °K, the change from n- to p-type occurs rather quickly and at a significant pace. Surprisingly, the change from p- to n-type does not occur with a continuously decreasing oxygen partial pressure. Only at temperatures above 1770 °K is the reverse p-to-n shift visible. The authors proposed that point defects of the interstitial type of chromium, which explain why the oxide has an n-type character at low partial pressure, and point defects of the lacuna type of chromium, which explain why the oxide has a p-type character at high partial pressure, are present in the oxide [36].

I.3. Applications of Cr_2O_3 films

There are many current and potential uses for chromium oxide, making it an intriguing oxide. In various areas of science, technology, and industry, it has been stated that Cr_2O_3 film is frequently employed, such as the fields of corrosion protection, wear resistance [37, 38], gas sensor [39], rechargeable lithium ion batteries [40] and optical applications which include electrochromic coatings and infrared (IR) transmitting coatings [41].

I.3.1. Gas Sensors applications

Continuous attempts are being made to create gas sensors in response to growing worries about chemical control and environmental pollution. Applications of chromium oxide in gas sensors have attracted much attention. Gases of interest include CO, H_2S, NH_3, and Cl_2.Various research reports on Cr_2O_3 thin film-based gas sensors have been reported.
Investigations on the conductometric gas sensing properties of Cr_2O_3 thin films for a variety of gases (CH_4, CO, NO_2, Cl_2, NH_3, and H_2S) as a function of operating temperature (between 30 and 300 °C) and gas concentration (1–30 ppm). At an operational temperature of 100 °C, we have discovered that Cr_2O_3 films are particularly sensitive to H_2S, while at a temperature of 220 °C, the films become selective to Cl_2 [39].

Thin films of Cr_2O_3:Al nanostructures have been created using the radio frequency (RF) magnetron sputtering process as a gas sensor for nitric oxide (NO_2). The best sample had a sensitivity of 32% at 200 °C, response times of under 15 s, and recovery times of 77 S [42].

The as-grown Cr_2O_3 structure is a suitable material for a hydrogen gas sensor. Gas sensor measurement of chromium oxide thin film grown with the magnetron RF sputter

technique was made separately before and after annealing. while the as-grown Cr_2O_3 structure in gas sensor measurements reacted to hydrogen gas at 200 °C and 300 °C [43].

The gas sensing properties of Cr_2O_3 thin films deposited by the ultrasonic nebulized spray pyrolysis are investigated in the temperature range of 200–375 °C for ethanol. The gas sensing studies reveal that the films show p-type conductivity and exhibit a fairly good sensor response when exposed to reducing gases like ethanol, n-hexane, benzene, ammonia and acetone; however the films were found to show a high relative response towards ethanol at 350 °C [44].

I.3.2. Solar cell applications

There have been many works done by others in the literature that describe the role of chromium oxide thin film on the performance of solar cells. Jae-Kwan Sim et al.[45], reported an reveals that the Cr_2O_3 layer formed on the surface of STS substrate by thermal oxidation process for 1 min at 600 ˚C in oxygen atmosphere plays an important role in increasing the performance of CIGS solar cells. It was found that the Cr_2O_3 thin layer was an effective diffusion barrier to reduce impurity diffusion into the CIGS layer. A device efficiency of 10.6% enhanced about 81% was achieved for flexible CIGS solar cell with the nanoscale Cr_2O_3 diffusion barrier layer.

Pingli Qin et al. reported organic solar cells with a p-type amorphous chromium oxide thin film as the hole-transporting layer. They demonstrate that 473 °K deposition temperature, $f(O_2)$ = 40%, and 10 nm thickness of the amorphous chromium oxide (ACO) layer are the best parameters for cell performance, and power conversion efficiency up to 3.28% on FTO has been achieved. Amorphous chromium oxide (ACO) layers are a great opportunity for large-area OSC fabrication [46].

I.4. Doped Cr_2O_3 thin films

Doping is a very important approach for Cr_2O_3 thin films to improve their properties. Numerous studies on the effect of doping on chromium oxide thin films utilized in a variety of applications have been published by numerous thin film deposition methods. As summarized in table I.3.

Table I.3: *Different types of dopant in chromium oxide thin films.*

Doping	**Technique**	**Substrate ST (°C)**	**Thickness**	**Transmittance Eg (eV)**	**Applications**	**Year / Ref**
Cu	spray pyrolysis	soda lime glass 400°C	/	/	antibacterial activity in dark-UV light	2023 [47]
Ni	pulsed laser deposition	sapphire substrate 500°C	/	2.9-3.1 eV	photoresponse	2021 [48]
Zn	PLD	glass substrate	/	Transmission decreased 2.78 to 2.50	NH_3 Gas Sensor	2021 [49]
Ti	PLD	glass substrates at room temperature	200nm	2.68 to 2.55 eV	NO_2 Gas Sensor	2020 [50]
Ni	pulsed laser deposition (PLD)	sapphire substrates 500°C	74 ± 2 nm	77–81% 3.64 to 3.48 eV	p-type TCO	2020 [1]
Al or Ir	radiofrequency (RF) magnetron sputtering system	a substrate temperature of 773 °K	/	/	the antiferromagnetic anisotropy KAF	2020 [51]
Cu	sol–gel dip-coating	glass substrate 400°C	/	98% to 90% 2.94-2.51 eV	/	2019 [52]

Ni	sol–gel dip-coating	glass substrate 400°C	/	more than90% 2.94-2.51 eV	/	2018 [53]
Cs	spray pyrolysis	glass substrate at temperature of 350°C	/	3.38-2.98 eV	Photocatalytic Degradation of Methylene Blue Dye under UV-Sunlight Irradiation	2017 [54]
Mg	electron-beam evaporation	c-plane sapphire	20 to 150 nm	/	/	2015 [34]
I	chemical spray pyrolysis	substrate temperature s(773°K) on glass substrate	2000 +20A˚	3.3-3.14 eV	/	2012 [55]
Mg-N	spray pyrolysis	glass substrates	150 nm	up to 65%	/	2011 [56]

I.5. Some methods of depositing Cr_2O_3 thin films

I.5.1. Physical vapor deposition (PVD)

The atomistic deposition technique known as PVD involves the physical discharge of atoms or molecules, followed by their condensation and nucleation onto a substrate in a vacuum, low pressure gaseous, or plasma environment. Sputtering, vacuum or thermal evaporation and PLD are the fundamental PVD processes.

I.5.1.1. Sputtering

Many researchers have studied the chromium oxide thin films using the RF reactive magnetron sputtering technique. A.M. Oje et al. [57] reported that RF powers have played a vital role in the formation of Cr_2O_3 rich films. The results show that the thin films are hydrophilic and optical transmittance decreases with an increase in RF power. The resistivity values varied from 0.061 Ω cm to 0.152 Ω cm. In addition, Cr_2O_3 films are formed after it anneals at 500 °C for 4 hours. The average roughness decreased from 8.22 nm to 6.97 nm,

and the grain sizes decreased from 131.78 nm to 95.63 nm, according to AFM data. After annealing, the Urbach energy drops from 1 eV to 666 meV [58].

K. Khojier et al. [59] addressed the structural, mechanical, and tribological properties of chromium oxide thin films annealed at different temperatures (200–600 C) by DC magnetron sputtering technique and then post-annealed at different temperatures (200–600 C). When the samples were annealed at 200°C and 300°C, the XRD patterns revealed Cr_3O structure, and when the samples were annealed at 500°C and 600 °C, they revealed Cr_2O_3 structure. According to the findings, this approach was effective for creating Cr_3O phases with higher hardness, lower scratch volumes, and higher values for friction coefficients, not Cr_2O_3.
Chromium oxide thin films (Cr_20_3) deposited by magnetron sputtering an optimal operating point is at temperatures above 300 °C, where the films consist of pure Cr_20_3 [60].

I.5.1.2. Thermal (or vacuum) evaporation

Lanping Zhang et al. [61] have prepared chromium oxide films by Cr vapor deposition on Pt (111) with different thicknesses. Structure observed of metastable Cr_2O_3. At higher coverage, formation of the stable Cr203 phase occurs.
Jul karnain et al. [62] have studied the effect of temperature on chromium oxide (Cr_2O_3) thin films using thermal evaporation. Amorphous Cr_2O_3 thin films have been discovered through X-ray diffraction (XRD) research, and the electrical conductivity shows a semiconducting behavior and a positive sign exhibiting P-type carriers.

Chromium oxide films were prepared on MgO (001) substrate at 300°C with different thicknesses. The XPS measurement suggests that the surfaces of all samples contain Cr_2O_3 and the transmittance ranges from 5% to 40%; this difference has been attributed to the different thickness [63].

I.5.1.3. PLD

A thin Cr_2O_3 deposit on a glass substrate was created using pulsed laser deposition with annealing temperatures of 300, 400, and 500 ^{O}C and the thickness was 160 nm. The NO_2 gas sensitivity of Cr_2O_3 films is low at room temperature and increases with temperature. All of the films are P type, according to the Hall measurement [64].

A Cr_2O_3 thin film with a preferred orientation along the (006) plane has been obtained by using the pulsed laser deposition technique on a sapphire substrate. The transmittance was recorded at 70% in the range of 200–800 nm with optical band gap energy of 3.24 eV, and the electrical resistivity was found to be 11.52 kΩ-cm [65].

S. Punugupati et al. report on the ferromagnetism of Cr_2O_3 thin films using pulsed laser deposition. The films are epitaxially grown on sapphire substrates, and there is no secondary

phase formation in the films, according to the XRD and TEM data. As-deposited films exhibit ferromagnetic behavior up to 400 K; however, ferromagnetism almost completely disappears following oxygen annealing [66].

A few-layer graphene (FLG) on nickel (Ni) substrate was coated with a Cr_2O_3 nanostructured thin film using a pulsed laser deposition process for usage as an anode material for lithium-ion batteries. The Cr_2O_3 deposit on FLG enhanced the electrochemical property, and the initial discharge capacity was improved to 1234.5 mA h g^{-1}. The reversible lithium storage capacity of the as-grown material is 692.2 mA h g^{-1} after 100 cycles [67].

I.5.2. Chemical Vapor Deposition (CVD)

The CVD process creates materials in the form of thin layers by using gaseous precursors that chemically react to generate these layers on a heated substrate. The different activation methods use heat, plasma, or light, and their respective CVD processes are denoted as HFCVD (or TACVD), PECVD, and LACVD [68, 69].

Electrical energy is employed in the PECVD method to start homogenous reactions in the gas phase. Weixin Yu et al. [70] reported that Chromium oxide coating is applied to alumina ceramics using atmospheric-pressure plasma enhanced chemical vapor deposition (AP-PECVD) to increase its flashover voltage in vacuum. The experimental results show that the surface flashover voltages are increased by 20% and 26% after the PECVD at atmospheric and subatmospheric pressures, respectively. Therefore, the deposition of chromium oxide films can effectively inhibit the surface charge accumulation and improve the surface flashover voltage in vacuum by reducing the trap energy level and its density. The results obtained by Jing Liang et al. [71] indicate that Cr_2O_3, can be easily prepared by PSE-CVD and is an active catalyst in the oxidation of C_3H_6. Jinwen Wang et al.[72], made a deposit of chromium oxide (Cr_2O_3) thin films by plasma-enhanced chemical vapor deposition on c-cut sapphire (Al_2O_3).

A concentrated laser beam will directly activate the source gas in the LACVD process. Sousa et al. [38] have reported on the growth of Cr_2O_3 onto sapphire substrates by low-pressure photolytic LCVD, using UV laser radiation and $Cr(CO)_6$ as well Ruihua Cheng et al. [73] obtained both Cr_2O_3 and CrO_2 in the film by using laser-initiated chemical vapor deposition through the oxidation of $Cr(CO)_6$ in an oxygen environment.

Or change the nature of the precursors by using the MOCVD process, which produces films from metal-organic precursors. Metal-organic MOCVD was used to develop thin chromium (Cr_2O_3) films for anti-wear protection on AISI 304 stainless steel, soda-lime glass, and (001) silicon substrates. All three substrates and all three precursors were crystalline films

with hexagonal Cr_2O_3 eskalonite structures. Carta et al. [74]. Yuneng Chang et al. [75] discussed the polycrystalline or amorphous chromium oxide (Cr_2O_3) thin films deposit MOCVD, where Oxygen concentration in gas phase is the key factor determining chromia film structure.

I.5.3. Sol gel

The sol-gel process is to the production of homogeneous materials in the form of thin layers. Which involves gel formation as one of its stages of processing. A network of oxides called "the gel" is created during a sol-gel synthesis by the molecular precursors present in the starting solution, or "the sol," through a variety of methods. Thin-film deposition can be achieved by different sol gel methods, namely dip-coating and spin-coating [73–75].

M.G. Tsegay et al. [79] have reported that Cr_2O_3 spectrally selective solar absorber nanocoatings were deposited by using drop and spin coatings at different rotational speeds on polished copper (Cu) substrates. The crystal structure showed a Cr_2O_3 crystalline phase. The existence of Cr_2O_3 on Cu substrates was demonstrated by EDS, Raman, and XPS spectroscopy. For the samples that were drop-coated and spin-coated at 600 rpm, the optical properties of the Cr_2O_3 showed a high solar absorptance value of 0.93 and a high thermal emittance of 0.23. These properties indicate that Cr_2O_3 nanocoatings are a potential candidate for selective solar absorber applications.

A. Zekaik et al. [80] discussed the effect of Cu doping on chromium oxide (Cr_2O_3) deposited by sol-gel dip coating method on glass substrates. According to XRD measurements, the crystallite size decreases as the amount of Cu doping increases, and the phase was Cr_2O_3. The UV-Vis spectra of the films showed improvement of transparency in the visible region with optical band gap shift from 2.94 to 2.51 eV.

H. R. Abedi et al. [81], studied the effect of surface roughness and the Cr_2O_3 oxide layer created by dip caoting on the absorptivity and formability of the samples in the laser-forming (LF) process with a ytterbium fiber laser beam. By increasing the surface roughness from Ra = 0.04 µm to Ra = 1.9 µm, light absorption was nearly doubled, the laser beam absorption coefficient was enhanced from 38% to 90%, and the created bending angle was increased from 3.43 to 7.43. In addition, the Cr_2O_3 layer up to 6 um led to an increase in the laser beam absorption from 38% to 70%, and the bending angle was increased from 3.43 to 5.1°. The optimal parameters include those that could enhance laser light absorption and bending angle for a surface roughness of 1.9 µm and an oxide layer thickness of about 1.7 µm.

A Cr_2O_3 electron-selective material for high-effective perovskite solar cells is synthesized by spin-coating on FTO substrates. The spin-coating speed is optimized for high

optical transmittance and superb electron extraction and carrier transport properties. The planar hybrid PSC based on the optimal Cr_2O_3 ESL achieves a power conversion efficiency of 16.23% [82].

I.5.4. Spray pyrolysis system

Chamberlin and Skarman first introduced the spray technique in 1963 [83]. Spray pyrolysis is a very simple and relatively cost-effective method to prepare dense and porous oxide films. The term "pyrolysis" refers to the breakdown of chemical compounds or solutions caused by extremely high temperatures acting on them. The word "pyrolysis" actually derives from "pyro" for "heat" and "lysis" for "breaking". In this method, a precursor solution is atomized and thrown over the heated substrate where the film will be created [81, 82].

An atomizer, a solution precursor, a heated substrate, and a temperature controller are the typical pieces of equipment utilized in the pyrolysis spray. **Figure I.6** shows the schematic of spray pyrolysis process. In general, some atomizers used for thin film preparations to produce a spray jet fall are given below [86]:

a) Ultrasonic nebulized atomization

The precursor solution is converted into uniformly distributed micrometer and submicrometer-sized droplets by the ultrasonic nebulizer (the ultrasonic power of the mist generator is about 100 W), which is operated at a frequency of 2.56 MHz. The vapor generated is transported by the carrier gas, air, through a pipe to the heated substrate, leading to the formation of thin solid films.

b) pneumatic spray atomization

In this case, it is the effect of the pressure of the carrier gas which causes the liquid to be sprayed into fine droplets.

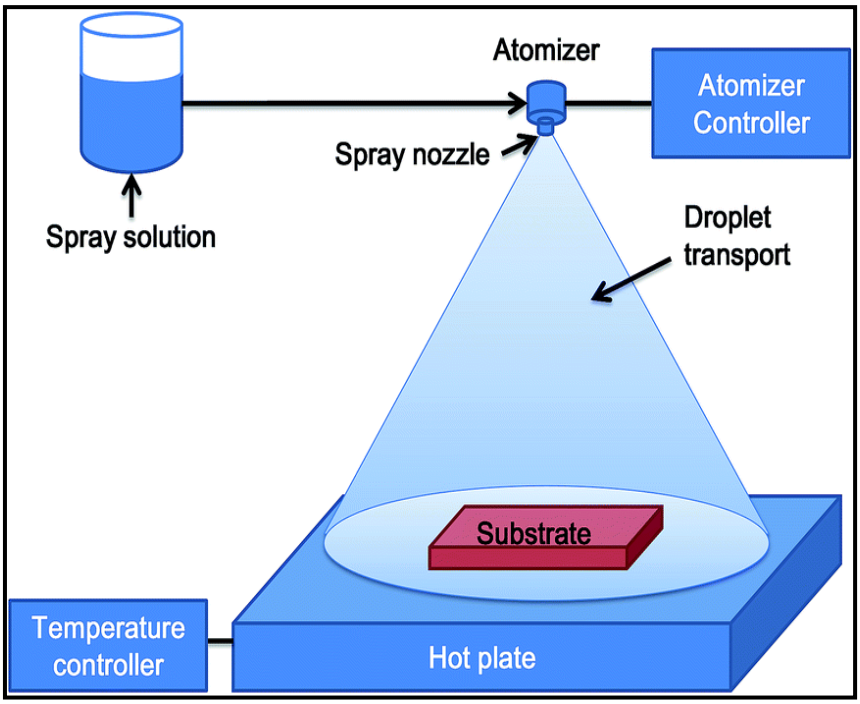

Figure I.6: Illustration of the spray system [87].

The spray pyrolysis method makes use of a variety of solvents. As metal-oxide precursors, typically, nitrates, chlorides, and acetates, which may be dissolved in aqueous and alcoholic solvents, are utilized. Depending on the nature, cost-effectiveness, and solubility of the solution precursors, transforming liquid precursor or solution of precursor in to micro sized droplets. Making solvent to evaporate is based on the type of atomizers employed in the system. The atomization technique frequently affects the size of the aerosol droplet. There are three main atomization methods: electrostatic, air blast, and ultrasonic, which are called electrostatic spray deposition, pressurized spray pyrolysis, and ultrasonic or normal spray pyrolysis (SP), respectively. The spray of the precursor solution is sprayed onto a heated substrate. When the spray collides with a surface, the atoms lose energy. After the impact, the atoms spread on the surface, interacting with other adsorbed atoms. A fraction of the atoms can initiate the formation of an island that can grow in size and coalesce, forming a continuous film [85, 86].

Vinayak B. Kamble et al. [90], deposited Cr_2O_3 thin film-based chemiresistive-type gas sensors by ultrasonic nebulized spray pyrolysis. The films deposited on glass were polycrystalline with nano-sized grains and highly porous. The films exhibit strong ethanol

sensitivity and a nearly linear response at temperatures that are approximately 75 °C below the typical chromium oxide ethanol-detecting temperature.

Spray pyrolysis was used to develop Cr_2O_3 thin films onto a glass substrate at a temperature of 450°C.The as-prepared film was annealed at a temperature 550 °C. Transmittance demonstrate that as the annealing temperature is raised to 550 °C, the optical constants of Cr_2O_3 films increase and the absorption edge experiences a red shift. The optical energy gap decreased from 3.08 to 2.95 eV [91] .

Amir F. Dawood et al. [92], used a chemical spray pyrolysis process at 400 °C to create chrome oxide (Cr_2O_3) thin films of varying thickness. The optical properties such as transmission, reflectance, refractive index, extinction coefficient, energy gap (5.862, 3.75 eV for 1350 and 1600, respectively), and dielectric constant in real and imagery parts, all as a function of the wavelength, decrease with increasing thickness except the absorbance.

Thin films Cu-doped Cr_2O_3 thin films were prepared using the spray pyrolysis technique on a pre-heated (400 °C) soda lime glass substrate. The films' polycrystalline nature and rhombohedral structure were confirmed by XRD investigation. The crystallite size decreases while lattice strain increases with an increase in the Cu/Cr ratio. The films' ability to inhibit the growth of two gram-positive (Bacillus subtilus and Bacillus meurellus) and two gram-negative (Escherichia coli and Acetobacter rhizopherensis) bacteria was examined. Antibacterial activity was significantly enhanced with the increase in the Cu/Cr ratio. Interestingly, the UVA light further enhanced the antibacterial effect against both types of bacteria [47].

I.6. Characterization techniques

I.6.1. Thickness measurements

The thickness of the deposited films was calculated with the help of a weight difference method using an electronic high-precision balance. Measure the mass of the film before and after the deposition process; the difference will give the mass of the film (m), and the film thickness d is determined as follows:

$$t = \frac{m}{\rho A} \qquad \textbf{(I.1)}$$

ρ: is the density of the film material.
A: is the area of the film.

I.6.2. X-ray diffraction (XRD)

The crystal structure of the obtained thin films was investigated by a Rigaku-Type MiniFlex600 diffractometer (LPCMA-University of Biskra) in the 2θ range of 20-80° with a

CuKα radiation, which has a wavelength of 1.541838 °A, with an accelerating voltage of 40 kV, and a current of 30 mA.

X-ray diffraction is a powerful technique for material characterization in order to examine and characterize the placement of atoms, their arrangement within each unit cell, and the distance between the atomic planes. The X-ray diffraction by periodic atomic planes and the angle- or energy-resolved detection of the diffracted signal are the foundation of the approaches. W.L. Bragg (Bragg, 1913) provided a geometrical explanation for the XRD phenomena (constructive interferences). Details about the geometrical prerequisites for diffraction are provided in **Figure I.7** [90, 91].

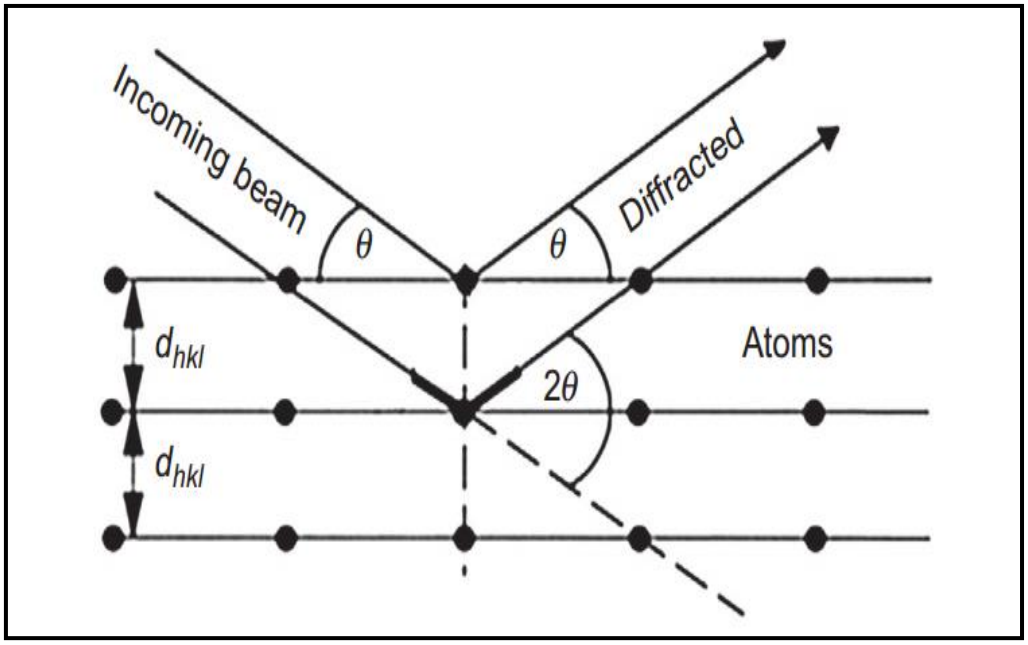

Figure I.7: Geometrical condition for diffraction from lattice planes [93].

The reflection according to the following Bragg's law:

$$2dsin\theta = n\lambda \qquad \textbf{(I.2)}$$

Where,

d: the distance between crystal planes.

θ: the incident angle of X-ray

λ: the wavelength of the X-ray

n: a positive integer.

X-ray diffraction having wide applications within major domains such as phase identification, crystal structure and size, crystallographic orientation, dislocation density, residual stress/strain.

- **Crystallite Size and Microstrain**

The diffraction spectra were used to determine the size of the crystallites in each sample the crystallite size of the Cr_2O_3 films were calculated from the peaks with the highest intensity by using Debye Scherrer's formula [95]:

$$\boldsymbol{D = \frac{0{,}9\lambda}{\beta\cos\theta}} \qquad \textbf{(I.3)}$$

Where:

λ: the applied X-ray wavelength (0.15418 nm for Cu Kα radiation).

θ:the diffraction peak angle.

β:the full-width at half-maximum (FWHM) in radian.

The strain is a macroscopic measure of deformation. The micro strain (ε) is calculated using the relation:

$$\boldsymbol{\varepsilon = \frac{\beta\cos\theta}{4}} \qquad \textbf{(I.4)}$$

I.6.3. Scanning electron microscopy (SEM) and Energy Dispersive Spectroscopy (EDS)

The morphology and compositional observations of the surfaces of the material, elemental analysis of specimen can be studied with a scanning electron microscope (SEM).

There are many signals that can be employed to provide details about properties at and near a specimen's surface through the interaction of the electrons with the specimens.

The specimen's atoms will be affected by elastic and inelastic scattering when the incident electron beam strikes the surface of the specimen. Incident electron undergoes elastic scattering. After the interaction, the electron continues on its course without losing kinetic energy (or the energy loss is insignificant) is called a "backscattered electron." Help to resolve topographical contrast and atomic number contrast with a resolution of >1 micron. The electrons scattered under angles larger than 90° are very useful. Secondary electrons are a result of the inelastic collision and scattering of incident electrons with specimen electrons, where the incident electron loses part of its kinetic energy and can activate other electrons or excite atoms of the specimen. They are generally characterized by possessing energies of less than 50 eV. They are used to reveal the surface structure of a material with a resolution of ~10 nm or better [93, 94]. A few interactions are shown in **Figure I.8**.

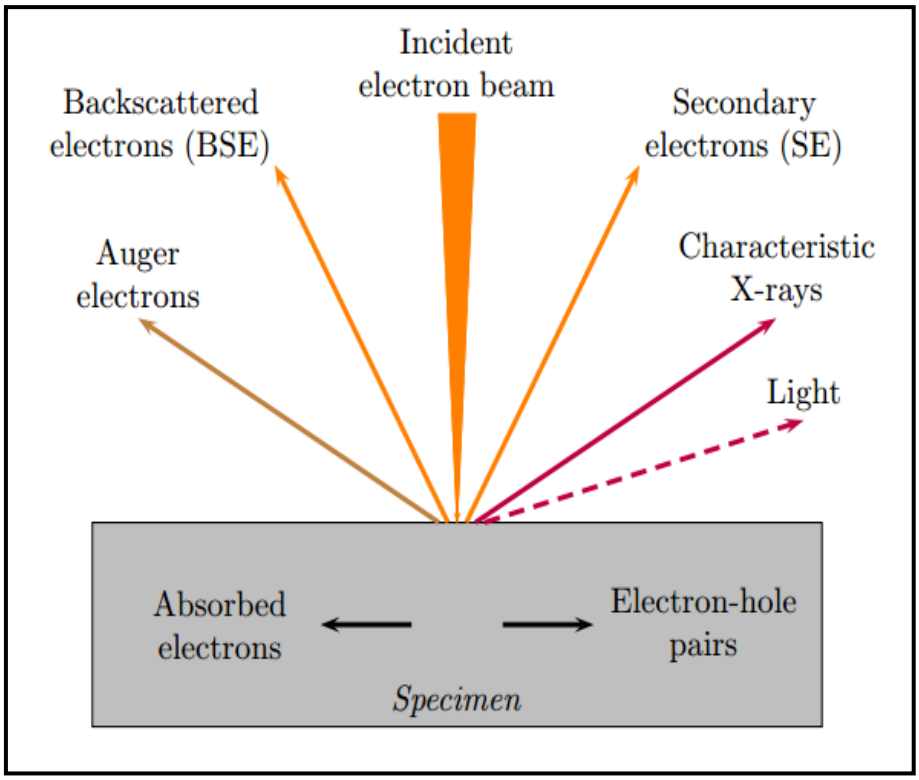

Figure I.8: The electron interaction with the sample [96].

EDS represented is the one of extensively employed approach to examine the elemental analysis and chemical characterization in the sample by considering the consideration of interaction between X-ray excitation and the sample [98]. Its characterization capabilities are due in large part to the fundamental principle that each element has a unique atomic structure allowing x-rays that are characteristic of an element's atomic structure to be identified uniquely from each other [99]. The peak positions are predicted by the Moseley's law with higher accuracy than experimental resolution of a typical EDS instrument. To stimulate the emission of characteristic X-rays from a sample, the electrons beam is focused into the sample being analyzed. In the ground state of an atom within the sample, an electron in an inner shell may excited by the he incident beam, ejecting it from the shell while creating an electron hole where the electron was. The hole was filled by an outer, higher-energy shell then fills the hole, and X-ray will be able to produce by the difference in energy between the higher-energy shell and the lower energy. The number and energy of the X-rays emitted from a sample will be measured by an energy dispersive spectrometer. Since the X-rays energies are characteristic of the difference in energy between the two shells and of the atomic structure of the emitting element, EDS allows the elemental composition of the sample to be measured [100].

I.6.4. UV-Visible spectroscopy

Ultraviolet and visible (UV-Vis) absorption spectroscopy is the measurement of the attenuation of a beam of light after it passes through a sample or after reflection from a sample surface [101].

When radiation interacts with matter, a number of processes can occur, including reflection, scattering, absorbance, fluorescence/phosphorescence (absorption and reemission), and photochemical reaction (absorbance and bond breaking) [102].

Optical transmission measurements are used to evaluate and test certain optical constants of materials that are critical for system fabrication and analysis. Among these optical constants: the absorption coefficients, the band gap energy, dielectric index, refractive index and and Urbach energy, it can also provide information on the thickness of the sample. The most common type of spectrophotometer is a double beam one as shown in **Figure I.9**. A spectrum of monochromatic wavelengths is continuously shone into a sample during a transmission measurement, and the emitted light is regularly measured as a function of the incident wavelength. A transmission spectrum is generated by plotting the relative intensity of the transmitted light to the incident light as a function of the wavelength, y application of the Beer-Lambert law [103].

$$\mathbf{T = T_0 e^{-\alpha t}} \qquad \textbf{(I.5)}$$

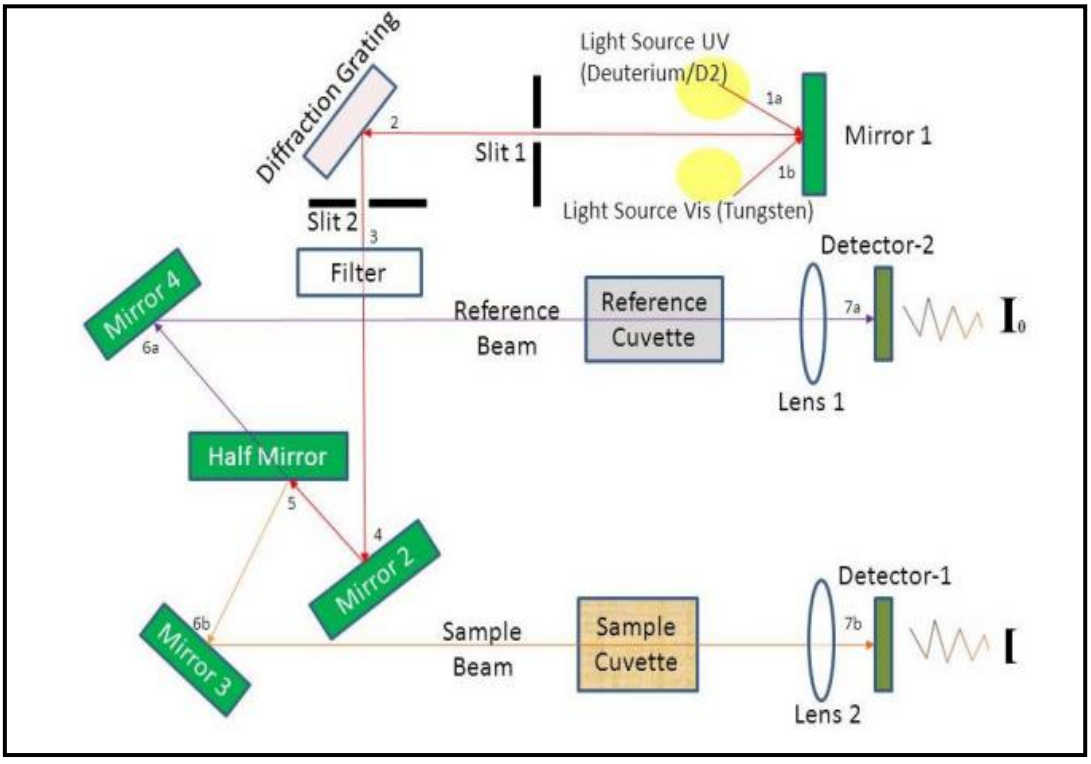

Figure I.9: Basic Double-beam UV-Vis spectrophotometer set-up [103].

a) Optical band gap (E_g)

The band gap energy corresponds to the excitation of an electron from the valance band to the conduction band. The optical gap energy of thin films is determined according to Tauc formula [95]:

$$(\alpha h\vartheta)^2 = A(h\vartheta - E_g) \qquad \textbf{(I.6)}$$

α: the absorption coefficient.

A: a constant (independent of photon energy ($h\vartheta$)).

h: the Planck constant.

E_g: the optical band gap.

E_g are determined by plotting $(\alpha h\upsilon)^2$ versus ($h\upsilon$) and extrapolating of the linear region of the plot to zero absorption ($(h\upsilon)^2 = 0$) as shown in **Figure I.10**.

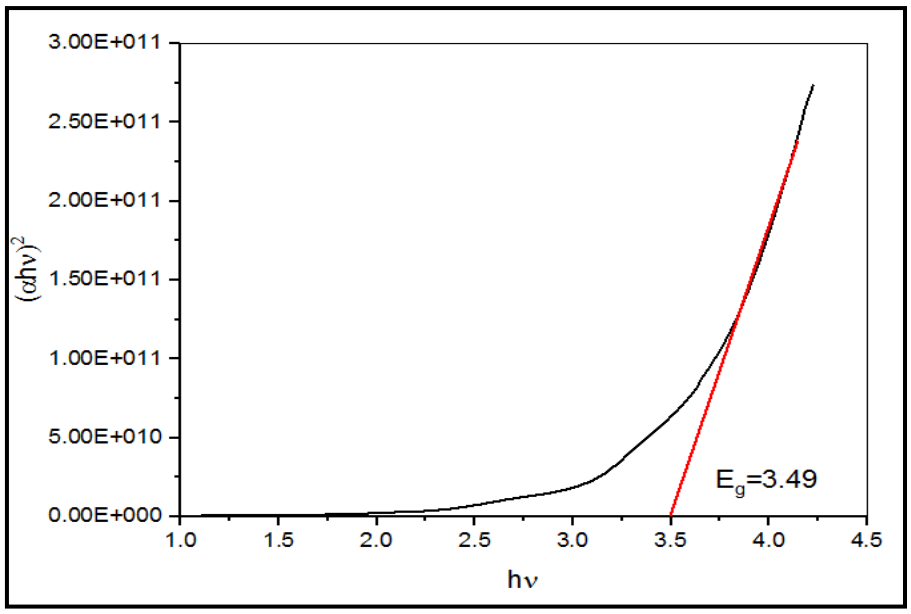

Figure I.10: Determination of the band gap (Eg) for the film Cr_2O_3.

b) Urbach energy (E_u)

Urbach energy (E_u) is used to determine the level of structural disorder existing in the film, which can be obtained using:

$$\alpha = \alpha_0 \exp\left(\frac{h\vartheta}{E_U}\right) \qquad \textbf{(I.7)}$$

The Urbach energy (E_u) can be estimated from the inverse slope of the linear plot between ln(α) and hυ as shown in **Figure I.11**.

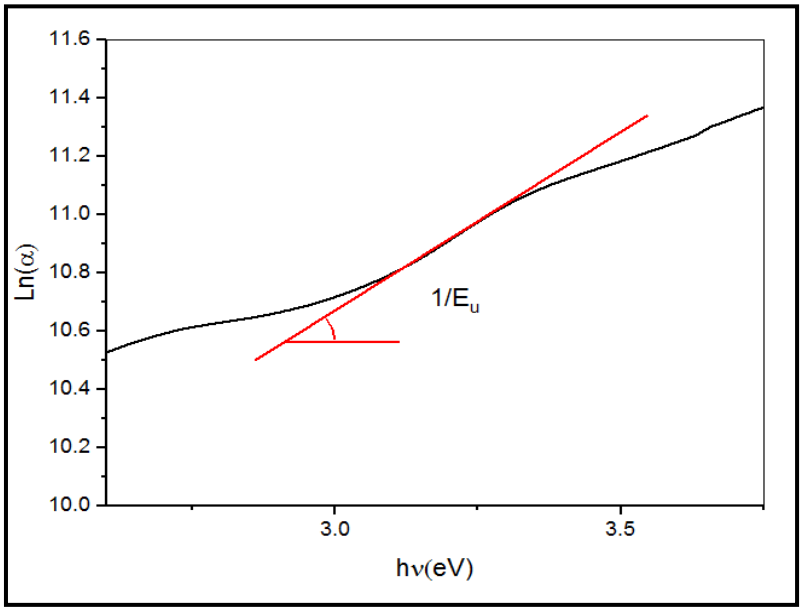

Figure I.11: Determination of Urbach energy (E_u).

I.6.5. Four point probe method

Four point probe method is used to check a material's electric properties. Due to the four points equally spaced that touched the sample surface, it is known as a four-point probe.

A constant electric current is streamed along the sample through two outermost probes. The voltage change is measured through two inner probes. These values of sourced current and measured voltage are used to determine the sample resistivity [101–103], as shown in **figure I.12**.

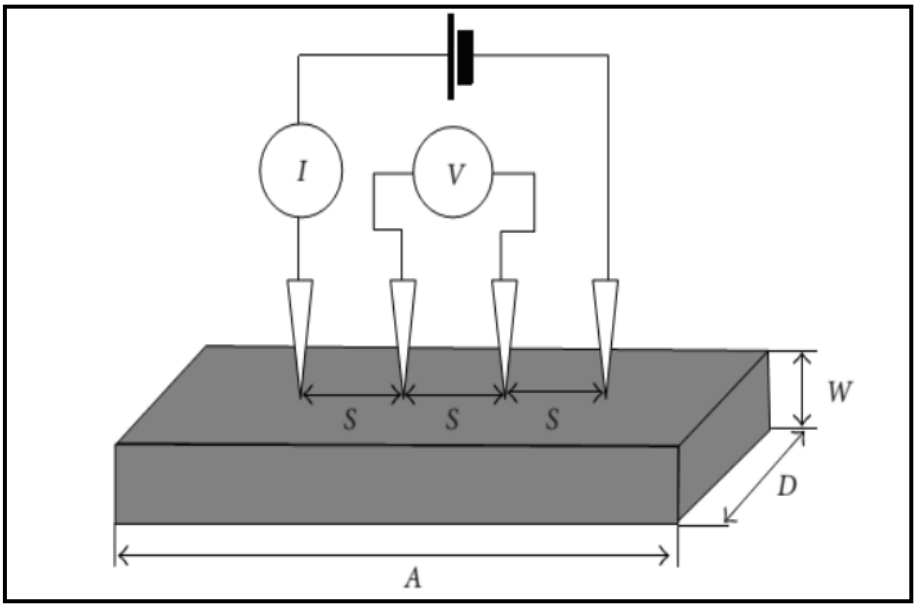

figure I.12: Schematic diagram of test circuit for measuring bar specimen resistivity with the four-point probe method [107].

A DC current is delivered through the outer probes to compute the sheet resistance (Rs), which causes a voltage to appear across the two inner probes. The sheet resistance can be calculated using Equation [108]:

$$R_S = \frac{\pi}{\ln(2)} \frac{\Delta V}{I} \qquad \textbf{(I.8)}$$

Rs: the sheet resistance.

ΔV: the voltage drop measured across the inner probes.

I: the current applied at the outer probes

The sheet resistivity of the thin film sheet is given by:

$$\rho_s = \frac{\pi t}{\ln(2)} \frac{\Delta V}{I} \qquad \textbf{(I.9)}$$

t: the thickness of the film.

The conductivity is: $\sigma = 1/\rho_s$ **(I.10)**

I.7.Figure of merit

Transparent thin films are gaining importance, which makes them a suitable material for a set of performance requirements that are significantly influenced by their optical and electrical properties. A crucial variable for applications involving optoelectronic devices is the figure of merit. The optical and electrical characteristics have a crucial influence in determining the film's quality, where it requires both high conductivity and high transparency over the visible light region.

TCOs are often assessed using the optical transmission and the sheet resistance known as the figure of merit, calculated from a formula by Haacke [109].

$$\Phi = \frac{T^{10}}{R_{sh}} \qquad \textbf{(I.11)}$$

References

[1] J. Singh, R. Kumar, V. Verma, and R. Kumar, "Materials Science in Semiconductor Processing Structural and optoelectronic properties of epitaxial Ni-substituted Cr_2O_3 thin films for p -type TCO applications," *Mater. Sci. Semicond. Process.*, no. September, p. 105483, 2020, doi: 10.1016/j.mssp.2020.105483.

[2] B. Chavillon, "Synthèse et caractérisation d ' oxydes transparents conducteurs de type p pour application en cellules solaires à colorant . To cite this version : HAL Id : tel-00674543 Synthèse et caractérisation d ' oxydes transparents conducteurs de type p pour applic," 2012.

[3] H. Sato, T. Minami, S. Takata, and T. Yamada, "Transparent conducting p-type NiO thin films prepared by magnetron sputtering," *Thin Solid Films*, vol. 236, no. 1–2, pp. 27–31, 1993, doi: 10.1016/0040-6090(93)90636-4.

[4] H. Kawazoe, M. Yasukawa, H. Hyodo, M. Kurita, H. Yanagi, and H. Hosono, "P-type electrical conduction in transparent thin films of CuAlO2," *Nature*, vol. 389, no. 6654, pp. 939–942, 1997, doi: 10.1038/40087.

[5] D. Mullarkey, "Utilising Chromium-Based p-Type Transparent Conducting Oxides in Photovoltaic Devices," no. January, 2018, [Online]. Available: http://www.tara.tcd.ie/bitstream/handle/2262/83110/Thesis.pdf?sequence=1

[6] A. Khan, "Synthesis of Strontium Cuprate (SrCu2O2) by MOCVD as a P-type Transparent Conducting Oxide Thin Film . Afzal Khan To cite this version : HAL Id : tel-00576634 « Afzal / KHAN »," 2011.

[7] L. Bottiglieri, "Out of stoichiometry CuCrO 2 as transparent p-type semiconductor for photovoltaics and transparent electronics," 2016.

[8] H. Kawazoe and H. Yanagi, "T ransparent p -Type Conducting Oxides : Design and Fabrication of p - n Heterojunctions," no. August, pp. 28–36, 2000.

[9] A. N. Banerjee and K. K. Chattopadhyay, "Recent developments in the emerging field of crystalline p-type transparent conducting oxide thin films," vol. 50, 2005, doi: 10.1016/j.pcrysgrow.2005.10.001.

[10] "Chromium, Molybdenum and Tungsten 23.1," pp. 1002–1039, doi: 10.1016/B978-0-7506-3365-9.50029-8.

[11] "CHROMIUM DIOXIDE – LOW TEMPERATURE THIN FILM GROWTH , STRUCTURAL AND," 2008.

[12] B. L. Chamberland, "The chemical and physical properties of CrO_2 and tetravalent

chromium oxide derivatives," vol. 8436, no. December, 2017, doi: 10.1080/10408437708243431.

[13] C. Madi, M. Tabbal, T. Christidis, S. Isber, B. Nsouli, and K. Zahraman, "Microstructural characterization of chromium oxide thin films grown by remote plasma assisted pulsed laser deposition," *J. Phys. Conf. Ser.*, vol. 59, no. 1, pp. 600–604, 2007, doi: 10.1088/1742-6596/59/1/128.

[14] H. Öztürk and C. Kürkçü, "Pressure-Induced Phase Transformations , Electronic Properties and Intermediate Phases of Chromium Dioxide," vol. 136, no. 1, pp. 26–32, 2019, doi: 10.12693/APhysPolA.136.26.

[15] V. Y. Irkhin and M. I. Katsnel, "Half-metallic ferromagnets," vol. 659.

[16] M. K. Trivedi *et al.*, "Characterization of Physical , Thermal and Structural Properties of Chromium (VI) Oxide Powder : Impact of Biofield Treatment To cite this version : HAL Id : hal-01398907 Powder Metallurgy & Mining Characterization of Physical , Thermal and Structural P," no. Vi, pp. 0–4, 2016, doi: 10.4172/2168-9806.1000128.

[17] P. Ajith, J. Agnes, and P. Raja, "Synthesis , characterizations and Antibacterial Studies of Chromium trioxide Nanoparticles," no. January, 2022, doi: 10.46501/IJMTST0801044.

[18] A. To *et al.*, "The Crystal Structure of ($Cr0_3$) ¢ o," pp. 222–226, 1968, doi: 10.1107/S0567740870002182.

[19] J. M. Schönle, "Synthesis and Characterisation of Chromium (III) Complexes with Polypyridyl Ligands," no. Iii, 2014.

[20] A. V Almaev, B. O. Kushnarev, E. V Chernikov, V. A. Novikov, P. M. Korusenko, and S. N. Nesov, "Superlattices and Microstructures Structural , electrical and gas-sensitive properties of Cr_2O_3 thin films," *Superlattices Microstruct.*, vol. 151, no. February, p. 106835, 2021, doi: 10.1016/j.spmi.2021.106835.

[21] P. Studies, "Synthesis and Characterization of Hard Cr_2O_3 and Superhard Cr-Zr-O PVD Coatings," 2019.

[22] P. Patnaik and D. Ph, *Handbook of Inorganic Chemicals*.

[23] P. P. Corporation and N. York, "This material is protected by copyright registered in," no. 1, pp. 42–46, 1977.

[24] N. Iwata and H. Yamamoto, "Growth and Evaluation of Magnetoelectric Cr_2O_3 Single Crystal Thin Films," no. June 2016, 2011, doi: 10.1557/PROC-1034-K10-67.

[25] A. S. Kao, M. F. Doerner, and V. J. Novotny, "Processing effects on the tribological characteristics of reactively sputtered chromium oxide (Cr_2O_3) overcoat films

Processing effects on the tribological characteristics of reactively sputtered chromium oxide (Cr_20_3) overcoat fUms," vol. 5315, no. 1989, 2013, doi: 10.1063/1.343722.

[26] S. Rekhi, L. S. Dubrovinsky, R. Ahuja, S. K. Saxena, and B. Johansson, "Experimental and theoretical investigations on eskolaite (Cr_2O_3) at high pressures," vol. 302, pp. 16–20, 2000.

[27] V. B. Pinho, "Experimental and theoretical study on Fe-Cr-O thin films : from fine structure to macroscopic behavior Pâmella Vasconcelos Borges Pinho To cite this version : HAL Id : tel-03917144 Experimental and theoretical study on Fe-Cr-O thin films : from fine struc," 2023.

[28] T. Ivanova, M. Surtchev, and K. Gesheva, "Characterization of CVD Chromium Oxide Thin Films," vol. 513, no. 2, pp. 507–513, 2001.

[29] D. D. E. La, C. Universite, and G. Alpes, "Oxydation thermique du chrome pur en atmosphère contrôlée : propriétés semiconductrices et structurales de la chromine," 2018.

[30] D. S. Mcclure, "Comparison of the Crystal Fields and Optical Spectra of Cr_2O_3 and Ruby," vol. 2289, no. 1963, 1998, doi: 10.1063/1.1733964.

[31] P. Taylor, "Phase Transitions : A Multinational," no. September 2013, pp. 37–41, doi: 10.1080/01411599108203448.

[32] A. Kasikov, A. Tarre, and M. Marandi, "Dispersion of chromia films (eskolaite) in UV-VIS," vol. 70, no. 7, pp. 36–43, 2019, doi: 10.2478/jee-2019.

[33] D. W. Fischer, "BAND SPECTRA AND MOLECULAR ORBITAL," 1971.

[34] L. Farrell, K. Fleischer, D. Caffrey, D. Mullarkey, E. Norton, and I. V Shvets, "Conducting mechanism in the epitaxial p -type transparent conducting oxide Cr_2O_3 : Mg," vol. 125202, pp. 1–10, 2015, doi: 10.1103/PhysRevB.91.125202.

[35] J. H. W. De Wit, "The Oxygen Partial Pressure Dependence of the Defect Structure of Chromium(Ill)Oxide," no. Ill, pp. 2257–2260.

[36] T. Massoud, L. U. Pierre, and E. T. Marie, "Nanostructure et propriétés électroniques locales des couches passives sur nickel et acier inoxydable To cite this version : HAL Id : tel-00833265," 2013.

[37] T. G. Wang *et al.*, "High-temperature thermal stability of nanocrystalline Cr_2O_3 films deposited on silicon wafers by arc ion plating," *Surf. Coatings Technol.*, vol. 228, pp. 140–147, 2013, doi: 10.1016/j.surfcoat.2013.04.020.

[38] P. M. Sousa, A. J. Silvestre, and O. Conde, "Cr_2O_3 thin films grown at room temperature by low pressure laser chemical vapour deposition," pp. 1–16, 1959.

[39] V. Balouria, A. Kumar, A. Singh, S. Samanta, A. K. Debnath, and A. Mahajan, "Author ' s personal copy Sensors and Actuators B : Chemical", doi: 10.1016/j.snb.2011.05.002.

[40] Y. I. Boldyrev, N. D. Ivanova, G. V. Sokolsky, S. V. Ivanov, and O. A. Stadnik, "Thin film nonstoichiometric chromium oxide-based cathode material for rechargeable and primary lithium batteries," *J. Solid State Electrochem.*, vol. 17, no. 8, pp. 2213–2221, 2013, doi: 10.1007/s10008-013-2082-7.

[41] M. F. Al-Kuhaili and S. M. A. Durrani, "Optical properties of chromium oxide thin films deposited by electron-beam evaporation," *Opt. Mater. (Amst).*, vol. 29, no. 6, pp. 709–713, 2007, doi: 10.1016/j.optmat.2005.11.020.

[42] E. Ahmed and M. Saeed, "Synthesis and characterization of Cr_2O_3 : Al thin films by plasma of R . F . magnetron sputtering for gas sensing application," vol. 10, pp. 4450–4455, 2023.

[43] S. Saritas, "Temperature-dependent gas sensor application of chromium oxide structure," *J. Mater. Sci. Mater. Electron.*, vol. 34, no. 7, pp. 1–12, 2023, doi: 10.1007/s10854-023-10083-9.

[44] V. B. Kamble and A. M. Umarji, "Gas sensing response analysis of p-type porous chromium oxide thin films," *J. Mater. Chem. C*, vol. 1, no. 48, pp. 8167–8176, 2013, doi: 10.1039/c3tc31830c.

[45] J. Sim, S. Lee, J. Kim, K. Jeong, H. Ahn, and C. Lee, "Applied Surface Science Efficiency enhancement of CIGS compound solar cell fabricated using homomorphic thin Cr_2O_3 diffusion barrier formed on stainless steel substrate," *Appl. Surf. Sci.*, vol. 389, pp. 645–650, 2016, doi: 10.1016/j.apsusc.2016.06.194.

[46] P. Qin *et al.*, "Organic solar cells with p-type amorphous chromium oxide thin film as hole-transporting layer," *Thin Solid Films*, vol. 519, no. 13, pp. 4334–4341, 2011, doi: 10.1016/j.tsf.2011.02.013.

[47] M. Ishtiaq *et al.*, "A comparison of antibacterial activity in dark-UV light in perspective of surface and structural properties of spray pyrolysis grown Cu doped Cr_2O_3 thin films," *Surfaces and Interfaces*, vol. 37, no. February, p. 102741, 2023, doi: 10.1016/j.surfin.2023.102741.

[48] Z. Fan, M. Zhu, S. Pan, J. Ge, and L. Hu, "Giant photoresponse enhancement in Cr_2O_3 films by Ni doping-induced insulator-to-semiconductor transition," *Ceram. Int.*, vol. 47, no. 10PA, pp. 13655–13659, 2021, doi: 10.1016/j.ceramint.2021.01.226.

[49] S. M. Abdul Kareem, M. H. Suhail, and I. K. Adehmash, "Fabrication of Cr_2O_3: ZnO

nanostructure thin film prepared by PLD technique as NH3gas sensor," *Iraqi J. Sci.*, vol. 62, no. 7, pp. 2176–2187, 2021, doi: 10.24996/ijs.2021.62.7.7.

[50] S. M. AbdulKareem, I. K. Jassim, and M. H. Suhail, "Cr_2O_3:TiO_2 nanostructure thin film prepared by pulsed laser deposition technique as NO_2 gas sensor," *Baghdad Sci. J.*, vol. 17, no. 2, pp. 329–335, 2020, doi: 10.21123/BSJ.2020.17.1(SUPPL.).0329.

[51] T. Nozaki, M. Al-Mahdawi, Y. Shiokawa, S. P. Pati, H. Imamura, and M. Sahashi, "Magnetic anisotropy of doped Cr_2O_3antiferromagnetic films evaluated by utilizing parasitic magnetization," *J. Appl. Phys.*, vol. 128, no. 2, 2020, doi: 10.1063/5.0009353.

[52] A. Zekaik, H. Benhebal, and B. Benrabah, "Synthesis and characterization of Cu doped chromium oxide (Cr_2O_3) thin films," *High Temp. Mater. Process.*, vol. 38, no. 2019, pp. 806–812, 2019, doi: 10.1515/htmp-2019-0037.

[53] A. Zekaik *et al.*, " Sol–Gel Synthesis of Nickel-Doped Cr_2O_3 Thin Films ," *J. Mol. Eng. Mater.*, vol. 05, no. 04, p. 1750012, 2017, doi: 10.1142/s2251237317500125.

[54] T. Larbi, M. A. Amara, B. Ouni, and M. Amlouk, "Enhanced photocatalytic degradation of methylene blue dye under UV-sunlight irradiation by cesium doped chromium oxide thin films," *Mater. Res. Bull.*, vol. 95, pp. 152–162, 2017, doi: 10.1016/j.materresbull.2017.07.024.

[55] Z. T. Khodair, G. A. Kazem, and A. A. Habeeb, "Studying the optical properties of (Cr_2O_3:I) thin films prepared by spray pyrolysis technique," *Iraqi J. Phys.*, vol. 10, no. 17, pp. 83–89, 2012.

[56] E. Arca, K. Fleischer, and I. V. Shvets, "Magnesium, nitrogen codoped Cr_2O_3: A p-type transparent conducting oxide," *Appl. Phys. Lett.*, vol. 99, no. 11, pp. 2011–2014, 2011, doi: 10.1063/1.3638461.

[57] A.M. Oje, A.A. Ogwu1, A.I.Oje, N.T. Tsendzughul, S.Ur Rahman, "Influence of RF power on the stoichiometry, optical, and electrical properties of chromium oxide coatings prepared by reactive magnetron sputtering" Materials Research Express, Volume 6, Number 6. 2019, **DOI** 10.1088/2053-1591/ab0d74.

[58] A. Tatarolu, A. M. Oje, and A. A. Ogwu, "Effect of thickness and type of substrate on optical properties of chromium oxide thin film prepared by sputtering magnetron Effect of thickness and type of substrate on optical properties of chromium oxide thin film prepared by sputtering magnetron", doi: 10.1088/1757-899X/1105/1/012065.

[59] K. Khojier, H. Savaloni, and N. Z. Dehnavi, "Structural , mechanical and tribological characterization of chromium oxide thin films prepared by post-annealing of Cr thin

films," no. November, 2013, doi: 10.1016/j.apsusc.2013.07.123.

[60] G. Contoux, F. Cosset, and J. Machet, "Deposition process study of chromium oxide thin films obtained by d . c . magnetron sputtering," vol. 292, pp. 75–84, 1997.

[61] L. Zhang, M. Kuhn, and U. Diebold, "Growth , structure and thermal properties of chromium oxide films on Pt (111)," vol. 375, pp. 1–12, 1997.

[62] J. Hossain, K. S. Sharif, and K. A. Khan, "Temperature effect on the electrical properties of chromium oxide (Cr_2O_3) thin films," vol. 13, no. 5, pp. 485–490, 2011.

[63] A. Kadari, T. Schemme, D. Kadri, and J. Wollschläger, "XPS and morphological properties of Cr_2O_3 thin films grown by thermal evaporation method," *Results Phys.*, 2017, doi: 10.1016/j.rinp.2017.08.036.

[64] J. J. Carey, M. Nolan, Y. Krockenberger, H. Irie, S. Chatterjee, and S. Chatterjee, "Effect of Thermal Annealing on the Electrical Properties and Gas Sensing for Pulsed Laser Deposition Cr_2O_3 Thin Films Effect of Thermal Annealing on the Electrical Properties and Gas Sensing for Pulsed Laser Deposition Cr_2O_3 Thin Films," no. Iii, 2021, doi: 10.1088/1742-6596/1829/1/012020.

[65] S. Arulkumar, S. Parthiban, A. Goswami, R. S. Varma, M. Naushad, and M. B. Gawande, "Ac ce pte d M us pt," *Mater. Today Proc.*, vol. 27, no. xxxx, pp. 0–31, 2019, [Online]. Available: https://doi.org/10.1016/j.matpr.2019.12.188%0Ahttps://doi.org/10.1016/j.matpr.2019.09.090%0Ahttps://doi.org/10.1080/14484846.2018.1432089

[66] S. Punugupati, J. Narayan, and F. Hunte, "Room temperature ferromagnetism in epitaxial Cr_2O_3 thin films grown on r-sapphire," vol. 193907, pp. 1–6, 2015.

[67] S. Khamlich *et al.*, "Pulsed laser deposited Cr_2O_3 nanostructured thin film on graphene as anode material for lithium-ion batteries," no. Iii, pp. 1–21.

[68] K. Larsson "Chapter 1", IP Address: 193.194.69.104 .doi: 10.1088/978-0-7503-3107-4ch1.

[69] B. D. Fahlman, "Recent Advances in Chemical Vapor Deposition," pp. 1021–1033, 2006.

[70] W. Yu *et al.*, "Jo ur of," *Surf. Coat. Technol.*, p. 126509, 2020, doi: 10.1016/j.surfcoat.2020.126509.

[71] J. Liang, G. F. Pan, S. Bin Fan, W. L. Cheng, and Z. Y. Tian, "CVD synthesis and catalytic combustion application of chromium oxide films," *Phys. Status Solidi Curr. Top. Solid State Phys.*, vol. 12, no. 7, pp. 1001–1005, 2015, doi: 10.1002/pssc.201510019.

[72] J. Wang, A. Gupta, and T. M. Klein, “Plasma enhanced chemical vapor deposition of Cr 2 O 3 thin films using chromium hexacarbonyl ($Cr(CO)_6$) precursor,” vol. 516, pp. 7366–7372, 2008, doi: 10.1016/j.tsf.2008.02.027.

[73] P. D. Publications, R. Cheng, P. A. Dowben, and S. Stadler, “DigitalCommons @ University of Nebraska - Lincoln Potential phase control of chromium oxide thin films prepared by laser-initiated organometallic chemical vapor deposition,” pp. 1–4, 2001, doi: 10.1063/1.1343846.

[74] B. G. Carta *et al.*, “A Comparative Study of Cr_2O_3 Thin Films Obtained by MOCVD using Three Different Precursors,” pp. 375–380, 2005, doi: 10.1002/cvde.200406360.

[75] “Polycrystalline and Amorphous Chromium Oxide MOCVD Yuneng Chang, Shengfu Huang, Minche Huang,” vol. 685, pp. 1–6, 2001.

[76] G. Bahuguna, N. K. Mishra, P. Chaudhary, A. Kumar, and R. Singh, “Thin Film Coating through Sol-Gel Gel Technique,” vol. 6, no. 7, pp. 65–72, 2016.

[77] N. Y. Abu-thabit, A. Salam, and H. Makhlouf, *Fundamental of smart coatings and thin films : synthesis , deposition methods , and industrial applications*. Elsevier Inc., 2020. doi: 10.1016/B978-0-12-849870-5.00001-X.

[78] C. A. B. Exploration and M. A. Butt, “Thin-Film Coating Methods : A Successful Marriage of,” 2022.

[79] M. G. Tsegay, H. G. Gebretinsae, G. G. Welegergs, M. Maaza, and Z. Y. Nuru, “Novel green synthesized Cr_2O_3 for selective solar absorber : Investigation of structural , morphological , chemical , and optical properties Novel green synthesized Cr 2 O 3 for selective solar absorber : Investigation of structural , morphological , c,” *Sol. Energy*, vol. 236, no. March, pp. 308–319, 2022, doi: 10.1016/j.solener.2022.03.011.

[80] A. Zekaik, H. Benhebal, and B. Benrabah, “Synthesis and characterization of Cu doped chromium oxide (Cr_2O_3) thin films,” pp. 806–812, 2019.

[81] H. Reza and M. Hoseinpour, “An experimental study of the effects of surface roughness and coating of Cr_2O_3 layer on the laser-forming process,” *Opt. Laser Technol.*, vol. 109, pp. 336–347, 2019, doi: 10.1016/j.optlastec.2018.07.064.

[82] J. Dong *et al.*, “ Annealing-Free Cr_2O_3 Electron-Selective Layer for Efficient Hybrid Perovskite Solar Cells ”, Materials Physical Chemistry, http://dx.doi.org/10.1002/cssc.201701864.

[83] R. AZIZI ,“ *The effect of doping on the properties of thin films of Indium oxide (In2O3) deposited by ultrasonic spray for optoelectronic application.*” 2020.

[84] V. K. Singh, “THIN FILM DEPOSITION BY SPRAY PYROLYSIS TECHNIQUES,”

vol. 4, no. 11, pp. 910–918, 2017.

[85] S. Rahemi, A. Sabour, R. Aghdam, M. Nazari, and A. Bayat, “Journal of Analytical and Applied Pyrolysis A comprehensive review on ultrasonic spray pyrolysis technique : Mechanism , main parameters and applications in condensed matter,” *J. Anal. Appl. Pyrolysis*, vol. 141, no. May, p. 104631, 2019, doi: 10.1016/j.jaap.2019.104631.

[86] P. S. Patil, “Versatility of chemical spray pyrolysis technique,” vol. 59, 1999.

[87] A. Manuscript, “Materials Chemistry A,” 2017, doi: 10.1039/C7TA03009F.

[88] S. M. Sabnis, P. A. Bhadane, and P. G. Kulkarni, “Process flow of spray pyrolysis technique,” vol. 4, no. 5, pp. 7–11, 2013.

[89] N. Synthesis, “Spray Pyrolysis,” pp. 23–30, 2013, doi: 10.1007/978-3-642-41275-2.

[90] V. B. Kamble and A. M. Umarji, “Chromium Oxide thin films by Ultrasonic Nebulized Spray Pyrolysis of Aqueous Combustion Mixture for Gas Sensing Application”.

[91] A. I. Journal, “Materials Science,” vol. 10, no. 6, 2014.

[92] N. A.-H. H. A. Al-husain, “Effect of Thickness on Some Optical Properties of Fe_2O_3 Thin Films Prepared by Chemical Spray Pyrolysis Technique,” *Al-Haitham Jour. Pure Appl. Sci.*, vol. 26, no. 2, pp. 137–142, 2013.

[93] J. Epp, *4 - X-ray diffraction (XRD) techniques for materials characterization*. Elsevier Ltd, 2016. doi: 10.1016/B978-0-08-100040-3.00004-3.

[94] A. Ali, Y. W. Chiang, and R. M. Santos, “X-ray diffraction techniques for mineral characterization : a re- view for engineers of the fundamentals , applications , and re- search directions,” no. December, 2021, doi: 10.20944/preprints202112.0438.v1.

[95] K. Nabila, “ Contribution à l’étude de couches minces d’oxydes transparents conducteurs à base de zinc et cobalt par spray pneumatique,” 2019.

[96] F. Oktober, “Scanning electron microscopy (SEM) analysis of tribofilms enhanced by fullerene-like nanoparticles,” 2012.

[97] S. Electron, M. Microscopy, and X. External, “Characterization Techniques,” pp. 19–34.

[98] C. Puttichaem *et al.*, “ENERGY-DISPERSIVE X-RAY SPECTROSCOPY CHARACTERIZATION OF ULTRA THIN DIAMOND-LIKE CARBON FILM ON MAGNETIC RECORDING HEAD,” 2021.

[99] “MODULE II ENERGY DISPERSIVE ANALYSIS OF X-RAYS (EDAX)”.

[100] S. CANLI “THICKNESS ANALYSIS OF THIN FILMS BY ENERGY DISPERSIVE X RAY SPECTROSCOPY,” December 2010, 77 pages

[101] A. F. Hussain, “UV-VISIBLE SPECTROMETRY,” no. December, 2019.

[102] T. Owen, “Fundamentals of modern UV-visible spectroscopy” Publication number 5980-1397E.

[103] P. Mechanics and I. A. Optics, “MINISTRY OF HIGHER EDUCATIONAND SCIENTIFIC Submitted to Institute of Optics and Precision Mechanics For the degree Doctorat LMD 3 rd cycle In Applied Optics and Photonics By Walid Allag Title Study of thin films for photovoltaic solar cells Par Walid Alla,” 2022.

[104] “FOR ELECTRICAL CHARACTERIZATION OF THIN FILMS,” 2010.

[105] R. S. Waremra and P. Betaubun, “Analysis of Electrical Properties Using the four point Probe Method,” vol. 9, pp. 1–4, 2018.

[106] S. Figure, “Four-Point Probe Manual,” pp. 1–3.

[107] Yahia .AnouarOptimization of indium oxide thin films properties prepared by sol gel spin coating process for optoelectronic applications2020 ”,.

[108] M. Naftaly *et al.*, “Sheet Resistance Measurements of Conductive Thin Films : A Comparison of Techniques,” 2021.

[109] G. Haacke, “New figure of merit for transparent conductors,” *J. Appl. Phys.*, vol. 47, no. 9, pp. 4086–4089, 1976, doi: 10.1063/1.323240.

Chapter II: *Influence of precursors on Cr_2O_3 thin film properties*

Introduction

The properties of the deposited Cr_2O_3 thin films are dependent on solvents, the nature of used precursors, and the processing conditions. Therefore in the present investigation, Cr_2O_3 thin films were obtained using spray pneumatic and the main purpose of this work is to study the influence of nature and the concentration of the precursor, on the structural, morphological, optical and electrical properties of the prepared films. In this work the spray solutions; hydrated chromium nitrate $Cr(NO_3)_3 \cdot 9H_2O$ and hydrated chromium chloride $CrCl_3 \cdot 6H_2O$, dissolved in distilled water after that were sprayed via atomization processes then condensed onto the heated substrates. The solutions are prepared with 0.02, 0.04, 0.06 and 0.08 mol/l as molar concentrations.

Part one: Experimental details

II.1. Experimental details

II.1.1 Experimental setup used (the spray pneumatic)

The simple and low-cost homemade pneumatic spray system (SP) technique is used to deposit the chromium oxide (Cr_2O_3) thin films, which have the shape and components shown in **figure II.1**.

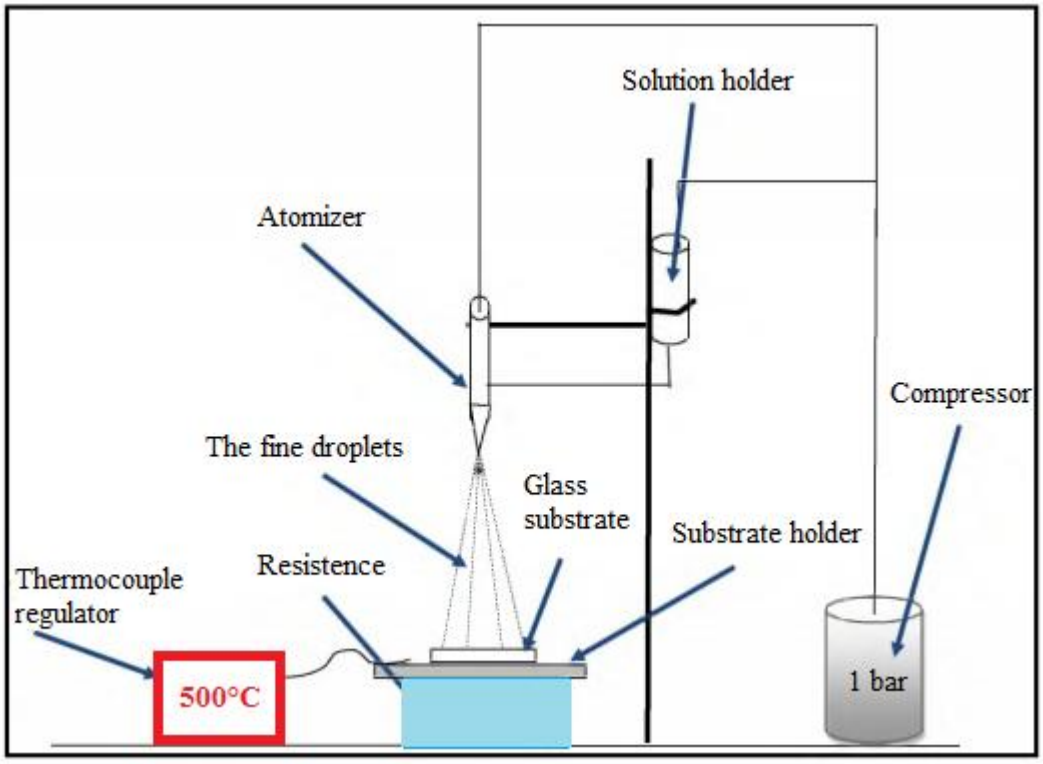

Figure II.1: The experimental setup for pneumatic spray (SP) deposition method.

A pneumatic spray system (SP) technique is used for depositing a wide variety of thin films. Compared to other deposition techniques, this method has a lot of benefits, such as simplicity and low cost with regard to equipment costs and energy needs, moderate temperature operation (100–550 °C), control of thickness, and solution flow rate control because it is quick and easy to execute, and good control over the material's chemical makeup.

Description of pneumatic spray system (SP) equipment

From Figure 1, the pneumatic spray technique involves mainly:

- **Compressor:** (in our case, it is air), which compresses the carrier gas under a controllable pressure (1 bar). This ensures the push of the solution to the spout and the transformation of the spray solution into a spray of fine droplets.
- **Atomizer:** With the application of pressure (1 bar), the starting solution is transformed through a nozzle. The nozzle converts the solution into small droplets, known as aerosols.
- **Substrate holder:** This is a plate (made of iron) with a diameter of 20 cm, supported on the electric heater, heated by the Joule effect. The temperature of which can be monitored using a temperature regulator that is connected to a thermocouple is fixed at the center of the iron plate.
- **Resistance:** To heat the substrate.
- **Solution holder:** is a burette in which the precursor solution is placed. The solution holder has a hole. This hole allows the solution to pass into an atomizer with a low flow rate that can be controlled by the compressor.
- **Control thermocouple:** It gives us the opportunity to detect the substrate's temperature while spraying in a relative manner by a thermocouple, placed on the heating plate and connected to a temperature regulator, allowing a direct reading of the temperature.

II.1.2. Preparation of the substrate

The investigated films were deposited on glass substrates (see **Figure II.2**) with dimensions of 2.5 cm in length and 2 cm in width; glass was chosen as the depot substrate for the following reasons:

• Cr_2O_3's thermal compatibility helps to reduce stress in the interface film/substrate.

After deposition, the sample (substrate and layer) will cool from the deposition temperature above 500°C to ambient temperature (25 °C), causing the two materials that make up the sample to become compressible. Since their expansion coefficients are similar, the stresses are kept to a minimum:

(α glass = 8.5×10^{-6} °K^{-1} , α Cr_2O_3 = 9.0×10^{-6} °K^{-1}) [1].

• For their transparency, this responds well to the optical characterisation of films in the visible.

•The conductivity measurement won't be impacted by it because it is an insulator.

• For economic reasons.

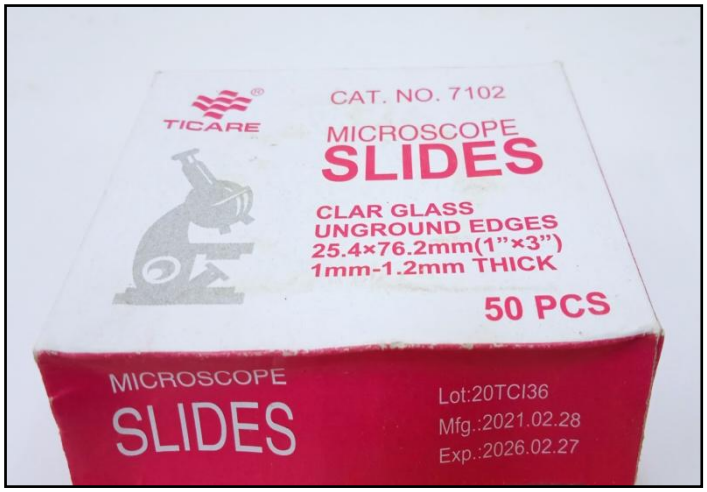

Figure II.2: Glass Substrates.

To guarantee that the layers prepared on the glass substrate adhere well. In our work, the substrates were cleaned of contaminants and degreased, which is one of the most important steps, as follows:

The substrates are cut using a pen with a diamond point.

- Washing with distilled water to clean any dust or attachments.
- Washing with acetone for 5 minutes.
- Rinsing with distilled water again
- Washing with ethanol for 5 minutes at ambient temperature
- Cleaning in a water-distilled bath
- The substrates were then left to dry in the air.

II.1.3. Preparation of the solution

For the preparation of thin films of chromium oxide Cr_2O_3, the spray solutions were obtained by dissolving hydrated chromium chloride $CrCl_3 \cdot 6H_2O$ in 50 ml of distilled water. A few drops of HCl acid have been added to the mixture. The solution was stirred at 50 ° C for 2 hours, resulting in the formation of a light green homogenous solution. The different properties of the elements used in the preparation of our samples are summarized in the table (II.1).

The calculation of mass as a function of concentration is given by using the following formulas

$$C = \frac{n}{V} \qquad \text{(II.1)}$$

With :

C: the concentration of the solution (mol/l).

n: The number of moles (mole).

V: the volume of the solvent (ml).

$$\boldsymbol{n = \frac{m}{M}} \qquad \text{(II.2)}$$

m: the mass (g).

M: the molar mass (g/mole).

Combining the two equations we find that:

$$\boldsymbol{M = C*V*M} \qquad \text{(II.3)}$$

Table II.1: *Some properties of chromium chloride hexahydrate.*

Synonym(s)	Chromium trichloride hexahydrate, Hexaaquachromium (III) chloride
Linear Formula	$CrCl_3.6H_2O$
Description	Green to dark green crystals / crystalline powder
Molecular Weight	266.45
Density (g/cm^3)	5.231

II.1.4. Depositing of thin films

Following the production of the substrates and precursor solutions, the deposition process for chromium oxide Cr_2O_3 thin films is described using the following steps:
To prevent thermal shock of the substrates, it is necessary to lay the substrate on the substrate holder and gradually raise the temperature from ambient to the deposit temperature. Setting of The distance between the atomizer and the substrate holder 30 cm. the applied Pressure on the solution to create droplets was adjusted through the compressor at 1 bar. Those droplets are then transported to the heated substrate for 3 minutes and, ultimately, result in the production of the thin layer.
These parameters (time, pressure, and distance atomizer-substrate) are optimized in our previous work [2].

The following chemical equation describes the thin layer formed by the pyrolysis reaction between the precursor solution and air in the heated medium [3]:

$$2CrCl_3 + 2H_2O \xrightarrow{Heat} Cr_2O_3 + 6HCl$$

We performed numerous series of samples in an effort to find the conditions for the development of the deposited films. Table (II.2) lists the conditions for film preparation :

- ✓ Concentration of different chemical precursors: 0.02, 0.04, 0.06 and 0.08 mol/l.
- ✓ Substrate temperature: 350 - 550 C°.

- ✓ Indium doped Cr_2O_3: 0, 2, 4, 6 and 8 wt. %.
- ✓ Copper doped Cr_2O_3: 0, 2, 4, 6 and 8 wt. %.

Table II.2: *Summary Table of the Experimental Conditions of the Four Series of Deposits Carried Out.*

Sample	concentration of different chemical precursors (mol/l)		Substrate temperature	doping (wt. %)	Time deposit (minute)	Pressure of air (bar)
Series 1	chromium chloride	chromium nitrate	450°C	/	3 min	1 bar
	0.02	0.02				
	0.04	0.04				
	0.06	0.06				
	0.08	0.08				
Series 2	0.04 mol/l		350°C	/	3 min	1 bar
			400°C			
			450°C			
			500°C			
			550°C			
Series 3	0.04 mol/l chromium chloride		500°C	Indium (In)	3 min	1 bar
				0.02		
				0.04		
				0.06		
				0.08		
Series 4	0.04 mol/l chromium chloride		500°C	Copper (Cu)	3 min	1 bar
				0.02		
				0.04		
				0.06		
				0.08		

Part Two: Influence of precursors on Cr_2O_3 thin films properties

II.2. Results and discussion

II.2.1. Thickness measurement and film formation mechanism

Under the above -stated conditions Cr_2O_3 films were elaborated from chromium chloride and chromium nitrate solutions. A thermal decomposition occurs to the fine droplets of the solutions after their falling over the hot substrate surface. resulting in the formation of uniform and well-adherent (hardly peeled with scotch tape test) thin films. The thickness of the deposited films was calculated with the help of a weight difference method using an electronic high-precision balance. Knowing the area of film and the density of Cr_2O_3 (5.22 g/cm3) [4], the film thickness **t** is determined as shown in equation (I.1) [5].

From table (II.3), we can notice that the thickness have a similar trend of variation with the rise in molar concentration. The continuous increase in thickness with precursor concentration indicates that the later may be governed by the Cr-containing species. It is difficult to control the incorporation of O^{2-} into the film during the growth process using the spray pyrolysis technique. The atmospheric conditions where the film growth takes place can't control accurately and hence the stoichiometry is only controlled by the Cr species.

The sample obtained by the nitrate solution is thinner than that deposited by the chloride solution, this is certainly due to the contribution of several physico-chemical factors entering into the film's growth mechanisms, such as the type of the solution (viscosity, density, surface tension, reactivity...), the aerodynamic effect and the volatility of the solution on the one hand and, with equal molarities, the chrome concentration in nitrate solution is lower than that in chloride solution on the other hand. The Chromium concentrations in the two solutions used are:

a (Chromium Chloride) **{**$C_{Cr}(a) = M(Cr)/ M(CrCl_3.6H_2O) = 51,996/266,44 = 0,20$**}**.

b (Chromium Nitrate) **{**$C_{Cr}(b)= M(Cr)/ M(Cr(NO_3)_3.6H_2O)= 51,996/400,15 = 0,13$**}**.

Which agree well with the atomic percentage of elements given by EDS analysis shown in table 2.

Table II.3: *Values of Crystallites size and strain (ε) of Cr_2O_3 thin films.*

	Chromium Chloride				Chromium nitrate			
M (mol/L)	(hkl)	Crystallites size (nm)	strain $*10^{-3}$	Thickness (nm)	(hkl)	Crystallites size (nm)	strain $*10^{-3}$	Thickness (nm)
0.02	110	33.20	1.044	274	116	/	/	270
0.04		56.69	0.611	334		/	/	307
0.06		47.24	0.734	513		37.97	0.913	455
0.08		35.42	0.979	666		18.99	1.826	632

II.2.2.Structural properties

In the field of material characterization, X-ray diffraction is a vital technique for extracting atomic-scale data from both crystalline and non-crystalline (amorphous) materials.In this study the X-ray diffraction traces of thin films deposited with different precursor solutions molarities with chromium chloride and chromium nitrate as precursors were taken at room temperature.

Figure II.3, shows the X-ray diffraction pattern of Cr_2O_3 thin films deposited with different precursor solutions molarities with (a) Cr chloride and (b) Cr nitrate as precursors. The XRD patterns show that all the films are polycrystalline, with Rhombohedral structure (using JCPDS 00-001-1294 as reference).

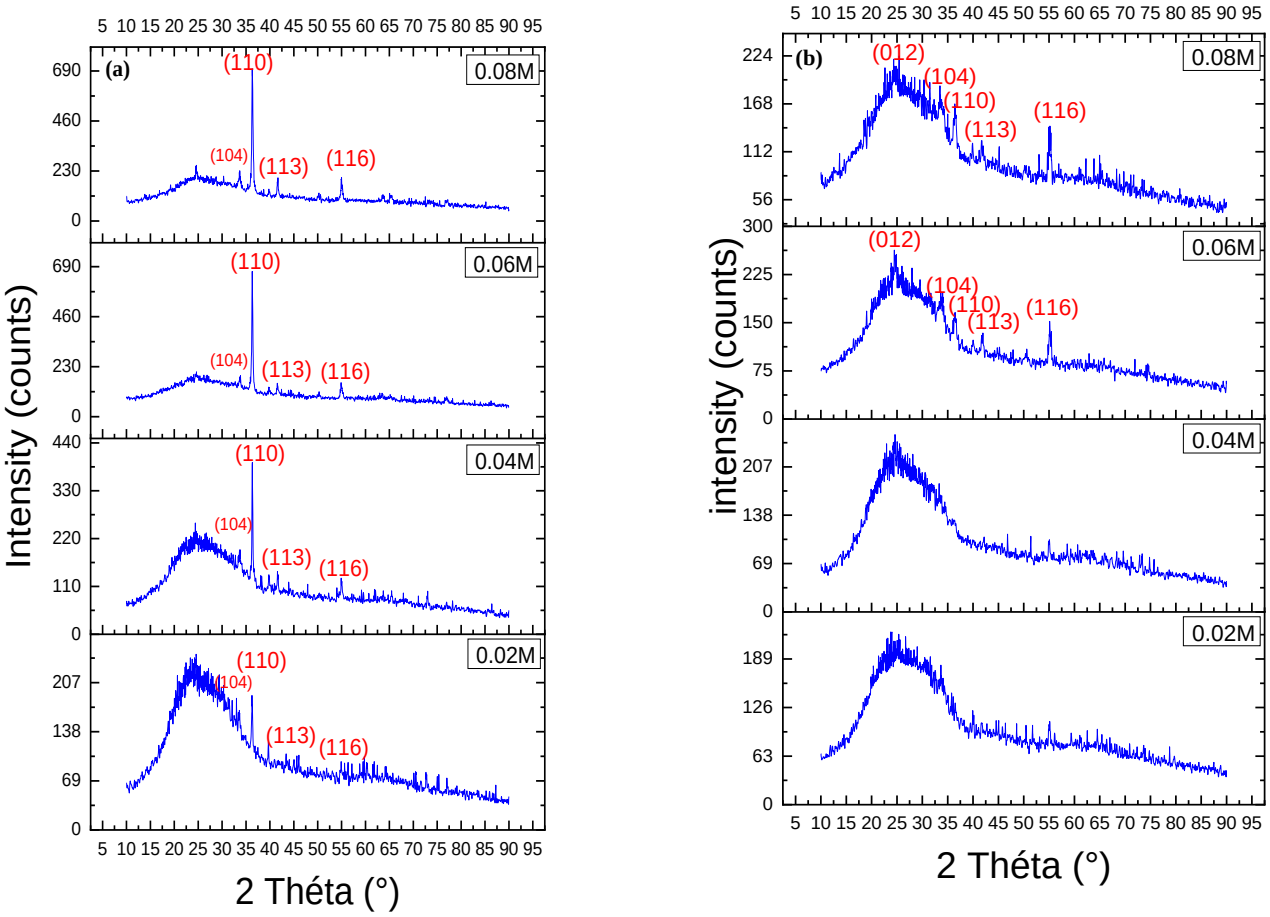

Figure II.3: XRD diffraction patterns of Cr_2O_3 thin film with different concentrations for **(a)** Chromium chloride and **(b)** Chromium nitrate precursors.

It is seen from **figure II.3. (a),** that the films exhibit a strong orientation along (110) at 36°. The increase in concentrations results in a continuous increase in (110) peak intensity, and also observed other peaks such as (104), (113) and (116). **figure II.3. (b),** shows the X-ray diffraction patterns of chromium nitrate films. For low concentrations (0.02M and 0.04M) we can see the poor crystallinity of the structure by increasing the molarity, peak appears at 55°, which is attributed to the (116) diffraction peak, other peaks assigned as (012), (104), (110) and (113) were also observed, which confirms the improvement of the film crystallinity [6].

However, we noticed the presence of a broad peak located between 10 and 30° for low concentrations (0.02M and 0.04M) for films prepared with chloride precursor and for all samples obtained by using nitrate precursors. This is an indication of the presence of an amorphous phase in

the film network. From this we inferred that films deposited with nitrate are composed of small crystallites embedded in an amorphous phase.

As can be seen there is a different behaviors between samples obtained by using chloride and those obtained using nitrate precursors, the chloride crystallization is better than nitrate, and of course this is due to the nature of each source.

The difference in the precursor properties alters the films growth mechanism which originates the difference in the pyrolytic reaction on the surface of the substrate produces the formation of the films with different thickness. The high Cr-containing species in chloride solution leads to the nucleation along the plane (110) since the latter requires less formation energy. However, when using the chromium nitrate as starting solution, decomposition may proceed through a series of oxide nitrates [6, 7]; this explains the obtained poor crystalline film structure.

The crystallite sizes of the Cr_2O_3 films were calculated from the peaks with the highest intensity. Since the intensity along the (110) plane for chromium chloride and (116) for chromium nitrate increases sharply as the precursor concentration increases, using the well-known Scherer formula (see eq. I.3).

The strain (ε) for an orientation of Cr_2O_3 thin films deposited at different molarities can be estimated using the formula given previously (eq. I.4); their estimated values are represented in Table (II.3).

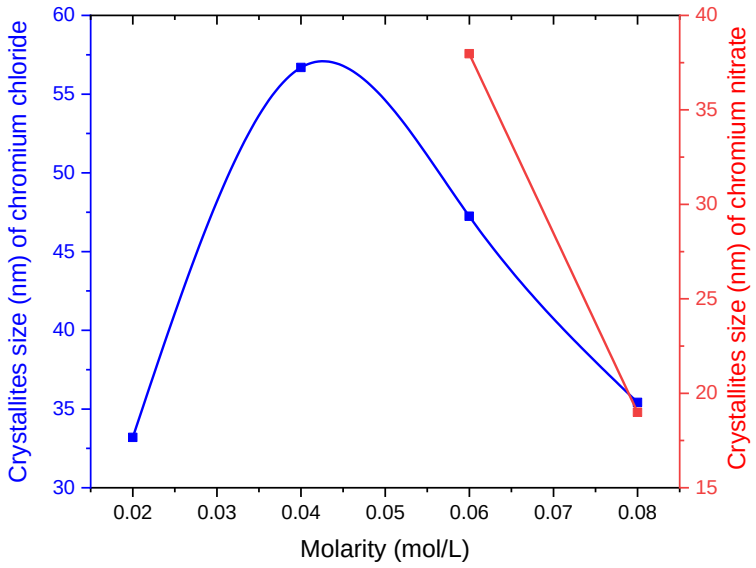

Figure II.4: Evolution of the grain size of Cr_2O_3 films with molarity.

It was observed from the **figure II.4,** that the crystallite size of the films decreases with the increase in concentration for both precursors which is probably due to the increased nucleation centers. We note that there is an inverse relationship between the crystal size and microstrain. Similar results

have been reported by T. Larbi et al. [9] and slightly greater than those obtained by Wang et al. [10].

It is clear from table1that the film deposited at 0.04 M with Chromium chloride has the larger crystallite size, which is probably due to the crystallites packed dominantly along the (110) plane thereby improving the crystallinity of the film. Nevertheless the later is less dense than those deposited at higher concentrations as suggested by the broad pick at the beginning of DRX diagram.

II.2.3. Elemental analysis and morphological study

The EDS spectrum and SEM surface images of Cr_2O_3 thin films deposited with the tow studied salts at different concentrations are shown in **Figure II.5, II.6,** respectively.

To confirm the composition of Cr_2O_3 films, EDS compositional analysis was employed. **Figure II.5,** shows an EDS spectrum of Cr_2O_3thin film deposited at various concentration. This spectrum confirms the presence of Cr and O elements. The presence of silicon peak may be due the glass substrate, this peak gets smaller and the Cr peak becomes more prominent as the molar concentration in both of chloride and nitrate precursors increases. This is due to increase in film growth on the glass substrate which suggests an increase in the quantity of the elements in the films, table (II.4) shows the atomic percentage of elements.

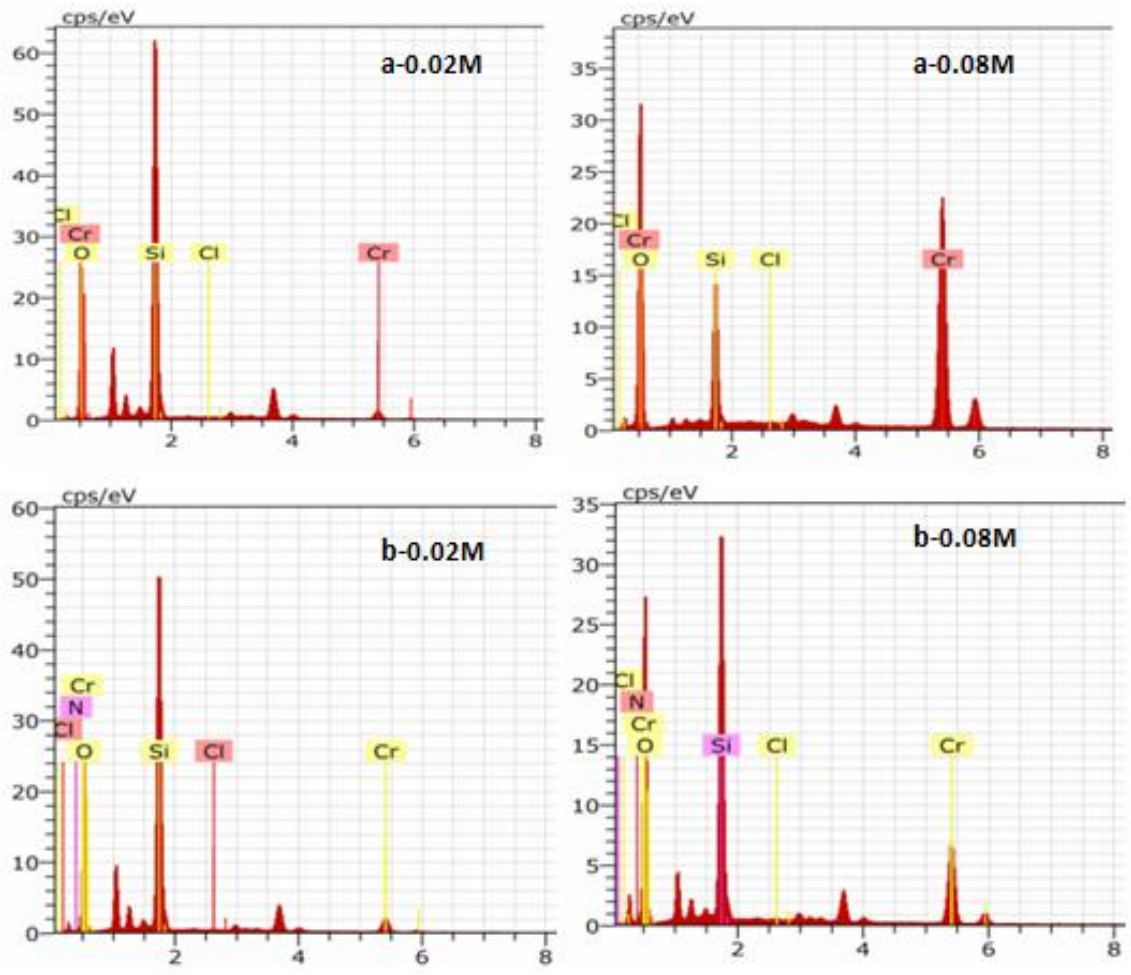

Figure II.5: EDS spectra of Cr_2O_3 films **(a)** Chrome chloride, **(b)** Chromium nitrate precursors.

Table II.4: *Atomic percentage of chemical composition in Cr_2O_3 films.*

	Chrome chloride [at. %]				Chromium nitrate [at. %]			
	0.02M	0.04M	0.06M	0.08M	0.02M	0.04M	0.06M	0.08M
O	85.22	82.66	73.09	68.81	84.92	81.71	80.06	78.45
Cr	14.78	17.24	26.91	31.19	15.08	18.29	19.94	21.55

As **Figure II.6,** shows the top view SEM images of the Cr_2O_3 taken using magnifications of about 2,000 indicate the polycrystalline nature. These images show that the surface morphology depends clearly on the nature of the used precursor.

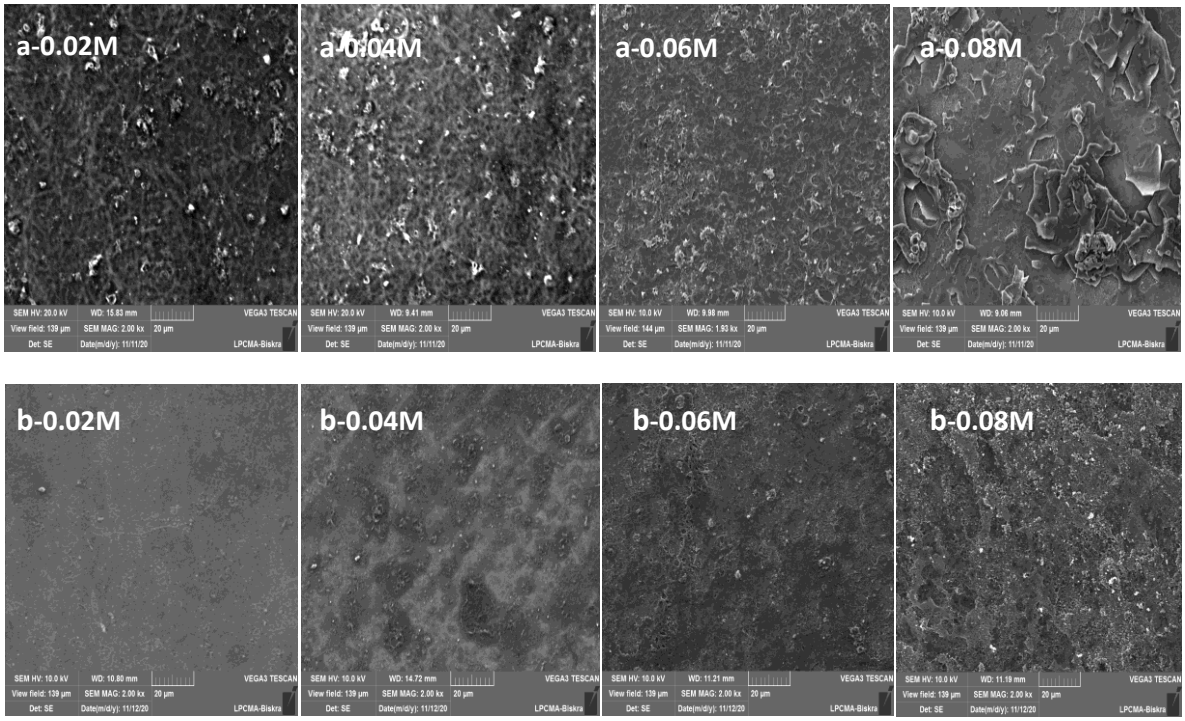

Figure II.6: SEM surface images of the Cr_2O_3 thin films deposited at various concentration for **(a)** Chrome chloride, **(b)** Chromium nitrate precursors.

The surface morphologies of the Cr_2O_3 films prepared with chromium nitrate as starting solution figure 3b have approximately the same density and smooth surface morphology at low concentrations. When the concentrations got higher, the film got rougher and more sintered structure can be found.

The micrographs of the films deposited with chromium chloride solution, clearly illustrate the formation of sub-micrometer crystallites distributed in a uniform manner over the surface. Although the films are well recovered and no cracks could be detected. The amount of solute increases in the solution as the concentration increases and therefore the electrostatic interaction between the solute particles becomes larger. As a result an increasing in the probability of gathering more solute to form more and denser grains leading to a rougher surface of the grown films; which is in good concordance with the above XRD analysis.

II.2.4. Optical properties

The optical measurement results include relations of the transmittance with wavelength for chromium oxide (Cr_2O_3) thin films with different molarities (0.02, 0.04,0.06 and 0.08 M) and computing some optical parameters like optical energy gap and Urbach energy by using UV–Vis spectrophotometer.

Figure II.7, shows the optical transmission of Cr_2O_3 thin films prepared with chromium chloride and chromium nitrate precursors as a function of the wavelength in the 290–1500 nm range for different concentrations.

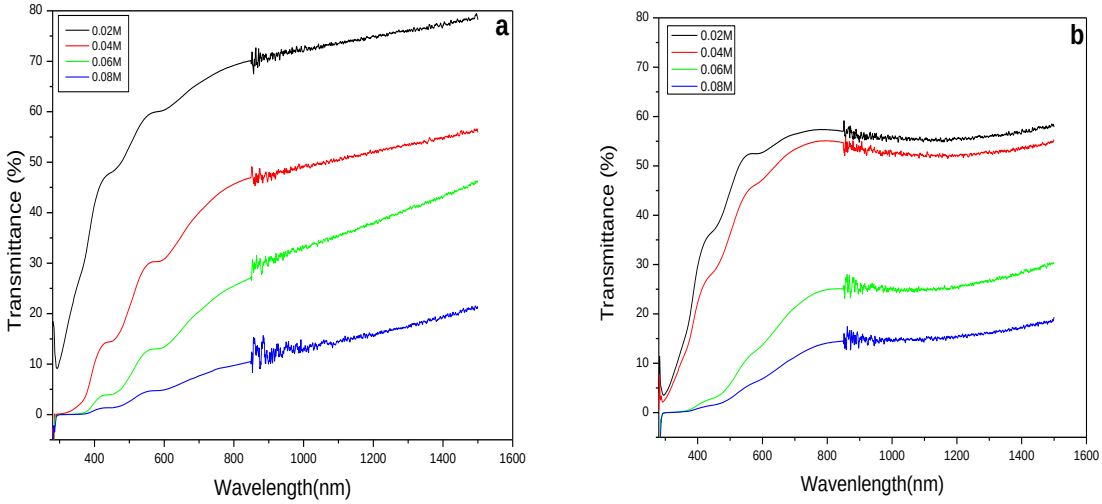

Figure II.7: Transmission spectra of Cr_2O_3 films prepared by different molar concentration (**a**) Chrome chloride, (**b**) Chromium nitrate precursors.

As observed, the average transmittance of these films overall decreased gradually versus the increase in the precursor concentration. The prepared film with Chrome chloride has a transparency of 75% to 15%, it is higher than that prepared with chromium nitrate 60% to 15%.The reduction of transmittance at higher molar concentration is due to the increase in the thickness of the films, and roughness of thin film can also affect its optical properties, i.e., more roughness causes the light scattering at the surface and degrade its transparency, which consistent with SEM images.

The 0.01M thin film shows sufficient transparency for applications in thin film solar cells and electro chromic windows.

Also, it can be seen in Fig.II.7, a fall in T% for wavelengths around 350 nm which is the absorption edge in the Cr_2O_3 films due to the transition electronic between the valence and the conduction bands. In addition to the absorption edge, two broad peaks are also observed at 455 and 600 nm, depicting two regions of d-d optical transitions. Absorption bands are assigned to the charge transfer of $^4A_{2g} \rightarrow {}^4T_{1g}$ at higher energy region and $^4A_{2g} \rightarrow {}^4T_{2g}$ at lower energy region of Cr^{3+} ions [10, 11]. The absorption edge of Cr_2O_3 thin films shifted towards a higher wavelength region (red shift) with the increase in the precursor concentration.

The optical energy gap (E_g) was calculated with the presumption that direct transitions between the edges of the valence and conduction bands were possible.

Equation (I.6) was used to calculate the energy gap, and by drawing a straight line between $(hv)^2$ and (hv) in eV, one may determine the direct band gap's value as shown in **figure II.8**.

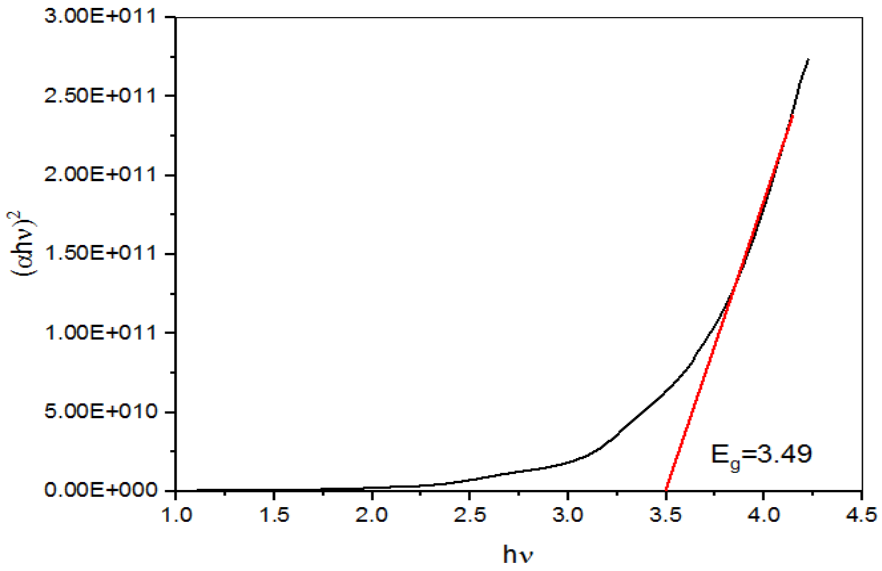

Figure II.8: Determination of the band gap (Eg) for the film Cr_2O_3 at 450°C.

The optical band gaps (Eg) of the films based on Tauc formula for direct band gap semiconductors and Urbach energy E_U (see eq I.7), which characterizes the disorder in the film, are presented in **figure II.9.**

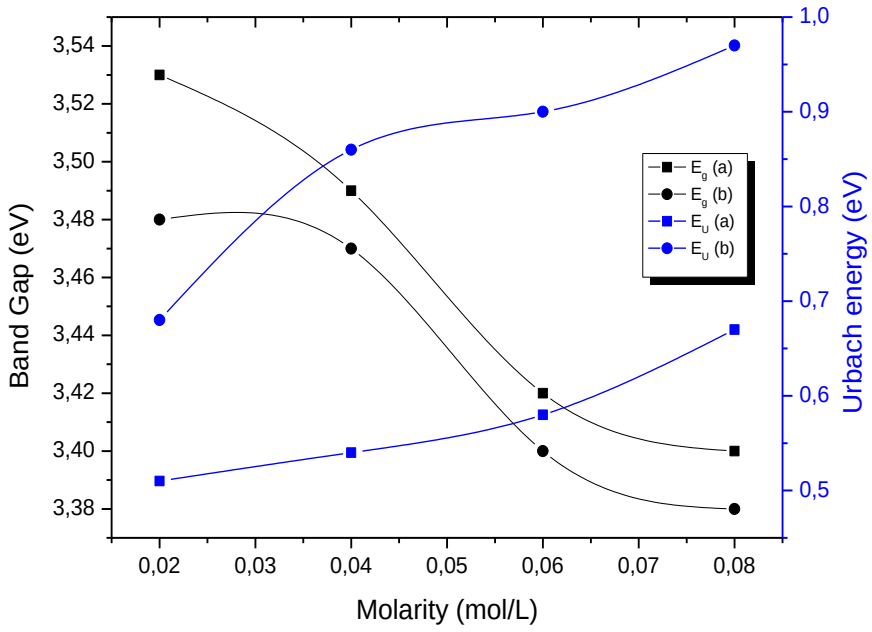

Figure II.9 Variation of band gap and band tail width versus solution concentration for films prepared with (a) Chrome chloride and (b) Chromium nitrate.

From table (II.5), we can see that the calculated optical band gap energy of Cr_2O_3 films prepared with chloride is larger than those prepared with nitrate. A slight decrease in optical band gap for both of them was observed with the increase of solution concentration.

This narrowing effect in band gap is referred to the increase in the band tail width (Urbach energy). Which is due to the formation of crystal defects which create lattice strain in the film due to their preparation conditions (as discussed in XRD analysis); this leads to the formation of allowed states between the forbidden gap [12, 13].

Analogous results of Eg values are reported by Jarnail Singh [11] (3.49-3.64 eV), T. Larbi [15] (3.38 eV). The values of Urbach energy (table II.5) for the films elaborated with chromium chloride is lower than the value for the films prepared with chromium nitrate; this is due to the poor crystallinity of the latter (presence of amorphous phase), as deduced from the XRD analysis. Our values of Eu are higher than the value obtained by Jarnail Singh [16] (0.28 eV) for the epitaxial Cr_2O_3 thin film prepared by PLD.

Table II.5: *The electrical and optical parameters values of the deposited Cr_2O_3 thin films.*

M (mol/L)	Chrome chloride					Chromium nitrate				
	Thickness (nm)	**Eg (eV)**	**E_U (eV)**	**R_{sh}* 10^2 (Ω)**	**σ $(\Omega.cm)^{-1}$**	**Thickness (nm)**	**Eg (eV)**	**E_U (eV)**	**R_{sh}* 10^2 (Ω)**	**σ $(\Omega.cm)^{-1}$**
0.02	274	3.53	0.51	73	4.99	270	3.48	0.68	67	5.53
0.04	334	3.49	0.54	58	5.16	307	3.47	0.86	66	4.94
0.06	513	3.42	0.58	65	2.99	455	3.40	0.90	65	3.38
0.08	666	3.40	0.67	64	2.35	632	3.38	0.97	59	2.68

II.2.5. Electrical properties

The sheet resistance (R_{sh}) of Cr_2O_3 thin films was measured by four-point probe method in dark and at room temperature. The conductivity (σ) of films can be estimated using the formula given previously (eq. I.10) [17].

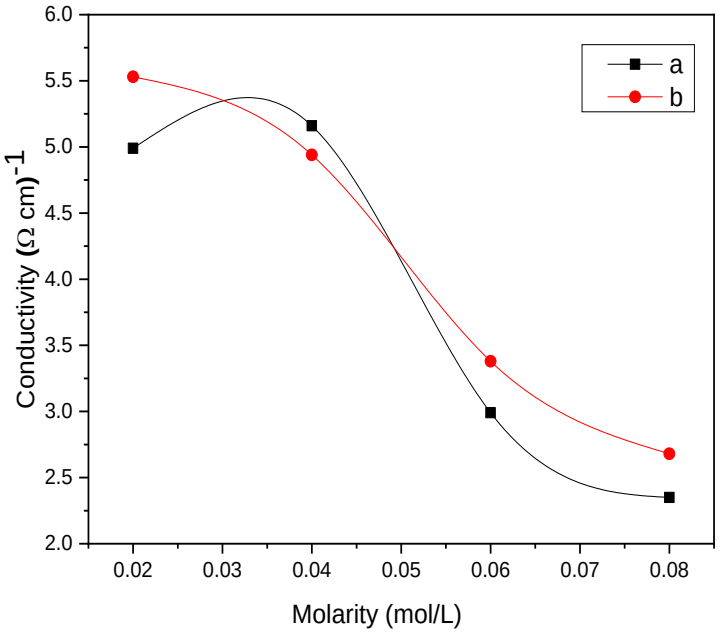

Figure II.10: Electrical conductivity variations of Cr_2O_3 thin films as a function of precursor molarity (a) Chrome chloride and (b) Chromium nitrate.

The electrical conductivity (σ) shows a decreases behavior with the increase of concentration from 0.02 M to 0.08 M. It is decreased from 4.99 $(\Omega.cm)^{-1}$ to 2.35$(\Omega.cm)^{-1}$ for Chromium chloride and from 5.53 $(\Omega.cm)^{-1}$ to 2.68 $(\Omega.cm)^{-1}$ for chromium nitrate. We believe that the decrease of conductivity is attributed to the decrease of carrier's mobility. The XRD and SEM analyses shown a decrease of crystallite size, this leads to an increase in the trapping states at grain boundaries and in the other hand the increase in band tail width (Urbach energy) which characterize the disorder in the film. For sheet resistance values in Table 3 we can see that the values are decreasing but the values are near to each other.

However, the obtained values of conductivity are much higher than those reported in the literature [11] where the work of Jarnail Singh (the order of $10^{-2}(\Omega.cm)^{-1}$) deals with Cr_2O_3 thin film prepared using the PLD technique and Elisabetta Arca [18] (the order of $10^{-3}(\Omega.cm)^{-1}$) for Cr_2O_3 thin film deposited by spray-pyrolysis.

Conclusion

In this study Cr_2O_3 thin films were grown on glass substrates using chromium chloride and chromium nitrate with different concentrations of precursor (0.02, 0.04, 0.06 and 0.08 mol/L) using home-made pneumatic spray pyrolysis system (SPT).

The sample obtained from the nitrate solution is thinner than that deposited using the chloride solution; this is certainly due to the contribution of several physico-chemical factors entering into the film's growth mechanisms. X-ray diffraction reveals a polycrystalline nature for all films prepared with chromium chloride with a preferred grain orientation along to (110) plane, whereas those prepared with low concentration of chromium nitrate have a poor crystallinity. Crystallites sizes of the films have been found to be decreasing from 56 to 33 nm and from 38 to 19 nm for chromium chloride and chromium nitrate respectively. SEM images revealed that the films were well adherent, uniform, pore and crack –free. The films prepared with chromium nitrate as starting solution have approximately the same density and smooth surface morphology at low concentrations. Whereas films obtained from chromium chloride were rough and consist sub-micrometer crystallites distributed in a uniform manner over the surface. The optical study confirms that the transmittance of Cr_2O_3films decreases with the increase of precursor concentration and are strongly affected by the nature of the starting solution. The average transmittance of the films deposited from chromium nitrate is in the range of 60 % (Eg varies from 3.38 to 3.48 eV) and for the films deposited from chromium chloride, it attains 75 % in the visible region (Eg varies from 3.40 to 3.53 eV).The electrical conductivity of the films found in the order of 5 $(\Omega.cm)^{-1}$.

Finally, the present contribution clearly indicated that the molarity and nature of the starting solution are important parameters and affects significantly the physical properties of Cr_2O_3 films. The combination of high visible transmittance, high conductivity, and good structural and morphological properties makes that the Cr_2O_3 films which are deposited especially using chromium chloride at 0.04mol/l are a suitable p-type transparent conducting oxide for usage in many optoelectronic devices and solar cells applications.

References

[1] T. G. Wang, Y. Dong, Y. Liu, S. Iyengar, K. H. Kim, and Z. Yang, “In-situ heat treatment study on the nanocrystalline Cr 2 O 3 film using an environmental scanning electron microscope,” *Coatings*, vol. 7, no. 12, 2017, doi: 10.3390/coatings7120225.

[2] Sâad RAHMAN, “Elaboration Et Caracterisation De Couches Minces Par Spray Pyrolyse Et Pulverisation Magnetron,” p. 158, 2008, [Online]. Available: http://thesis.univ-biskra.dz/1064/1/phy_d1_2008.pdf

[3] Z. T. Khodair, G. A. Kazem, and A. A. Habeeb, “Studying the optical properties of (Cr2 O3:I) thin films prepared by spray pyrolysis technique,” *Iraqi J. Phys.*, vol. 10, no. 17, pp. 83–89, 2012.

[4] R. Gago, M. Vinnichenko, R. Hübner, and A. Redondo-cubero, “Bonding structure and morphology of chromium oxide fi lms grown by pulsed-DC reactive magnetron sputter deposition,” *J. Alloys Compd.*, vol. 672, pp. 529–535, 2016, doi: 10.1016/j.jallcom.2016.02.194.

[5] A. Abdelkrim, S. Rahmane, K. Nabila, A. Hafida, and O. Abdelouahab, “Polycrystalline SnO2 thin films grown at different substrate temperature by pneumatic spray,” *J. Mater. Sci. Mater. Electron.*, vol. 28, no. 6, pp. 4772–4779, 2017, doi: 10.1007/s10854-016-6122-9.

[6] Kouidri , Nabila and Rahmane , Saâd, “Effect of Cobalt Chloride Concentration on Structural, Optical and Electrical Properties of Co3O4 Thin Films Deposited by Pneumatic Spray,” *J. New Technol. Mater.*, vol. 10, no. 1, pp. 56–62, 2020, doi: 10.12816/0058152.

[7] K. H. Stern, “High Temperature Properties and Decomposition of Inorganic Salts Part 3, Nitrates and Nitrites,” *J. Phys. Chem. Ref. Data*, vol. 1, no. 3, pp. 747–772, 1972, doi: 10.1063/1.3253104.

[8] A. Malecki, B. Malecka, R. Gajerski, and S. Labuś, “Thermal decomposition of chromium(III) nitrate(V) nanohydrate. Different chromium oxides CrO1.5+y formation,” *J. Therm. Anal. Calorim.*, vol. 72, no. 1, pp. 135–144, 2003, doi: 10.1023/A:1023915618876.

[9] T. Larbi, M. A. Amara, B. Ouni, and M. Amlouk, “Enhanced photocatalytic degradation of methylene blue dye under UV-sunlight irradiation by cesium doped chromium oxide thin films,” *Mater. Res. Bull.*, vol. 95, pp. 152–162, 2017, doi: 10.1016/j.materresbull.2017.07.024.

[10] J. Wang, A. Gupta, and T. M. Klein, “Plasma enhanced chemical vapor deposition of Cr 2 O 3 thin films using chromium hexacarbonyl (Cr (CO) 6) precursor,” vol. 516, pp. 7366–7372, 2008, doi: 10.1016/j.tsf.2008.02.027.

[11] J. Singh, R. Kumar, V. Verma, and R. Kumar, “Structural and optoelectronic properties of epitaxial Ni-substituted Cr2O3 thin films for p-type TCO applications,” *Mater. Sci. Semicond. Process.*, vol. 123, no. September 2020, p. 105483, 2021, doi: 10.1016/j.mssp.2020.105483.

[12] M. Roy, S. Ghosh, and M. K. Naskar, “Solvothermal synthesis of Cr 2 O 3 nanocubes via template-free route,” vol. 159, pp. 101–106, 2015.

[13] A. Abdelkrim, S. Rahmane, O. Abdelouahab, A. Hafida, and K. Nabila, “Optoelectronic properties of SnO2 thin films sprayed at different deposition times,” *Chinese Phys. B*, vol. 25, no. 4, 2016, doi: 10.1088/1674-1056/25/4/046801.

[14] H. Attouche, S. Rahmane, S. Hettal, and N. Kouidri, “Precursor nature and molarities effect on the optical, structural, morphological, and electrical properties of TiO2 thin films deposited by spray pyrolysis,” *Optik (Stuttg).*, vol. 203, 2020, doi: 10.1016/j.ijleo.2019.163985.

[15] T. Larbi, B. Ouni, A. Gantassi, K. Doll, M. Amlouk, and T. Manoubi, “Structural, optical and vibrational properties of Cr2O3 with ferromagnetic and antiferromagnetic order: A combined experimental and density functional theory study,” *J. Magn. Magn. Mater.*, vol. 444, pp. 16–22, 2017, doi: 10.1016/j.jmmm.2017.07.103.

[16] S. Arulkumar, S. Parthiban, A. Goswami, R. S. Varma, M. Naushad, and M. B. Gawande, “Ac ce pte d M us pt,” *Mater. Today Proc.*, vol. 27, no. xxxx, pp. 0–31, 2019, [Online]. Available: https://doi.org/10.1016/j.matpr.2019.12.188%0Ahttps://doi.org/10.1016/j.matpr.2019.09.090%0Ahttps://doi.org/10.1080/14484846.2018.1432089

[17] A. Abdelkrim, S. Rahmane, O. Abdelouahab, N. Abdelmalek, and G. Brahim, “Effect of solution concentration on the structural, optical and electrical properties of SnO2 thin films prepared by spray pyrolysis,” *Optik (Stuttg).*, vol. 127, no. 5, pp. 2653–2658, 2016, doi: 10.1016/j.ijleo.2015.11.232.

[18] E. Arca, K. Fleischer, S. A. Krasnikov, and I. Shvets, “Effect of chemical precursors on the optical and electrical properties of p-Type transparent conducting Cr2O3:(Mg,N),” *J. Phys. Chem. C*, vol. 117, no. 42, pp. 21901–21907, 2013, doi: 10.1021/jp404230k.

Chapter III: *Influence of substrate temperature on Cr_2O_3 thin films properties*

Introduction

The property of the film depends upon several factors such as the molar concentrations, the thickness, the doping agent, the annealing temperature and even the measurement conditions.

In this chapter, the effect of substrate temperature on the structural, morphological, optical and electrical properties of chromium oxide films is studied. Cr_2O_3 solution was prepared by dissolving 0.04M of chromium chloride hexahydrate ($CrCl_3 \bullet 6H_2O$) dissolved in distilled water. The solution was sprayed on heated glass substrates at various substrate temperatures (350 - 550 °C) by spray pyrolysis method.

III. Results and discussion

III.1. Adhesion and Thickness measurement

The ribbon (scotch) tape test is the quickest qualitative measure of film adhesion, and it has shown that our films have good adhesion and uniformity. Except for the film deposited at 350 °C, which had a rough surface and poor adhesion, which is due to the insufficient temperature to complete the chemical reaction and decompose the sprayed droplets of Cr ions from the solution.

Cr_2O_3 is produced as a result of the fine droplets of aqueous chromium chloride solution thermally decomposing on the glass substrate. The possible chemical reaction is as follows:

$$2CrCl_3 \cdot 6H_2O \rightarrow Cr_2O_3 + 6HCl \uparrow + 9H_2O \uparrow$$

The thicknesses of the films can be estimated using the formula given previously (eq. I.1) which is listed in Table 2. It is clear from the **figure III.1** that the thicknesses of the Cr_2O_3 thin films decreases with increasing the substrate temperature. This decrease may be attributed to re-evaporation of film material after deposition at higher substrate temperatures which results to removal of the secondary volatile products or to thermal convection of the sprayed droplet during the deposition process [1]. In addition, Water loss or interlayer water removal with subsequent formation of the compact Cr_2O_3 film is another factor that may explain the thickness decrease [2].

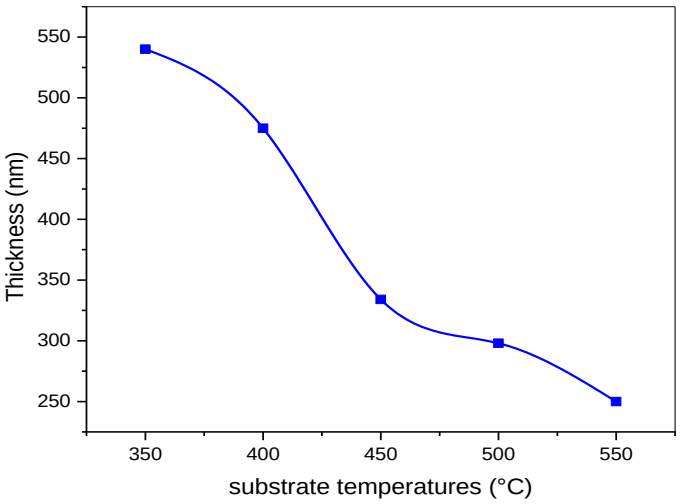

Figure III.1: Variation of the thickness of the Cr_2O_3 thin films as a function of the substrate temperature.

III.2. Structural properties

Figure III.2 shows the X-ray diffraction (XRD) patterns of Cr_2O_3 thin films at various substrate temperatures 350, 400, 450,500 and 550°C.

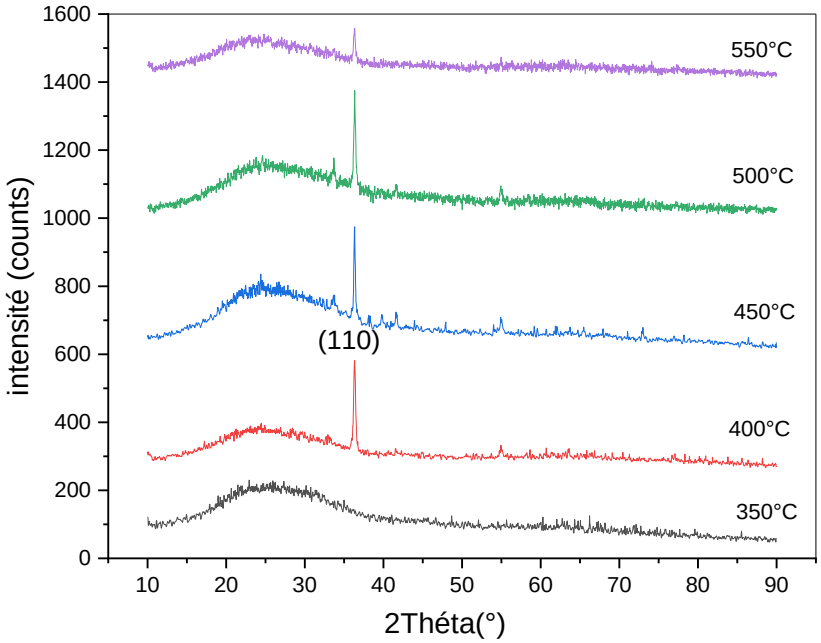

Fig III.2: XRD diffraction patterns of Cr_2O_3 thin film with different substrate temperature.

As observed, the film at 350˚C shows that the film is amorphous. As reported by J. Liang et al [3]. This shows that low temperature is not enough for the formation of the crystallization process, which limits the crystal's ability to grow because of the limited atomic mobility [4]. Whereas at high substrate temperature from 400 to 550 °C the films are crystalline. The patterns display diffraction peak at a value of 36°, which corresponds to the (110) crystalline plane of the Cr_2O_3 with a rhombohedral structure. This means that the Cr_2O_3 films showed a preferred orientation to the substrate surface (using JCPDS 00-001-1294 as reference). It can be noticed that the (110) peak becomes more intense and sharper with increasing substrate temperature from 400 °C to 500 °C, indicating film crystallinity improvement. At high substrate temperature (550 °C) the intensity of the peak (110) decreases this results from the atom's disintegrated and re-evaporated at high temperatures [5].

The crystallite size and strain of the Cr_2O_3 films were calculated from the intense peak (110).

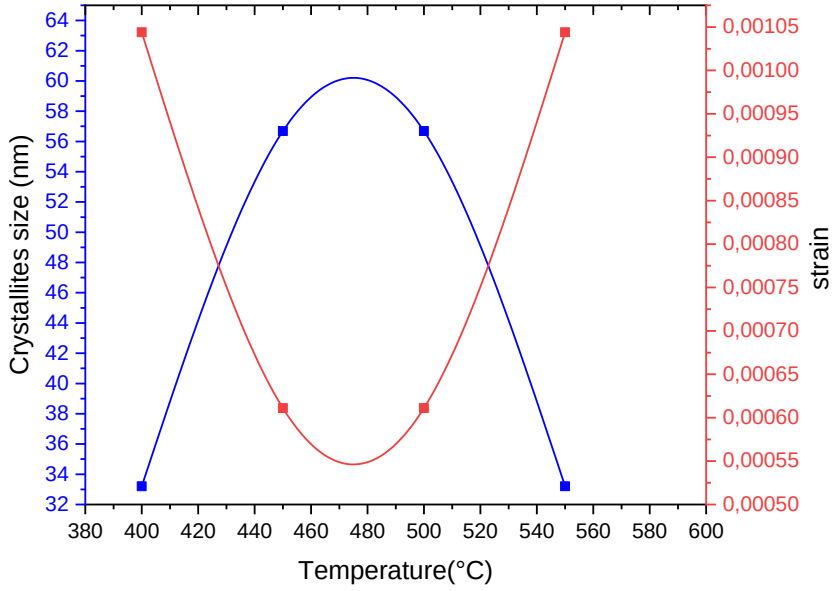

Figure III.3: Variation of the crystallite size and strain of the Cr_2O_3 thin films as a function of the substrate temperature.

It was observed from the **Figure III.3** that the crystallite size of the films increases with the increase in substrate temperature from 400 to 500°C then the crystallite size decreases at temperature 550°C. We note that there is an inverse relationship between the crystal size and microstrain. The increase in crystallite size (film crystallinity improvement)

may be due to the atoms' diffusion activation energy being sufficient for them to occupy the energetically ideal location in the crystal lattice.

III.3. Elemental analysis and morphological study

Figure III.4 shows the scanning electron micrographs of Cr_2O_3 films at different substrate temperatures using spray pyrolysis. The surface morphologies show that the growth mechanism of the thin film depends clearly on substrate temperatures.

The film prepared under 400 °C is inhomogeneous and has a rougher surface and forms degraded agglomerations. The more roughness is probably due to temperature witch is not sufficient to make complete diffusion, when most microdroplets arrive at the substrate surface in a wet state; the low deposition temperature is insufficient to evaporate the droplets. Higher temperatures result in a smoother and more homogeneous surface. The atoms absorb more energy from the substrate and then undergo a pyrolytic process on the substrate's surface. Where the rate of evaporation is high enough to create a more complete and evenly distributed film. It was determined that the surface homogeneity of the films improves with increasing substrate temperature[6].

In addition, EDX spectra revealed the presence of Cr and O atoms in the synthesized films. The Si element may have resulted from the glass substrates. It was clearly seen from the table (III.1) that the atomic percentage of Cr element decreased and Si increased with increasing substrate temperature, which may be due to the decrease in the film thickness.

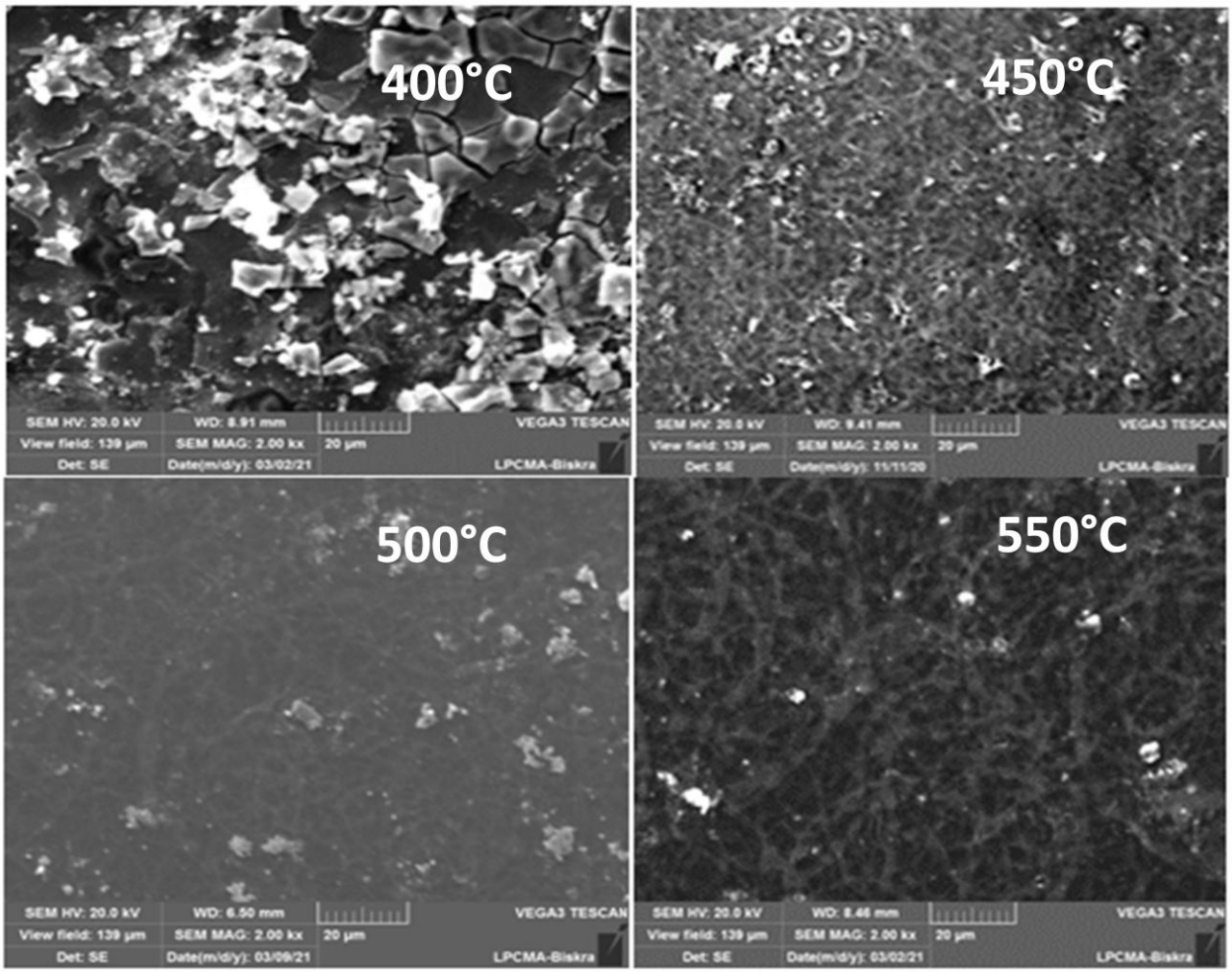

Figure III.4: SEM surface images of the Cr_2O_3 thin films deposited with different substrate temperature.

Table III.1: *Atomic percentage of chemical composition in Cr_2O_3 films.*

[at. %]				
	400°C	**450°C**	**500°C**	**550°C**
Cr	24.38	17.24	27.82	16.24
O	75.62	82.66	72.18	83.76

III.4. Optical properties

Figure III.5 represents the optical transmission of Cr_2O_3 thin films in the wavelength range of 290 to 1500 nm for different substrate temperature (350–550°C).The transmission spectra can be roughly divided into three regions : transparent region (600–1500 nm) the average transmittance value within the region was found for the films prepared at 400 °C,

450 °C, 500 °C and 550 °C reaches to 48%, 55%,68% and 76%, respectively, medium absorption region (400–600 nm) and strong absorption region (300–400 nm). The spectra exhibit a shift in the fundamental absorption edge towards low wavelengths due to the variation of substrate temperature. We note a low transmittance value and disappearing the absorption edge at temperature 350°C due to the surface roughness and a large thickness of the film. It can be seen that the optical transmittance increases with increasing temperature, the same behavior is reported by Pingli Qin et al [6, 7,8]. This increase in transmittance of the films is related to improvement of crystallinity and surface homogeneity of the films may be due to the decreased in optical scattering and defects.

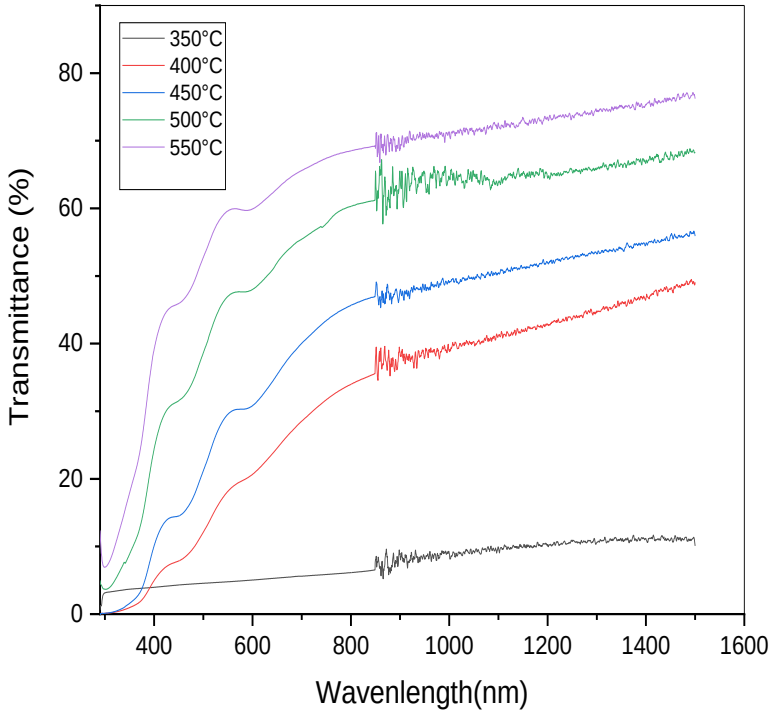

Figure III.5: The transmittance of Cr_2O_3 thin films for different substrate temperatures.

Figure III.6 shows the reflectance spectra of Cr_2O_3 thin layers at different temperature. It was observed that the reflectance of films increased with increasing substrate temperature and decreases with an increase in wavelength. It was seen that the reflection values are low in the visible and near IR region may be due to some optical transitions at the band gap.

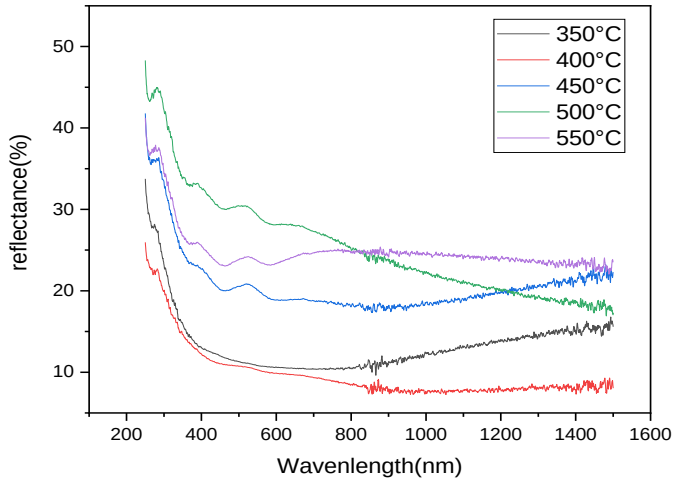

Figure III.6: The reflectance of Cr_2O_3 thin films for different substrate temperatures.

Table III.2: *The electrical and optical parameters values of the deposited Cr_2O_3 thin films.*

T(°C)	Chrome chloride				
	Thickness (nm)	**Eg (eV)**	**E_U (eV)**	**R_{sh} (Ω)**	**σ $(\Omega.cm)^{-1}$**
350	540	/	/	/	/
400	475	3.46	0.62	6100	3.45
450	334	3.49	0.54	5800	5.16
500	298	3.52	0.23	2020	16.61
550	250	3.58	0.21	3225	12.40

The optical gap energy of thin films is determined according to Tauc formula (equation I.6), E_g are determined by plotting $(\alpha h\upsilon)^2$ versus $(h\upsilon)$ and extrapolating of the linear region of the plot to zero absorption($(h\upsilon)^2= 0$). The Urbach energy (E_U) can be estimated from the inverse slope of the linear plot between $\ln(\alpha)$ and $h\upsilon$.

The optical band gap energy (E_g) and the Urbach energy E_U of the Cr_2O_3 thin film are shown in **Figure III.7** as a function of the substrate temperature.

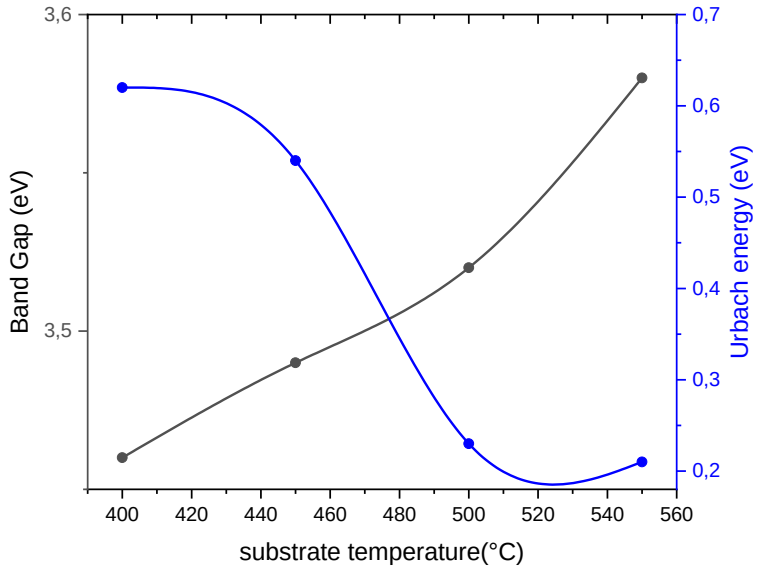

Figure III.7: Variation of band gap and band tail width for different substrate temperatures.

The estimated values of the optical band gap and Urbach energy are plotted in **figure III.7** as a function of substrate temperature. It was observed that the band gap increases from 3.46 to 3.58 eV with increase in substrate temperature, the same variation was observed in literature [7][10]. This widening of band gap leading to a blue shift of the optical transmittance may be accused by populating states within the valence band with holes as the oxygen concentration increases, the Fermi level is pushed to a lower energy, which increases the band gap calculated from the start of inter-band absorption. Which was in good agreement with report[11].

The Urbach energy is related to the disorder in the film network. We can see that Urbach energy decreases with increase in substrate temperature, where the decrease in Urbach energy is attributed to the decrease of the defects, which is attributed to the improvement in the crystal structures.

III.5. Electrical properties

Table (III.2) shows the sheet resistance (R_{sh}) and conductivity of Cr_2O_3 thin films measured at different substrate temperatures. Here, R_{sh} values decrease with substrate temperature up to 500 °C and then increase for the film deposited at 550 °C. As the electrical conductivity is inversely proportional to the sheet resistance.

Figure III.11 shows the variation of electrical conductivity of Cr_2O_3 thin films as a function of the substrate temperature. From this figure, we observe that the conductivity increases with substrate temperature. The increase in conductivity is probably caused by an increase in free charge carriers (holes) in the layers, which can be explained by an increase of oxygen absorption from air[11].

However, the structural and surface qualities of the films improved with rising substrate temperature, as seen by XRD patterns and SEM micrographs.The increase of the grain size gives rise to a reduced concentration of structural defects such as dislocations and grain boundaries. It is possible to explain the increase in conductivity by the increase in free charge carriers (holes) and/or by the increase of carrier's mobility in the layers as a result of the decreased stress. As can be seen, The maximum recorded value was 16 $(\Omega.cm)^{-1}$ for the film deposited at 500°C.

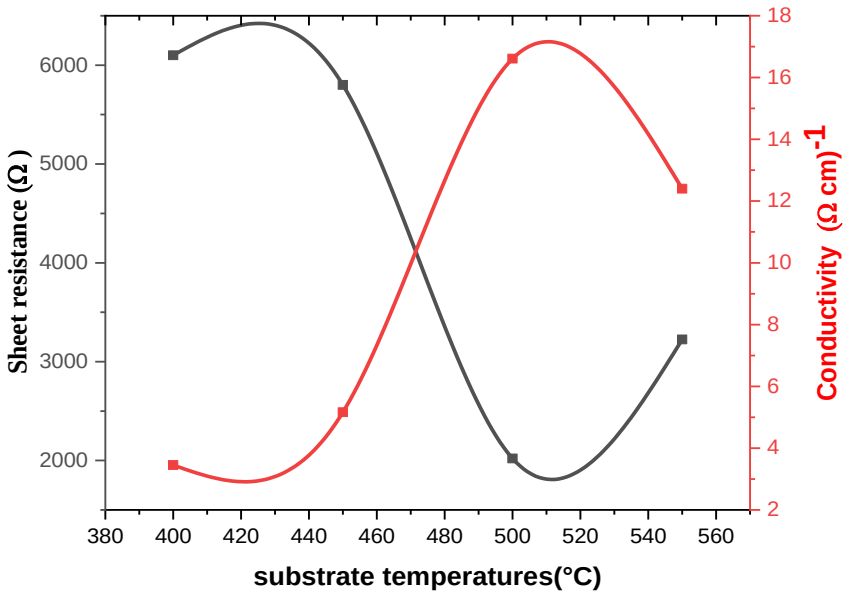

Figure III.8: Variation of electrical conductivity and sheet resistance of Cr_2O_3 thin films for different substrate temperatures.

Conclusion

In the present work, Chromium oxide thin films have been successfully deposited onto glass substrates using a pneumatic spray pyrolysis system (SPT) at various substrate temperatures (350-550 °C). All films have a rhombohedral structure with preferred orientation along the (110) plane at 2θ = 36° except for the film deposed at 350 °C, which has poor crystallinity. The crystallite size of the films has been found from 33 to 58 nm. The surface homogeneity of the films improves with increasing substrate temperature. The optical study confirms that the transmittance of Cr_2O_3 films increases with increasing substrate temperature and the energy gap increases from 3.46 to 3.58 eV. Electrical measurements showed that substrate temperatures increase the electrical conductivity from 3.45 to 16.61 $(\Omega.cm)^{-1}$ and sheet resistance decreases with substrate temperature increase.

References

[1] H. Kamal, E. K. Elmaghraby, S. A. Ali, and K. Abdel-Hady, "Characterization of nickel oxide films deposited at different substrate temperatures using spray pyrolysis," *J. Cryst. Growth*, vol. 262, no. 1–4, pp. 424–434, 2004, doi: 10.1016/j.jcrysgro.2003.10.090.

[2] S. A. Mahmoud, A. Shereen, and M. A. Tarawnh, "Structural and Optical Dispersion Characterisation of Sprayed Nickel Oxide Thin Films," *J. Mod. Phys.*, vol. 02, no. 10, pp. 1178–1186, 2011, doi: 10.4236/jmp.2011.210147.

[3] J. Liang, G. F. Pan, S. Bin Fan, W. L. Cheng, and Z. Y. Tian, "CVD synthesis and catalytic combustion application of chromium oxide films," *Phys. Status Solidi Curr. Top. Solid State Phys.*, vol. 12, no. 7, pp. 1001–1005, 2015, doi: 10.1002/pssc.201510019.

[4] S. J. Kang, Y. H. Joung, H. H. Shin, and Y. S. Yoon, "Effect of substrate temperature on structural, optical and electrical properties of ZnO thin films deposited by pulsed laser deposition," *J. Mater. Sci. Mater. Electron.*, vol. 19, no. 11, pp. 1073–1078, 2008, doi: 10.1007/s10854-007-9469-0.

[5] M. Liu *et al.*, "Effect of temperature on pulsed laser deposition of ZnO films," *Appl. Surf. Sci.*, vol. 252, no. 12, pp. 4321–4326, 2006, doi: 10.1016/j.apsusc.2005.07.038.

[6] A. V Almaev, B. O. Kushnarev, E. V Chernikov, V. A. Novikov, P. M. Korusenko, and S. N. Nesov, "Superlattices and Microstructures Structural , electrical and gas-sensitive properties of Cr 2 O 3 thin films," *Superlattices Microstruct.*, vol. 151, no. February, p. 106835, 2021, doi: 10.1016/j.spmi.2021.106835.

[7] P. Qin *et al.*, "Organic solar cells with p-type amorphous chromium oxide thin film as hole-transporting layer," *Thin Solid Films*, vol. 519, no. 13, pp. 4334–4341, 2011, doi: 10.1016/j.tsf.2011.02.013.

[8] A. B. C. Ekwealor, "Variations of optical and structural properties with temperature for CrxOy thin films synthesized in a polymer matrix by chemical bath deposition technique," *Dig. J. Nanomater. Biostructures*, vol. 9, no. 1, pp. 423–431, 2014.

[9] M. Hamam, Y. El-Gendy, M. S. Selim, A. M. Salem, and N. H. Teleb, "Optical properties of thermally evaporated AgSbSe2 thin films," *J. Appl. Sci. Res.*, vol. 5, no. 12, pp. 2323–2331, 2009.

[10] M. N. Adabiah, "Substrate temperature effects on reactively sputtered Cr 2 O 3 / n-Si heterojunctions Substrate temperature effects Cr 2 O 3 / n-Si heterojunctions on

reactively sputtered", doi: 10.1088/1742-6596/707/1/012026.

[11] N. Kouidri, S. Rahmane, and A. Allag, "Substrate temperature-dependent properties of sprayed cobalt oxide thin films," *J. Mater. Sci. Mater. Electron.*, vol. 30, no. 2, pp. 1153–1160, 2019, doi: 10.1007/s10854-018-0384-3.

Chapter IV: *Structural, optical and electrical properties of In-doped Cr_2O_3 thin films*

Introduction

Doping is an important approach for enhancing the optical and electrical properties of Cr_2O_3 thin films. For instance, Zn-doped chromium oxide (Cr_2O_3) and Ti-doped chromium oxide (Cr_2O_3) provided high sensitivity and rapid presence times for NH_3 and NO_2 gases, respectively [4,5]. Kamble et al. [6] reported that Pt-doped Cr_2O_3 leads to the enhancement of sensor response, as well as, an improvement in its kinetics. Arca et al. [8] reported that the Co-doping of Cr_2O_3 thin films with magnesium and nitrogen produces a p-type oxide with low resistivity and high transparency in the visible region. The results obtained by Larbi et al. [9] state that Cs-doped Cr_2O_3 promotes good photocatalytic activity under sunlight for methylene blue degradation. Zihao Fan et al. [10] revealed that the Ni-doped Cr_2O_3 films have remarkable photoelectric response during the infrared, visible and ultraviolet light range. Also, many researchers have studied the effect of Cu and Mg-doped Cr_2O_3 on the structural, electrical, and optical transmission properties[11,12]. In the literature, there is no study on In-doped Cr_2O_3. Indium (In) is a potential dopant thanks to its considerable chemical stability, high electrical conductivity, and high transparency. Furthermore, we expect that Cr_2O_3 doping with indium should improve its optical and electrical properties to produce efficiency-enhanced electronic devices for optoelectronic applications.

Pneumatic spray pyrolysis is a simple and low-cost method. To improve the properties of chromium oxide thin films, In-doped Cr_2O_3 thin films were prepared by using the spray pyrolysis technique. The effects of indium concentrations (wt. %) on the structural, morphological, optical, and electrical properties were investigated and discussed.

IV.1. Experimental details

Indium-doped Cr_2O_3 thin films were prepared onto a glass substrate of the type (TLC Silica gel 60 F254), with different Indium concentrations (0, 2, 4, 6, and 8 wt. %) by using a homemade spray pyrolysis experimental setup[13]. The spray solution was prepared by dissolving 0.04 M Chromium(III) chloride hexahydrate $CrCl_3 \cdot 6H_2O$ into distilled water, then indium chloride ($InCl_3$) was added into the solution as a dopant whose content was varied from 0 to 8wt. %.The sprayed solution was magnetically stirred to obtain a homogenous solution. The solution was sprayed on heated substrates at 500°C for 3min. The nozzle was located at a distance of 30 cm above the substrate. After deposition, the In-doped Cr_2O_3 thin films were allowed to cool to room temperature.

IV.2. Results and discussion

IV.2.1. Thickness measurements

A thermal decomposition occurs to the fine droplets of the solutions after their falling over the hot substrate surface resulting in the formation of uniform and well adherent (hardly peeled with scotch tape test) thin films. The film thickness (t) of Cr_2O_3 thin film is measured with the help of weight difference method using an electronic high-accuracy balance as shown in equation (I.1).

As listed in Table1, It can be seen that the thickness increases slightly from 298 to 362 nm with the increase of Indium doping concentration. For high values of In, there will be more Indium in the pulverized solution which leads to an increase in the mass transfer and solute atoms from the atomizer to the substrate; as a result, the reaction kinetics is accelerated, making a faster growth rate and thicker films.

IV.2.2.Structural properties

Figure IV.1 shows XRD patterns of In-doped Cr_2O_3 thin films which are polycrystalline and exhibit a strong orientation along (110) at 36°(ICDD n°: 00-038-1479). All the peaks corresponded to the pure rhombohedral structure of Cr_2O_3 thin films deposited at 500 °C with no other crystallographic phases related to In or impurity phase found in any of the thin films. It is observed that doping by 2, 4, and 8 wt. % of indium led to an obvious reduction in the intensity of the peak corresponding to the lattice plane (110), implying the deteriorated crystallinity. The decreasing peak intensity of Cr_2O_3 may be caused by a restrained quantity of indium atoms exists as interstitials sharing the oxygen with Cr atoms. A similar result has been reported for Ti and Cu doped Cr_2O_3[5,15], or by the formation of stress due to the difference in ionic radius between In^{3+} ions (0.80 A°) [16] and Cr^{3+} ions (0.63 A°)[17]. While 6 wt. % In-doped film shows enhancement in intensities of the peak caused by relaxed strain, which means that it has better crystallization.

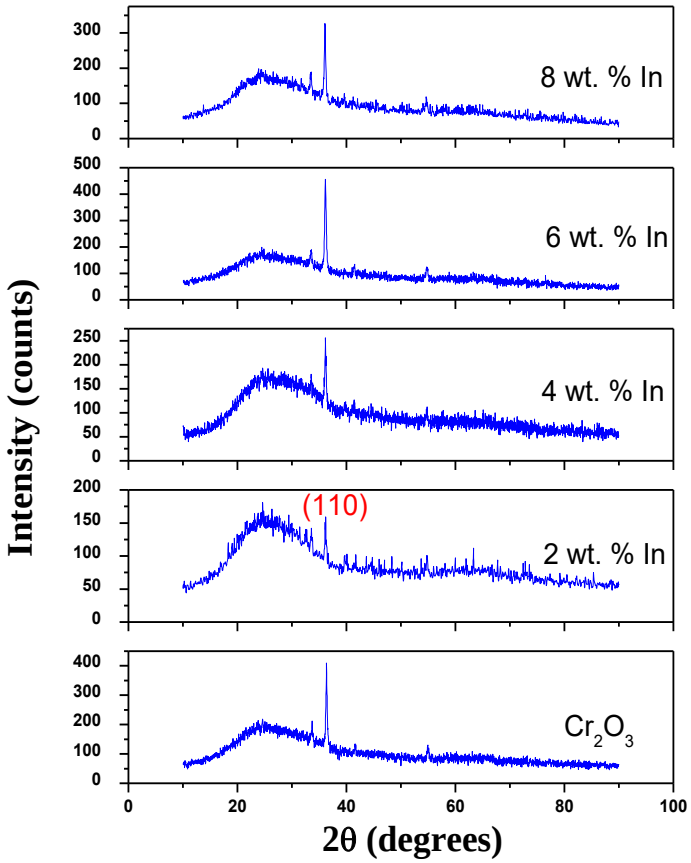

Figure IV.1: XRD pattern of In-doped Cr_2O_3 thin films.

The crystallite size (D) and the microstrain (ε) were calculated using (110) peak at angle θ=36 degrees by using the following formulas [18] (eq. I.4). The calculated values are given in table IV.1.

Table IV.1. *Values of Crystallites size and strain (ε) of In-doped Cr_2O_3 thin films.*

In concentration (wt. %)	Thickness (nm)	Crystallite size [nm]	Microstrain (ε) × 10^{-3}
Cr_2O_3	298	56.69	0.611
2	308	23.23	1.49
4	314	29.04	1.19
6	321	35.40	0.979
8	362	47.22	0.734

Figure IV.2 shows the crystallite size and the microstrain at different percentages of indium doping. The crystallite size decreases from 57 nm of the un-doped to 23 nm at 2 wt. % of indium

doped and it increases thereafter. This shows that, for the sample doped with 2%, indium could acts as a growth inhibitor of crystallites and then leads to a depressed crystallinity phenomenon, which may be due to the larger ionic radius of In^{+3} ions than Cr^{3+} ions. On the other hand, the microstrain increases up to 2% with the increase of In element and then it decreases. This behavior may be due to the formation of more structural disorders for the sample doped with 2% indium arising from In incorporation in the chromium oxide matrix during the chemical crystal growth process and leading to internal stress in the host lattice. Thereafter, the increase of crystallite size with the increase of dopant concentration is due to the strain relaxation process in the films. Similar results of estimated crystallite size have been reported by T. Larbi et al. [9] for Cs-doped Cr_2O_3 thin films that are greater than those obtained by Zekaik et al. [19] for Ni-doped Cr_2O_3 thin films.

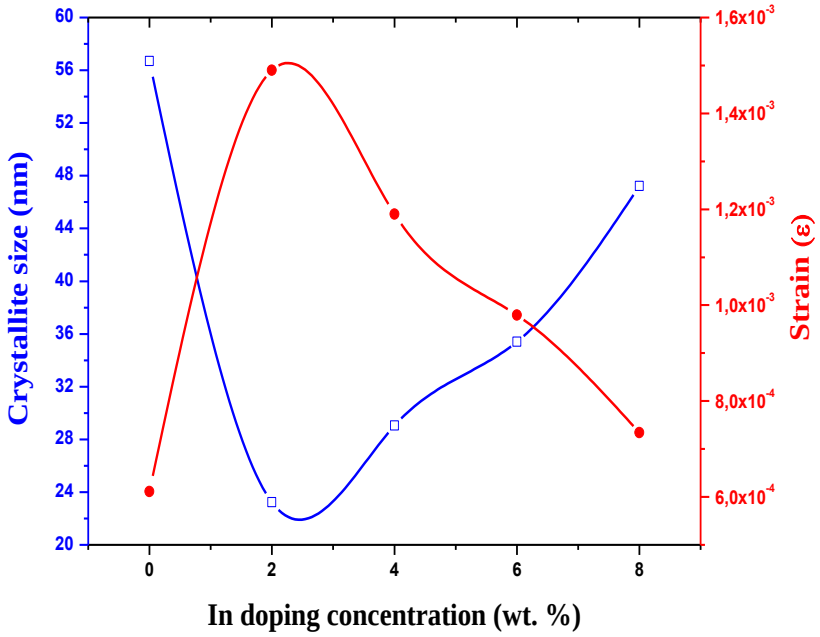

Figure IV. 2: The Variation of the crystallite size and strain versus indium concentrations.

IV.2.3.Elemental analysis and morphological study

The elemental analysis of un-doped and In-doped Cr_2O_3 thin films was determined by EDS. The atomic percentages of chemical composition are summarized in Table IV.2.

Table IV.2: *Atomic percentage of chemical composition of un-doped and In-doped Cr_2O_3 thin films.*

Chemical element	Atomic percentage				
	0%	2%	4%	6%	8%
Cr	27.82	15.38	15.25	20.21	19.03
In	0	0.73	0.74	1.06	1.17
O	72.18	83.89	84.01	78.83	79.80

The EDS spectra of films shown in **Figure IV.3** confirm the presence of Cr_2O_3, and indium in the films. The presence of Si element in films is probably from the glass substrate. The atomic percentage of indium in the doped films increased as the doping ratio, was increased while the Cr element decreases for 2 and 4 wt. %. As remarked, the variation of Cr percentage has the same tendency with grain size which may be the cause of the remarked behavior for chromium presence in the films. These results agree well with the XRD study, which very well supports the substitution of indium in the Cr sites as well, demonstrating that the indium is effectively doped in the Cr_2O_3 film.

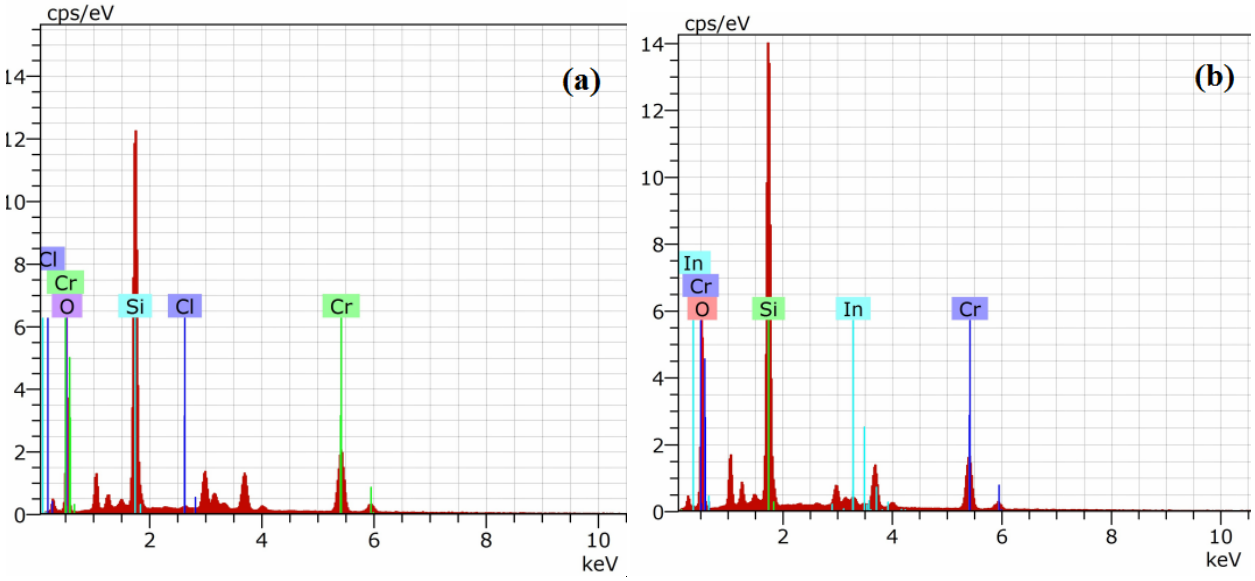

Figure IV.3: EDS spectra of: (a) intrinsic Cr_2O_3 and (b) 6 wt.% In-doped Cr_2O_3.

Figure IV.4 shows the SEM images of the indium-doped Cr_2O_3 films deposited with various concentrations of In (0–8 wt. %). Surface morphology analysis indicates that the substrates are well covered by all the films without cracks. The In-doped Cr_2O_3 films consist of grains that increase with the increase of In doping concentration. This is due to the large radius of In^{3+} ions with Cr^{3+}ions, which results in the appearance of defects and distortions at the level of the crystal lattice, which directly affects the surfaces of the films.

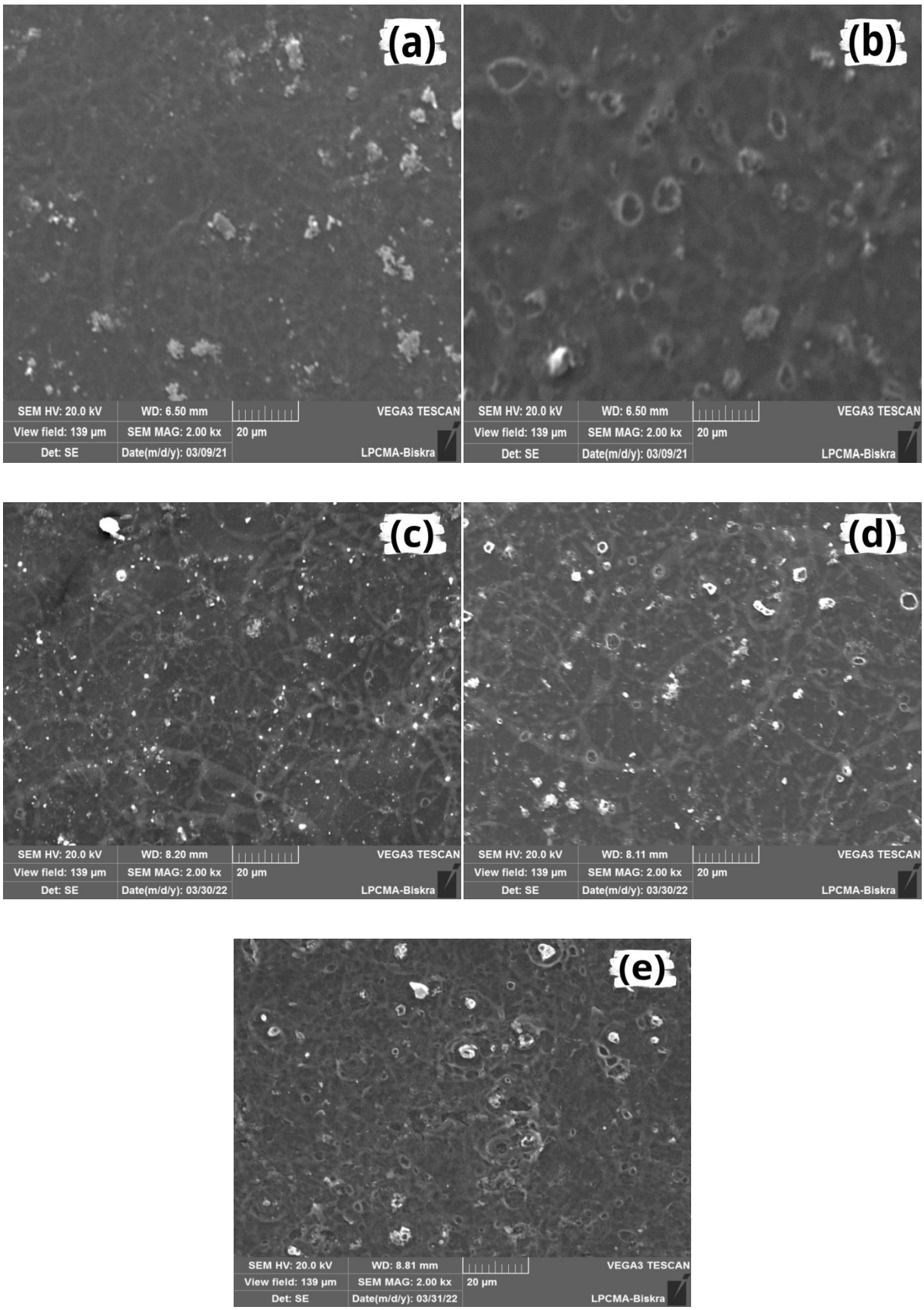

Figure IV.4: SEM images of In-doped Cr_2O_3: (a) Pure Cr_2O_3, (b) 2 wt.%, (c) 4 wt.%, (d) 6 wt.%, and (e) 8 wt.%.

IV.2.4. Optical properties

Optical transmission spectra of the pure and In-doped chromium oxide films in the wavelength region of 290–1500 nm are shown in Fig IV.5. The transmittance of un-doped Cr_2O_3 thin film is about 65%. It has been observed that the indium-doped chromium oxide improved the optical transmittance. A similar result has been reported for In-doped CdO [20]. The transparency increases from 65 to 94% with the increase of indium concentration up to 4wt. % in Cr_2O_3 films and then it decreases. The decrease in transmittance above 4 wt. % of In-doping may be due to the incorporation of more indium in the lattice sites and the interstitial positions, thus leading to an increase in the absorption, or the increase in the thickness of the films, as the density of the atoms leads to more optical scattering phenomenon in Cr_2O_3. The enhanced optical transmittance of Cr_2O_3 films may be due to the change in the grain size on In-doping up to 4 wt. % as the result of the incorporation of In^{3+} ions with a difference ionic radius to that of Cr^{3+} ions or this may be due to the systematic difference in the surface roughness leading to large scattering loss and the increasing bandgap. The indium doping at 4 wt. % has maximum average transmittance compared to other films. However, the obtained values of transmittance are much higher than those reported in the literature, [5,21] where the optical transmittance decreases with the increase of dopes concentration.

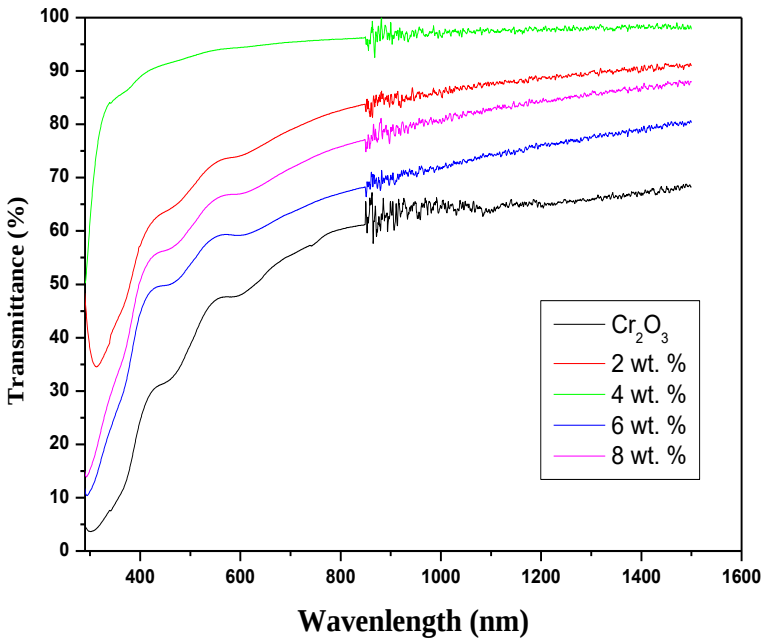

Figure IV.5: The transmittance of un-doped and In-doped Cr_2O_3 thin films.

The optical band gap energy (*Eg*) and Urbach energy (*Eu*), that characterize the disorder in the film, were evaluated from Tauc's formula; calculation details are given elsewhere (equation I.6) [14]. Figure IV.6 shows the variation of band gap and Urbach energy at various concentrations of Indium. The optical band gap values are determined as 3.52, 3.60, 3.93, 3.49, and 3.46 eV at 0, 2, 4, 6, and 8 wt. % of indium content, respectively. We can observe that *Eg* increases to 3.93 eV with the increase of indium concentration to 4 wt. %, while the Urbach energy decreases to 183 meV. On one hand, the increase of *Eg* may be due to a reduction in crystallite sizes as the result of the incorporation of In^{3+} ions with a different ionic radius to that of Cr^{3+} ions. The blue shift of the band edge and reduction of crystallite size confirms the substitution of Cr by indium ions within the Cr_2O_3 lattice, and hence, supports XRD results. On the other hand, as the oxygen content increases (Table II), holes populate states within the valence band, which pushes the Fermi level to lower energy. Consequently, the measured band gap determined from the onset of interband absorption moves to higher energy (i.e. suffers "a blue shift") [15,19,22]. The Increase of In concentration beyond 4 wt. % led to the formation of new donor levels located inside the bandgap, which in turn, displaced the valence band edge to higher energies, leading to a decrease in the energy gap values.

It is clear that, Urbach energy changes inversely with the optical band gap. These results support our interpretation of the increase of band gap with doping concentration as mentioned before since the increase of E_U with doping concentration is an indication of the higher density of localized states. This also means that, as the doping concentration increases, the influence of tailing on the bandgap energy becomes significant[22,23].

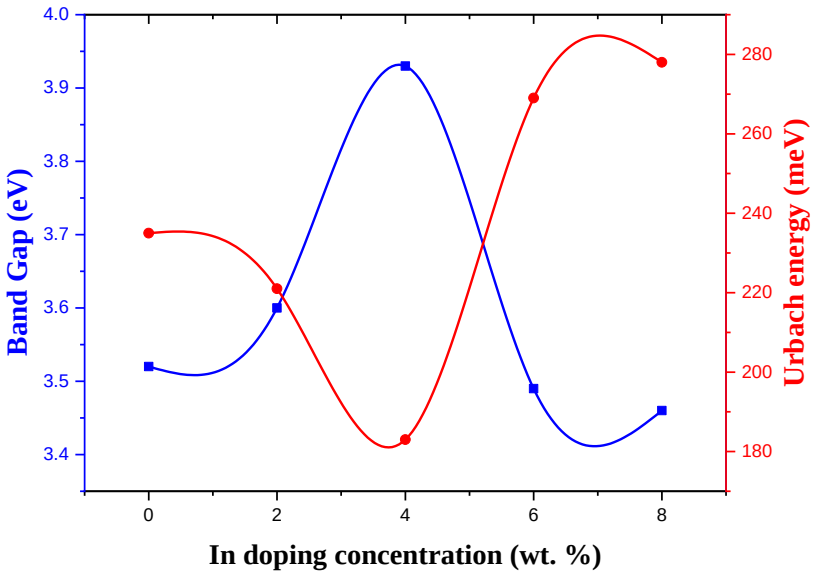

Figure IV.6: Variation of optical band gap and Urbach energies versus indium concentrations.

IV.2.5.Electrical properties

The sheet resistance (R_{sh}); in the linear four-point probe technique, the current (I) is applied between the outer two leads and the potential difference (V) is measured across the inner two probes. Since negligible contact and spreading resistance are associated with the voltage probes, one can obtain a fairly accurate estimation of R_{sh} using the equation (I.8).

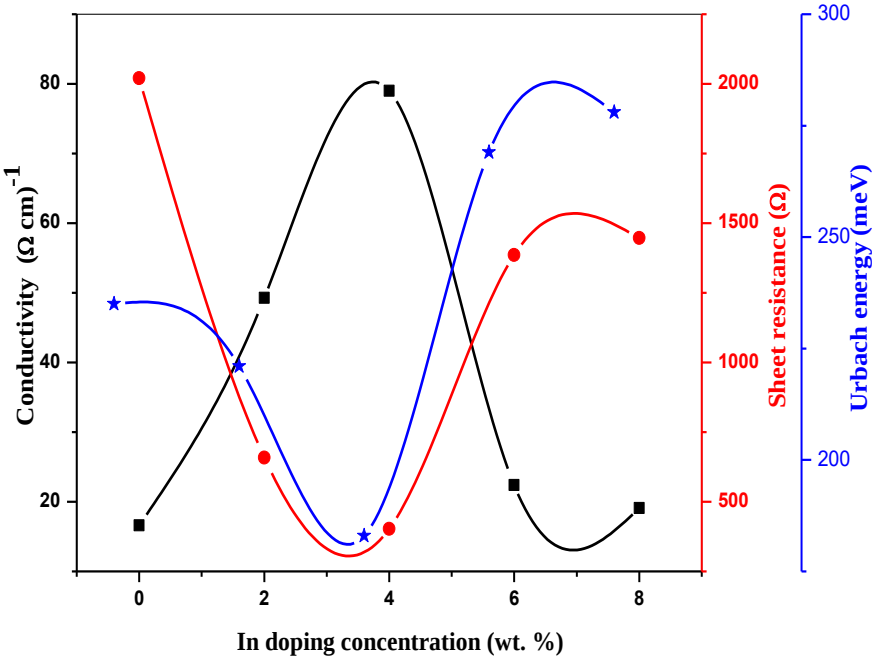

Figure IV.7: Variation of electrical conductivity, band tail width and sheet resistance of In-doped Cr_2O_3 thin films.

Figure IV.7, presents the conductivities, band tail width, and sheet resistance of un-doped and In-doped Cr_2O_3 thin films as a function of the indium content, and their values are summarized in Table III. The pure Cr_2O_3 film has the highest value of sheet resistance which is 2020 Ω. The sheet resistance decreases with the increase in the doping content and reaches the lower value of 403 Ω for a doping content of 4 wt. %. On the other hand, the conductivities of thin films increase with the increase of indium concentration up to 4 wt. %. We can observe that, the highest conductivity was achieved with the 4 wt. % of indium corresponding to 79 $(\Omega.cm)^{-1}$. This value is higher than those reported in literature[8] for Cr_2O_3 doped with magnesium and nitrogen and [10] for Ni-doped Cr_2O_3. The reason for such an increase in the electrical conductivity can be explained by the decrease in the band tail width (Urbach energy) which contributes to increasing the mobility of the charge carriers. However, when the indium doping ratio exceeds 4 wt. %, the electrical conductivity rapidly decreases. This is due to the concentration of free carriers in *p*-type Cr_2O_3 films that are

compensated with indium incorporation because indium acts as a donor atom, i.e., when the free electron concentration in the conduction band increases with indium incorporation, the free hole concentration in the valence band decreases to provide charge valence[24].

IV.2.6. Figure of merit

The figure of merit is an important parameter for optoelectronic device applications. The optical and electrical characteristics have a crucial influence in determining the film's quality, where it requires both high conductivity and high transparency over the visible light region. The figure of merit values was calculated using Haacke's formula as shown in equation (I.11) [14]

Table IV.3: *The optical and electrical parameters values of the deposited In-doped Cr_2O_3 thin films.*

In concentration (wt. %)	Eg (eV)	E_U (eV)	R_{sh} (Ω)	σ $(\Omega.cm)^{-1}$	Figure of merit x10^{-4} $(\Omega)^{-1}$
0	3.52	0.235	2020	16.61	0.0021
2	3.60	0.239	658	49.27	0.568
4	3.93	0.183	403	79.02	12
6	3.49	0.278	1386	21.52	0.031
8	3.46	0.269	1447	19.93	0.093

The figure of merit values for un-doped and indium-doped Cr_2O_3 thin films are presented in Table 3. We observed that, it increases with the increase of indium concentration to 4 wt. % and then decreases. The highest value of the figure of merit obtained is 1.2×10^{-3} (Ω^{-1}) for 4 wt. % (Table IV.3). This is possibly due to the formation of a good-quality film in terms of conductivity and transmittance. The best-obtained value is higher than those reported in the literature ($7.2x\ 10^{-6}$ (Ω^{-1}) for Cr_2O_3 co-doped with Mg and N [8], and ($6.7x\ 10^{-6}$ (Ω^{-1}) for Mg-doped Cr_2O_3 [12].

Conclusion

Thin films of un-doped and In-doped Cr_2O_3 were deposited on glass substrates at 500°C with various concentrations of indium (0, 2, 4, 6, and 8 wt. %) using a home-made pneumatic spray pyrolysis instrument. The X-ray diffraction shows that the films are polycrystalline with a rhombohedral structure oriented along the (110) plane. Doping with indium did not change the structure of Cr_2O_3. The crystallite size decreases from 57 nm of the un-doped to 23 nm at 2 wt. % of indium doped and increases thereafter. SEM images revealed that the films were well-adherent, uniform, pore, and crack–free. The optical results confirmed that the transmittance of thin films was affected by indium dopant and improved on the optical transmittance. A higher transmittance was present in an indium concentration of 4 wt. % (94%). The optical band gap varied between 3.93 and 3.46 eV. The indium-doped Cr_2O_3 films pose low sheet resistance and an increase in conductivity. The greatest figure of merit value 1.2×10^{-3} (Ω^{-1}) is obtained for Cr_2O_3 thin film In-doped with 4 wt. %. The best value of the figure of merit achieved in the present study is found to be the highest among the reported values for Cr_2O_3 films doped with different elements.

So it can be concluded from the present contribution that favorable structural, electrical, and optical properties of In-doped Cr_2O_3 thin films, especially those doped with 4 wt. % indium, are a convenient p-type transparent conducting oxide for usage in many optoelectronic devices and solar cell applications.

References

1. V.B. Kamble, A.M. Umarji, Gas sensing response analysis of p-type porous chromium oxide thin films. *J. Mater. Chem.* (2013) doi:10.1039/c3tc31830c

2. T. Nozaki, M. Sahashi, Magnetoelectric manipulation and enhanced operating temperature in antiferromagnetic Cr_2O_3 thin film. *Jpn. J. Appl. Phys.* (2018) doi:10.7567/JJAP.57.0902A2

3. D. Zhang, X. Li, B. Qin, X. Li, X. Guo, C. Lai, Fabrication of Chromium (III) Oxide (Cr_2O_3) Coating by Electrophoretic Deposition.*J. Am. Ceram. Soc.* (2014) doi:10.1111/JACE.13147

4. S.M. Abdul Kareem, M.H. Suhail, I.K. Adehmash, Fabrication of Cr_2O_3: ZnO nanostructure thin film prepared by PLD technique as NH3gas sensor. *Iraqi J. Sci.* (2021) doi:10.24996/ijs.2021.62.7.7

5. S.M. AbdulKareem, I.K. Jassim, M.H. Suhail, Cr_2O_3:TiO_2 nanostructure thin film prepared by pulsed laser deposition technique as NO2 gas sensor. *Baghdad Sci. J.* (2020) doi:10.21123/BSJ.2020.17.1(SUPPL.).0329

6. V.B. Kamble, A.M. Umarji, Effect of Pt doping on the gas sensing properties of porous chromium oxide films through a kinetic response analysis approach. *RSC Adv.* (2015) doi:10.1039/C5RA02186C

7. T. Nozaki, M. Al-Mahdawi, Y. Shiokawa, S.P. Pati, H. Imamura, M. Sahashi, Magnetic anisotropy of doped Cr_2O_3antiferromagnetic films evaluated by utilizing parasitic magnetization. *J. Appl. Phys.* (2020) doi:10.1063/5.0009353

8. E. Arca, K. Fleischer, I.V. Shvets, Magnesium, nitrogen codoped Cr_2O_3: A p-type transparent conducting oxide. *Appl. Phys. Lett.* (2011) doi:10.1063/1.3638461

9. T. Larbi, M.A. Amara, B. Ouni, M. Amlouk, Enhanced photocatalytic degradation of methylene blue dye under UV-sunlight irradiation by cesium doped chromium oxide thin

films. *Mater. Res. Bull.* (2017) doi:10.1016/J.MATERRESBULL.2017.07.024

10. Z. Fan, M. Zhu, S. Pan, J. Ge, L. Hu, Giant photoresponse enhancement in Cr_2O_3 films by Ni doping-induced insulator-to-semiconductor transition. *Ceram. Int.* (2021) doi:10.1016/j.ceramint.2021.01.226

11. A. Zekaik, H. Benhebal, B. Benrabah, Synthesis and characterization of Cu doped chromium oxide (Cr_2O_3) thin films. *High Temp. Mater. Process.* (2019) doi:10.1515/HTMP-2019-0037/MACHINEREADABLECITATION/RIS

12. L. Farrell, K. Fleischer, D. Caffrey, D. Mullarkey, E. Norton, I.V. Shvets, Conducting mechanism in the epitaxial p -type transparent conducting oxide Cr_2O_3:Mg. *Phys. Rev. B - Condens. Matter Mater. Phys.*(2015) doi:10.1103/PHYSREVB.91.125202/FIGURES/11/MEDIUM

13. A. Abdelkrim, S. Rahmane, O. Abdelouahab, N. Abdelmalek, G. Brahim, Effect of solution concentration on the structural, optical and electrical properties of SnO_2 thin films prepared by spray pyrolysis. *Optik.***(**2016) doi:10.1016/J.IJLEO.2015.11.232

14. A. Abdelkrim, S. Rahmane, K. Nabila, A. Hafida, O. Abdelouahab, Polycrystalline SnO_2 thin films grown at different substrate temperature by pneumatic spray. *J. Mater. Sci. Mater. Electron.*(2017) doi:10.1007/S10854-016-6122-9/FIGURES/7

15. K. Mohanapandian, A. Krishnan, SYNTHESIS, STRUCTURAL, MORPHOLOGICAL AND OPTICAL PROPERTIES OF Cu^{2+} DOPED Cr_2O_3 NANOPARTICLES. *Int. J. Adv. Eng. Technol.*II, II (2016).

16. K. Adaikalam, S. Valanarasu, A.M. Ali, M.A. Sayed, W. Yang, H.S. Kim, Photosensing effect of indium-doped ZnO thin films and its heterostructure with silicon. *J. Asian Ceram. Soc.*(2022) doi:10.1080/21870764.2021.2015847

17. A.R. Chavan, S.B. Somvanshi, P.P. Khirade, K.M. Jadhav, Influence of trivalent Cr ion

substitution on the physicochemical, optical, electrical, and dielectric properties of sprayed $NiFe_2O_4$spinel-magnetic thin films.*RSC Adv.* (2020) doi:10.1039/d0ra04319b

18. A. Abdelkrim, S. Rahmane, O. Abdelouahab, A. Hafida, K. Nabila, Optoelectronic properties of SnO_2 thin films sprayed at different deposition times. *Chinese Phys. B* (2016) doi:10.1088/1674-1056/25/4/046801

19. A. Zekaik, H. Benhebal, B. Benrabah, A. Chibout, N. Tayebi, A. Kharroubi, A. Ammari, C. Dalache, Sol–Gel Synthesis of Nickel-Doped Cr_2O_3 Thin Films. *World Scientific Publishing Company.* (2018) doi:10.1142/S2251237317500125

20. R. Kumaravel, K. Ramamurthi, V. Krishnakumar, Effect of indium doping in CdO thin films prepared by spray pyrolysis technique. *J. Phys. Chem. Solids*(2010) doi:10.1016/j.jpcs.2010.07.021

21. Z.T. Khodair, G.A. Kazem, A.A. Habeeb, Studying the optical properties of (Cr_2O_3:I) thin films prepared by spray pyrolysis technique. *Iraqi J. Phys.*10, 17 (2012).

22. N. Kouidri, S. Rahmane, A. Allag, Substrate temperature-dependent properties of sprayed cobalt oxide thin films. *J. Mater. Sci. Mater. Electron.*(2019) doi:10.1007/S10854-018-0384-3/FIGURES/7

23. S.J. Ikhmayies, R.N. Ahmad-Bitar, A study of the optical bandgap energy and Urbach tail of spray-deposited CdS:In thin films. *J. Mater. Res. Technol.* (2013) doi:10.1016/J.JMRT.2013.02.012

24. M. Nesa, M. Sharmin, K.S. Hossain, Structural , morphological , optical and electrical properties of spray deposited zinc doped copper oxide thin films. *J. Mater. Sci. Mater. Electron.*(2017) doi:10.1007/s10854-017-7075-3

Chapter V: *Structural, optical and electrical properties of Cu-doped Cr_2O_3 thin films*

Introduction

To enhance the properties of Cr_2O_3 thin films, doping is a very important approach to influencing the material properties. Chromium oxide doped has been used for applications such as gas sensors (Ti and Zn doped Cr_2O_3 thin film) [1-2] and photocatalytic degradation (Cs doped Cr_2O_3) [3]. In this study, an attempt was made to deposit Cu-doped Cr_2O_3 thin films to influence their structural, optical, and electrical properties by using the spray pyrolysis technique.

V.1. Experimental details

Undoped Cr_2O_3 and Cu doped Cr_2O_3 thin films were deposited on glass substrates by using a home-made spray pyrolysis experimental setup at a deposition temperature of 500 ◦C with different copper concentrations (0, 2, 4, 6 and 8 wt. %).The precursor solution was prepared by dissolving 0.04 M of Chromium (III) chloride hexahydrate $CrCl_3•6H_2O$ into distilled water, then copper chloride dihydrate ($CuCl_2•2H_2O$) was added into the solution as dopant in content varied from 0 to 8 wt. %.

V.2. Results and discussion

V.2.1. Thickness measurements

The films had good adherence to the substrate and the thicknesses of the deposited films were measured by using a weight difference method using an electronic high-precision balance. The film thicknesses of un-doped and copper doped Cr_2O_3 thin films with various Cu of 0, 2, 4, 6 and 8 wt.% were determined to be about 298, 302, 309, 316 and 321 nm. There is a small variability variation in the film thickness, it has no direct correlation with Cu doping.

V.2.2. Structural properties

X-ray Diffraction (XRD) was used to categorize the crystalline quality and phases that occur in the crystal structure during structural analyses of deposited thin films. The XRD patterns of non-doped and Cu-doped Cr_2O_3 films on glass substrates with varying Cu concentrations (2–8 wt%) are shown in **Figure V.1,** which reveals the polycrystalline structure of Cr_2O_3 thin films with a rhombohedral phase and exhibit a strong orientation along (110) at 36° (JCPDS n°: 00-001-1294), other peaks with low intensity assigned as (104), (113) and (116) were also observed. As the Cu doping level increased, the (110) peak intensity tended to decrease. Due to the fact that Cu^{2+} ions (0.73 Å)[4], entering in the Cr_2O_3 structure, have a larger radius compared with the Cr^{3+} ions (0.63 A°)[5], leading to its crystal structure deterioration. The crystallinity is visibly lowered when copper is used as a dopant,

which is in agreement with the report [6]. Moreover, no other phase has been observed in samples corresponding to either Cu. This indicates that copper has not altered the structure of the rhombohedral chromium (III) oxide and that the Cr_2O_3 sites have been replaced by the Cu^{+2} ions, which proves that the phases that have developed are stable and that the amount of copper does not affect how they form[7].

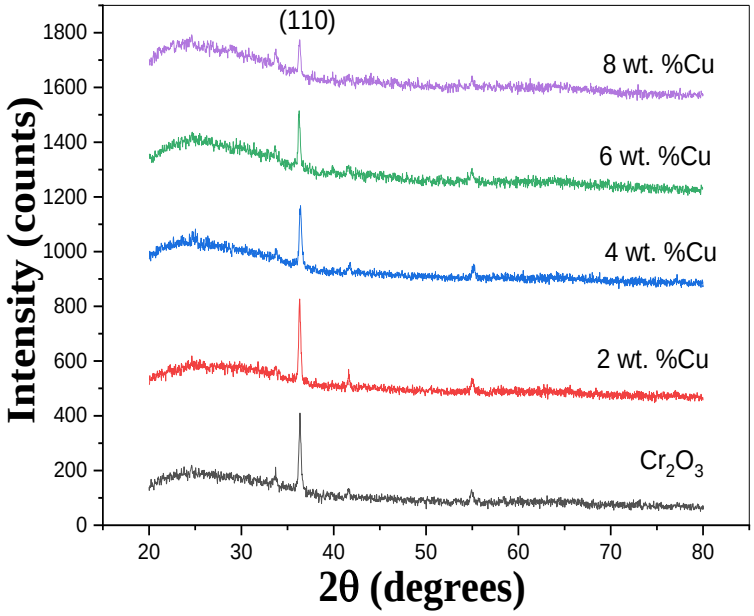

Figure V.1: XRD pattern of Cu-doped Cr_2O_3 thin films.

The calculated crystallite size, the microstrain and full width at half maximum of the peak (FWHM) from the most intense peak (110) for undoped and Cu-doped Cr_2O_3 at different concentrations are tabulated in Table V.1.

Table V.1: *Values of FWHM, Crystallites size and microstrain (ε) of Cu-doped Cr_2O_3 thin films.*

In concentration (wt. %)	FWHM (°)	Crystallite size [nm]	Microstrain (ε) × 10^{-3}
Cr_2O_3	0.147	56.69	0.611
2	0.157	53.15	0.652
4	0.236	35.28	0.970
6	0.255	32.70	1.060
8	0.269	31.03	1.170

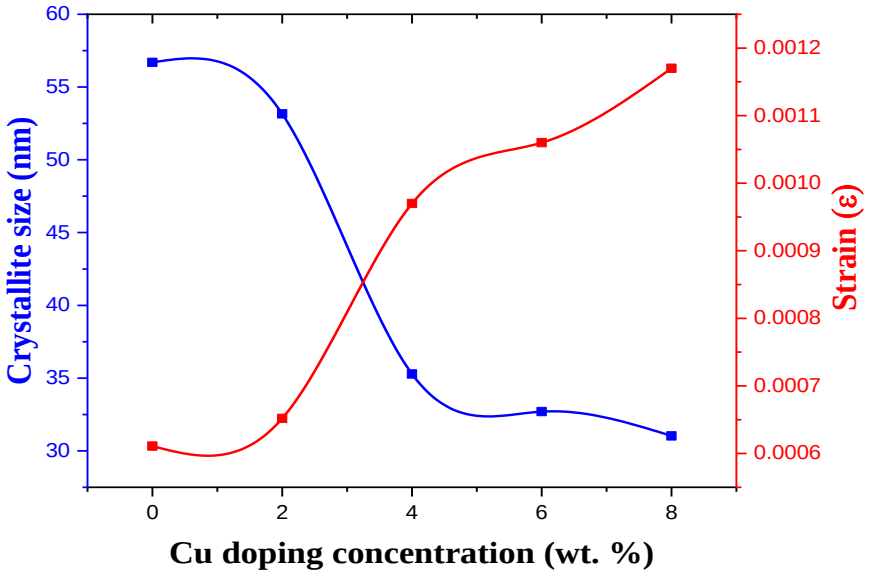

Figure V.2: Variation of the crystallite size and strain versus Cu concentrations.

The crystallite size and the microstrain at different percentages of copper doping are represented in **Figure V.2**. It was found that the crystallite size decrease with the increase in doping percentage. The decrease in X-ray peak intensity leads to an increase in full width at half maximum (FWHM), indicating deterioration in crystallinity and a decrease in crystallite size, a similar behavior has been reported [7]. The decrease in crystallite size could be due to the internal stress adversely affecting the structural properties, which is caused by the difference in ionic radius between Cr^{3+} and Cu^{2+}.These stresses may result in the formation of microstrains in the films, indicating that Cu^{+2} substitute into the Cr^{+3} or incorporate into interstitial sites in the lattice of Cr_2O_3.

V.2.3. Elemental analysis and morphological study

From scanning electron microscopy coupled with X-ray microanalysis, we verified the surface morphology and chemical composition of the deposited layers.

The atomic percentages of chemical composition of un-doped and Cu-doped Cr_2O_3 thin films are summarized in Table V.2. The EDS analysis results for Cu-doped Cr_2O_3 thin films are shown in **Figure V.3**. The EDS data confirm the presence of elemental peaks of Cr, O and Cu (dopant) in the films. The atomic percentages of Cu and Cr increased for 2 and 4 wt. %. and then decreased with the increase in Cu concentration. These results agree well with

the XRD study, demonstrating that the copper is effectively doped in the Cr_2O_3 film. The presence of Si element in films might be probably from the glass substrate. In addition, the oxygen content in the doped thin films was higher than that in the undoped thin film.

Table V.2: *Atomic percentage of chemical composition of un-doped and Cu-doped Cr_2O_3 thin films.*

Chemical element	**Atomic percentage**				
	0%	2%	4%	6%	8%
Cr	27.82	23.96	35.63	24.48	20.02
Cu	0	0.68	1.34	1.06	0.65
O	72.18	75.36	63.03	74.45	79.33

Figure V.3, shows the surface morphologies of the copper-doped Cr_2O_3 films deposited with various concentrations of Cu (0 – 8 wt. %). It is observed that the surface morphology of the films is affected by copper doping and the substrates are well covered by all the films without cracks. For the Cu doping concentration 2 and 4 wt. %. films have large grains with polyhedron like shape and agglomerations with random orientations .The grains were agglomerated and are non-uniform shapes, this is due to the increase of atomic percentages of Cu in the film (Cu^{3+} ions radius is larger than Cr^{3+} ions), where Cu could be found as clusters on the grain boundaries. With the increase of Cu concentration (6-8 wt. %), these structures have begun to disappear.

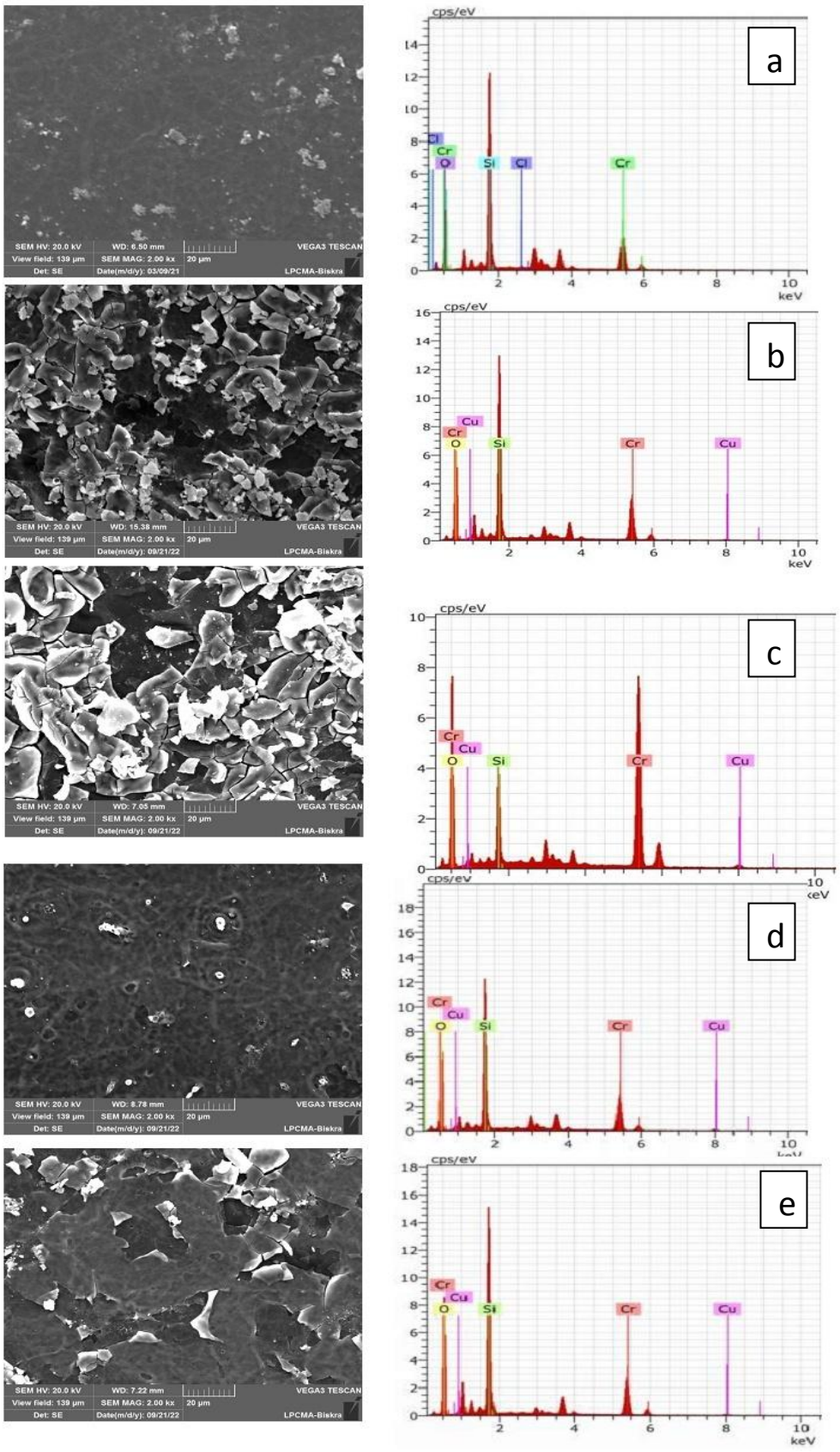

Figure V.3: SEM images and EDS spectra of Cu-doped Cr_2O_3: (a) 0 wt.%, (b) 2 wt.%, (c) 4 wt.%, (d) 6 wt.% and (e) 8 wt.%.

V.2.4. Optical properties

The optical transmittance curves as a function of wavelength were investigated using a UV-Vis-NIR spectrophotometer.

Figure V.4, shows the optical transmittance of different concentrations of Cu-doped Cr_2O_3 thin film (0, 2, 4, 6 and 8 Wt. %) in the 290–1500 nm spectral range. It was found that the undoped chromium oxide films exhibit a transmittance in the range of 65%. It is seen that the transmittance of Cr_2O_3 films is strongly affected by the Cu doping concentration, where the transmittance decreases from 65% to 45% as the Cu doping concentration increases from 2% to 8 %. Furthermore, the absorption edge shifts toward a longer wavelength as doping concentration increases. This drop in transmittance is attributed to a rise in photon scattering generated by doping-induced crystal defects, a similar result has been reported in literature [2-5].

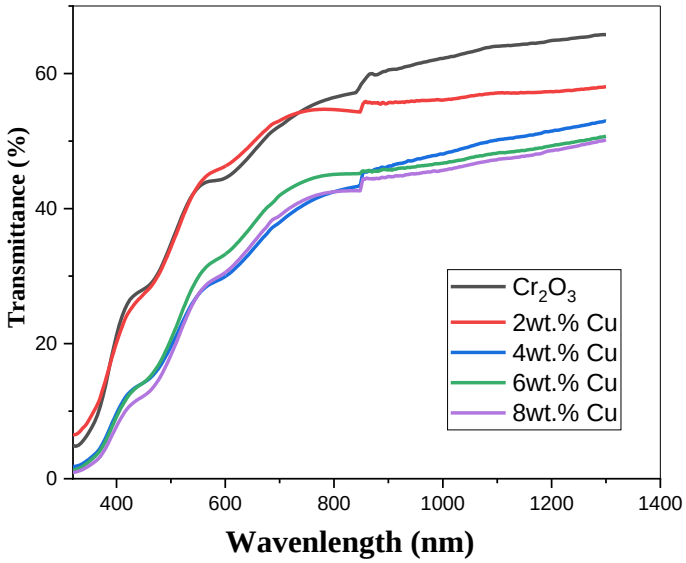

Figure V.4: Transmittance of un-doped and Cu-doped Cr_2O_3 thin films.

In order to calculate the band gap energy, which corresponds to the excitation of an electron from the valance band to the conduction band, we used Tauc's equation by plotting $(\alpha h\upsilon)^2$ versus $(h\upsilon)$ and extrapolating of the linear region of the plot to zero absorption($(h\upsilon)^2$= 0) the optical band gap of all thin films was determined.

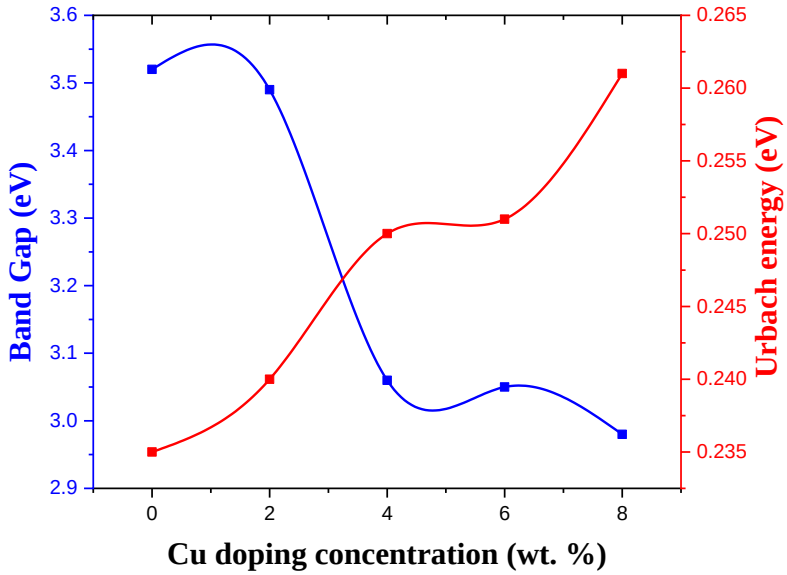

Figure V.5: Variation of optical band gap and Urbach energy versus Cu concentrations.

Figure V.5, displays the optical band gap (E_g) and Urbach energy (E_u) of thin films of Cu-doped Cr_2O_3 films. The optical band gap values are determined as 3.52, 3.49, 3.06, 3.05 eV and 2.98 eV at 0, 2, 4, 6 and 8 wt. % of Cu content respectively. The band gap energy of the pure chromium oxide thin film is 3.52 eV this value is very close to value reported by D. Zuili[10]. With the incorporation of Cu into Cr_2O_3 thin films, a reduction in optical band gap value was noted. Due to the formation of acceptors between the forbidden gap when Cu^{2+} cations replace Cr^{3+} lattice sites, which causes the optical band gap energy to narrow. Such behavior was also reported by Singh et al [11]. New donor levels that are formed inside the band gap cause the valence band edge to be moved to higher energies, decreasing the energy gap values.

The display of situational positions' tails within the optical range gap is made by Urbach (E_u). E_u is a measure of the high concentration of defect states in a material that perturbs the band structure. With increasing Cu doping content, the E_u values were found to range from 235 to 261 meV. It is clear that the E_u increases if the ratio of Cu-doping rises. Deterioration in crystallinity and a decrease in crystallite size are crystalline defects that can contribute to the establishment of local cases within the forbidden band gap, which confirms the increased disorderliness of these films.

V.2.5. Electrical properties:

The sheet resistance of un-doped and Cu-doped Cr_2O_3 thin films was measured by the four-point method. The values of the conductivity are calculated according to equation (I.10). **Figure V.6,** shows the conductivity and the sheet resistance of un-doped and Cu-doped Cr_2O_3 thin films deposited on glass substrates by the spray method.

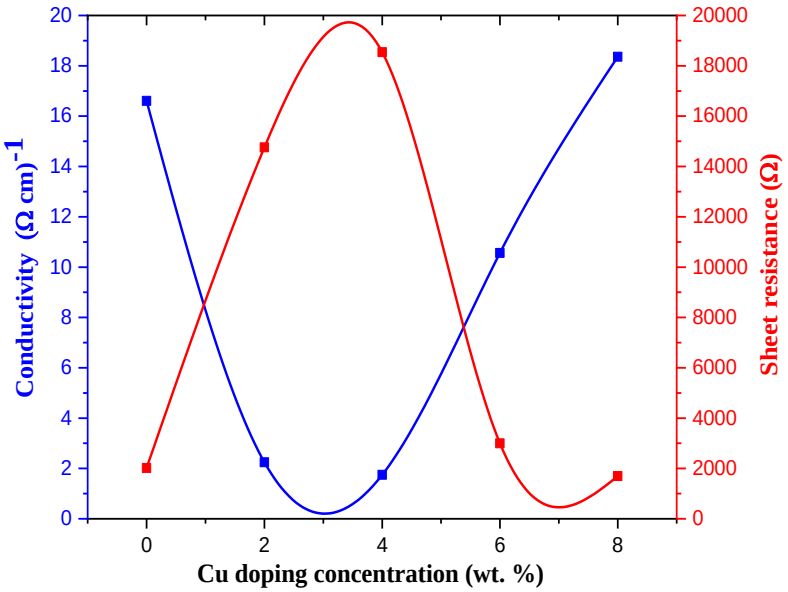

Figure V.6: Variation of electrical conductivity and sheet resistance of Cu-doped Cr_2O_3 thin films.

We observe that the sheet resistance increases with doping content and reaches a maximum of $18{,}538.10^3$ (Ω) for a doping content of 4 wt. %. On the other hand, the variation of electrical conductivity is inversely of the sheet resistance and decreases with Cu doping due to the poor crystallinity, Cu doping induced defect states, and stress generation. With the dopant concentration increase (6 and 8. Wt. %), the electrical conductivity increased. The increase in conductivity may be attributed to the increase in acceptor states associated with the integration of Cu impurities into the Cr sites of the Cr_2O_3 lattice. The incorporation of Cu into the Cr_2O_3 host matrix by replacing Cr^{3+} sites with Cu^{2+} results in an increased concentration of free charge carriers (holes) in the layers, which can be explained by an increase in oxygen.

V.2.6. Figure of merit

A crucial variable for applications involving optoelectronic devices is the figure of merit. The quality of the film is significantly influenced by its optical and electrical properties, when there is a need for high transparency over the visible light domain as well as good conductivity. Haacke's formula was used to calculate the figure of merit values, as shown in equation (I.11).

Table V.3: *The optical and electrical parameters values of the deposited Cu-doped Cr_2O_3 thin films.*

In concentration (wt. %)	Eg (eV)	E_U (eV)	R_{sh} (Ω)	σ $(\Omega.cm)^{-1}$	Figure of merit x10^{-7} $(\Omega)^{-1}$
0	3.52	0.235	2020	16.61	2.1
2	3.49	0.240	14706	2.24	0.658
4	3.06	0.250	18538	1.74	0.015
6	3.05	0.252	2995	10.56	0.255
8	2.98	0.261	1696	18.36	0.438

The figure of merit values for un-doped and copper-doped Cr_2O_3 thin films are presented in Table V.3. We observed that it decreased with the increase in copper concentration to 4 wt. % while it was increased over that value. These values are less than those of indium-doped Cr_2O_3 thin films. The highest value of the figure of merit obtained is 2.1×10^{-7} (Ω^{-1}) for un-doped Cr_2O_3 thin film. This is possibly due to a decrease in conductivity and transmittance. These values are close to those of co-doped Mg and N Cr_2O_3 thin film [12] and Mg-doped Cr_2O_3 thin film [13].

Conclusion

In this chapter, a study was done on how doping copper affected the structural, morphological, optical, and electrical properties of Cr_2O_3 thin films. Thin films of un-doped and Cu-doped Cr_2O_3 were deposited on a glass substrate at 500°C with various concentrations of copper (0, 2, 4, 6, and 8 wt.%) by using a home-made pneumatic spray pyrolysis instrument. The EDS analysis of films confirms the presence of elemental peaks of Cr, O, and Cu in the films. The X-ray diffraction shows that the films are polycrystalline with Rhombohedral structure oriented along the (110) plane. The (110) peak intensity tended to decrease as the Cu doping concentration increased. The crystallite sizes of the films have been found in the range of 58, 53, 35, 32, and 31 nm for 0, 2, 4, 6, and 8 wt.%, respectively. SEM images revealed that the films were well adherent, uniform, pore and crack–free. The optical results confirmed that the transmittance decreases from 65% to 45% as the Cu doping concentration increases from 2% to 8%. The optical band gap varied between 3.52 and 2.98 eV. The copper-doped Cr_2O_3 films have low conductivities and increase sheet resistance.

References

[1] S. M. AbdulKareem, I. K. Jassim, and M. H. Suhail, "Cr2O3:TiO2 nanostructure thin film prepared by pulsed laser deposition technique as NO2 gas sensor," *Baghdad Sci. J.*, vol. 17, no. 2, pp. 329–335, 2020, doi: 10.21123/BSJ.2020.17.1(SUPPL.).0329.

[2] S. M. Abdul Kareem, M. H. Suhail, and I. K. Adehmash, "Fabrication of Cr2O3: ZnO nanostructure thin film prepared by PLD technique as NH3gas sensor," *Iraqi J. Sci.*, vol. 62, no. 7, pp. 2176–2187, 2021, doi: 10.24996/ijs.2021.62.7.7.

[3] T. Larbi, M. A. Amara, B. Ouni, and M. Amlouk, "Enhanced photocatalytic degradation of methylene blue dye under UV-sunlight irradiation by cesium doped chromium oxide thin films," *Mater. Res. Bull.*, vol. 95, pp. 152–162, 2017, doi: 10.1016/j.materresbull.2017.07.024.

[4] S. Muthukumaran and M. Ashok, "Structural , FTIR and photoluminescence properties of ZnS : Cu thin films by chemical bath deposition method," *Mater. Lett.*, vol. 93, pp. 223–225, 2013, doi: 10.1016/j.matlet.2012.11.091.

[5] A. R. Chavan, S. B. Somvanshi, and K. M. Jadhav, "In fl uence of trivalent Cr ion substitution on the fi lms," pp. 25143–25154, 2020, doi: 10.1039/d0ra04319b.

[6] Z. Sheikhi Mehrabadi, A. Ahmadpour, N. Shahtahmasebi, and M. M. Bagheri Mohagheghi, "Synthesis and characterization of Cu doped cobalt oxide nanocrystals as methane gas sensors," *Phys. Scr.*, vol. 84, no. 1, 2011, doi: 10.1088/0031-8949/84/01/015801.

[7] A. Zekaik, H. Benhebal, and B. Benrabah, "Synthesis and characterization of Cu doped chromium oxide (Cr2O3) thin films," *High Temp. Mater. Process.*, vol. 38, no. 2019, pp. 806–812, 2019, doi: 10.1515/htmp-2019-0037.

[8] A. Zekaik *et al.*, " Sol–Gel Synthesis of Nickel-Doped Cr 2 O 3 Thin Films ," *J. Mol. Eng. Mater.*, vol. 05, no. 04, p. 1750012, 2017, doi: 10.1142/s2251237317500125.

[9] Z. T. Khodair, G. A. Kazem, and A. A. Habeeb, "Studying the optical properties of (Cr2 O3:I) thin films prepared by spray pyrolysis technique," *Iraqi J. Phys.*, vol. 10, no. 17, pp. 83–89, 2012.

[10] D. Zuili, V. Maurice, P. Marcus, and M. Curie, "In situ Scanning Tunneling Microscopy Study of the Structure of the Hydroxylated Anodic Oxide Film Formed on Cr (110) Single-Crystal Surfaces," no. 110, pp. 7896–7905, 1999.

[11] B. Singh, S. B. Shrivastava, and V. Ganesan, "Effects of Mn Doping on Zinc Oxide Films Prepared by Spray Pyrolysis Technique," *Int. J. Nanosci.*, vol. 16, no. 1, pp. 581–587, 2017, doi: 10.1142/S0219581X16500241.

[12] E. Arca, K. Fleischer, and I. V. Shvets, "Magnesium, nitrogen codoped Cr2O3: A p-type transparent conducting oxide," *Appl. Phys. Lett.*, vol. 99, no. 11, pp. 2011–2014, 2011, doi: 10.1063/1.3638461.

[13] L. Farrell, K. Fleischer, D. Caffrey, D. Mullarkey, E. Norton, and I. V Shvets, "Conducting mechanism in the epitaxial p -type transparent conducting oxide Cr 2 O 3 : Mg," vol. 125202, pp. 1–10, 2015, doi: 10.1103/PhysRevB.91.125202.

Conclusion and perspectives

This study focuses on the deposition and characterization of p-type semiconductor oxide (Cr_2O_3) thin films elaborated successfully by the pneumatic spray pyrolysis system (SPT) on glass substrates.

Our work will focus on studying the effect of the deposition parameters (concentration of different chemical precursors and substrate temperature) and the influence of In and Cu doping concentrations on the structural, morphological, optical, and electrical properties of chromium oxide films to obtain good-quality films for photovoltaic applications.

For this purpose, the crystallographic properties, surface morphology, chemical composition, optical properties (transmittance, gap energy, and Urbach energy), and electrical conductivity of the elaborated films were investigated using X-Ray diffraction (XRD), TESCAN VEGA3 SEM, energy dispersive spectroscopy (EDS), UV-Vis-NIR spectrophotometer, and four-point probe techniques, respectively.

From the results obtained from the present work, the most important findings are as follows:

At first, we studied the effect of concentration using chromium chloride and chromium nitrate (0.02-0.08 mol/l) on Cr_2O_3 thin films properties. XRD analysis confirms a polycrystalline nature for all films prepared with chromium chloride with a preferred grain orientation along (110) plane, whereas those prepared with chromium nitrate have a poor crystallinity. Crystallites sizes of the films have been found to be decreasing from 56 to 33 nm and from 38 to 19 nm for chromium chloride and chromium nitrate respectively. SEM images revealed that the films were well adherent, uniform, pore and crack – free. The sample obtained from the nitrate solution is thinner and have approximately the same density and smooth surface morphology than that deposited using the chloride solution. The optical study

confirms that the transmittance of Cr_2O_3 films decreases with the increase of precursor concentration. The average transmittance of the films deposited from chromium nitrate is in the range of 60 % (Eg varies from 3.38 to 3.48 eV) and for the films deposited from chromium chloride, it attains 75 % in the visible region (Eg varies from 3.40 to 3.53 eV).The electrical conductivity of the films found in the order of 5 $(\Omega.cm)^{-1}$. The Cr_2O_3 film deposited using chromium chloride at 0.04 mol/l is a suitable p-type transparent conducting oxide because it has a combination of high visible transmittance, high conductivity, and good structural and morphological properties.

The impact of substrate temperature on Cr_2O_3 thin films grown on glass substrates has been studied. The optimal orientation for all films is along the (110) plane at 2 = 36° with a rhombohedral structure. The crystallite size of the films varies from 33 to 58 nm. SEM images showed that the surface homogeneity of the films improved with increasing substrate temperature. Analysis of UV-VIS spectra confirms that the transmittance of Cr_2O_3 films increases with increasing substrate temperature, and the energy gap increases from 3.46 to 3.58 eV. Electrical measurements showed that substrate temperatures increase the electrical conductivity from 3.45 to 16.61 $(\Omega.cm)^{-1}$.

The effect of Indium doped Cr_2O_3 thin films on structural, morphological, optical and electrical properties with different concentrations of indium (0, 2, 4, 6, and 8 wt. %) has been discussed. The X-ray diffraction shows that the films are polycrystalline with a rhombohedral structure preferentially oriented along the (110) direction. The crystallite size is in the range of 47–58 nm. SEM images revealed that the films were well adherent and crack – free. The optical transmittance of films increased up to 94% for 4 wt. % In-doped Cr_2O_3 films and then decreased at 6 and 8 wt. %. The optical band gap varied between 3.93 and 3.46 eV. The highest conductivity value of 79 $(\Omega.cm)^{-1}$ is obtained for the 4 wt. % In-doped Cr_2O_3 films.

The effects of doping copper with various concentrations (0, 2, 4, 6, and 8 wt. %) on the structural, morphological, optical, and electrical properties of Cr_2O_3 thin films were investigated. XRD analysis indicates that the undoped and copper-doped Cr_2O_3 thin films showed a preferential orientation along the (110) plane with rhombohedral structure, and the (110) peak intensity tended to decrease as the Cu doping concentration increased. The crystallite size decreased with the increase in doping percentage from 58 to 31 nm. The optical band gap values are determined as 3.52, 3.49, 3.06, 3.05 eV, and 2.98 eV at 0, 2, 4, 6, and 8 wt. % of Cu content, respectively. The electrical conductivity decreases with Cu doping.

So it can be concluded from the present contribution that favorable structural, electrical, and optical properties of In-doped Cr_2O_3 thin films, especially those doped with 4 wt. % indium, are a convenient p-type transparent conducting oxide for usage in many optoelectronic devices and solar cell applications.

Finally, the different perspectives that can be considered for the continuation of this work are:

- Analyzing the deposited films' photocatalytic and self-cleaning characteristics to verify the findings of this research.
- Integrating Cr_2O_3 thin films optimized in transparent pn-junctions.

Abstract

Chromium oxide (Cr_2O_3) thin films have been deposited by the pneumatic spray method on glass substrates to obtain good optoelectric properties for use in photovoltaics. We studied the effect of the molar concentration of chromium chloride and chromium nitrate, substrate temperature, indium doping and copper doping on the structural, morphological, optical, and electrical properties (by various techniques XRD, SEM, EDS, UV-Visible, and the four probe technique) to improve the quality of Cr_2O_3 thin films. X-ray diffraction (XRD) study shows that the chromium chloride crystallization is better than that of nitrate, with a (110) preferred orientation in rhombohedral structure. SEM images revealed that the films were well adherent, uniform, pore and crack – free. The optimal temperature of the substrate is 500 °C, the average transmittance of the films is in the range of 60% (Eg varies from 3.46 to 3.58 eV), and the electrical conductivity is $16.61(\Omega.cm)^{-1}$.

The In and Cu doped chromium oxide films with percentages of dopant (0, 2, 4, 6, and 8 wt.%) were examined. The films doped with indium revealed improvements in their optical and electrical properties. Contrary to films doped with Cu.

The highest transmittance value of 94% and a better conductivity value of 79 $(\Omega.cm)^{-1}$ with the greatest figure of merit value 1.2×10^{-3} (Ω^{-1}) are obtained for the 4 wt.% In doped Cr_2O_3 films, making it a convenient p-type transparent conducting oxide for use in many optoelectronic devices and solar cell applications.

Résume

Des films minces d'oxyde de chrome (Cr_2O_3) ont été déposés par la méthode de spray pneumatique sur des substrats en verre afin d'obtenir de bonnes propriétés optoélectriques pour une utilisation dans le domaine photovoltaïque. Nous avons étudié l'effet de la concentration molaire du chlorure de chrome et du nitrate de chrome, de la température du substrat, du dopage à l'indium et du dopage au cuivre sur les propriétés structurelles, morphologiques, optiques et électriques (par diverses techniques DRX, MEB, EDS, UV-Visible et la technique des quatre sondes) afin d'améliorer la qualité des films minces de Cr_2O_3. La caractérisation par diffraction des rayons X (DRX) montre que la cristallisation du chlorure de chrome est meilleure que celle du nitrate, avec une orientation préférentielle (110) dans la structure rhomboédrique. Les images MEB ont révélé que les films étaient bien adhérents, uniformes, sans pores ni fissures. La température optimale du substrat est de 500 °C, la transmittance moyenne des films est de l'ordre de 60 % (Eg varie de 3,46 à 3,58 eV), et la conductivité électrique est de $16,61(\Omega.cm)^{-1}$.

Les films dopés à l'In et au Cu avec des pourcentages de dopant (0, 2, 4, 6, et 8 wt. %) ont été examinés. Les films dopés à l'indium ont révélé des améliorations de leurs propriétés optiques et électriques. Contrairement aux films dopés au Cu.

Les films de Cr_2O_3 dopés à l'indium à 4 % en poids présentent la plus grande valeur de transmission (94 %) et une meilleure valeur de conductivité (79 $\Omega.cm)^{-1}$ avec le plus grand facteur de mérite ($1,2\times 10^{-3}$ (Ω^{-1})), ce qui en fait de lui un oxyde conducteur transparent de type p utilisable dans de nombreux dispositifs optoélectroniques et dans les systèmes photovoltaïques.